FINAL TECHNICAL REPORT

Project Title: **"Studies on Anisotropy and Vortex Motion in Melt Texture Grown Superconductors".**

Principal Investigator:

Dr. Syed Khurshid Hasanain
Associate Professor
Department of Physics
Quaid-i-Azam University, Islamabad

Project No. **PSF/RES/C-QU/PHYS(90)**

Submitted by: **Dr. S.K. Hasanain**
Associate Professor

Dated: 19/8/98

Summary:

The focus of this project was to prepare and study the magnetic and transport properties of oriented, polycrystalline high T_c superconductors, with special emphasis on their anisotropy. It had further been planned that the behavior of the magnetic flux, (so called vortices) would be analyzed in terms of the dynamics of these entities, subjected to the thermal and anisotropic conditions. During the period of this grant proposal, we have been able to achieve almost all the goals envisaged in the proposal. These are illustrated by the 10 publications directly related to the project, which have been published in quality international journals during this period. (List attached). We have also produced two Ph.D. theses in superconductivity during this period, one of which was submitted by the Research Officer, supported by this project.

We have prepared very good quality *melt textured high T_c superconductors*, which were required for performing the studies on anisotropy of the magnetization of these materials. We have also conducted and published the dc and ac magnetization studies of these materials focusing on the properties of the vortices and obtained an understanding of the factors limiting the critical currents in various crystallographic directions. We have also studied in detail the dynamics of vortex motion in these materials by the methods of magnetic relaxation, field sweep rate dependence and ac susceptibility in superposed dc fields. Our studies have enabled us to draw a comprehensive picture that the barriers to vortex motion, and subsequent dissipation, are lowered in dc fields and in particular in crossed ac and dc fields the effects are drastic. We have also found that the decrease in critical currents with increasing fields can be explained on the basis of the so-called *Critical state model* for fields applied parallel to the c-axis, while the behavior perpendicular to the same is quite different. We have conducted transport measurements and identified the role of the (JxB) force as well as an angle independent, phase slip contribution to the dissipation. Our studies therefore constitute part of the major international effort to determine the electrodynamics of layered, anisotropic superconductors, the mechanisms determining the losses, and the anisotropy of their response.

Introduction:

The discovery of high T_c superconductors in 1985-86 has spurred efforts in two major directions (a) To understand the mechanism of superconductivity, (b) to comprehend the complex and anisotropic magnetic and transport properties of these materials. Our efforts have been directed towards the second, (b), of the above. The specific need for this arises because the well understood electrodynamics of conventional superconductors was based on isotropy both of the superconducting (SC) order parameter, and the coherence and penetration depths. The layered and almost 2-D nature of the new materials made the older theories obsolete or at least incomplete. The need was to comprehend how the response varied magnetically when the essential entities, the quantum of flux "vortices", would themselves be quasi-discontinuous or would lose coherence as they traversed the inter-plane distance.

In this context the major questions we chose to address experimentally were as follows :

(1) How does the magnetic response to dc fields vary as the field is applied at different direction to the c-axis of the perovskite structure ?

(2) How do the E(j) characteristics, which define the dissipation in a conductor, vary as the magnetic field or fields (superposed ac + dc fields) increase in magnitude, and in different applied directions ?

(3) The barriers to vortex motion, the so called *activation energy barriers* U or *pinning energies* U_0 are crucial for the loss less transport of current. These can be measured magnetically. How do these activation barriers vary in different conditions of orientations , field, etc.

(4) Investigation of vortex dynamics and the role of intra-granular and intergranular sources of dissipation; as well as the role of the Lorentz like (JxB) force in dissipation and the isotropic weak link dissipation.

(5) Investigation of the ac response χ_{ac}. as a function of the dc field, sweep rate, and temperature. This is usually performed with a view to identifying the factors controlling the penetration of flux into the superconductor.

Results:

This section will be divided into four main sub-sections.

a) Preparation of melt-texture grown, anisotropic samples and their magnetic characterization.
b) DC magnetization studies including $M(H)$, $M(\dot{H})$, $M(\theta)$.
c) Transport measurements $\rho(H,\theta)$.
d) dc magnetization and the effects of *superposed dc and ac fields*.

a) **Melt Texture growth:**

The first task before us was to prepare the $Y_1Ba_2Cu_3O_{7-x}$ superconductors which would possess overall bulk orientation and anisotropy. (The general method of power reaction yields granular, polycrystalline and isotropic materials). To prepare the melt texture grown materials we proceeded as planned except that since we had not been provided a tube furnace in the approved budget, we had to restrict ourselves in various ways. We were unable to provide a temperature gradient to the materials during the slow cooling step. However, we modified our existing box furnace so as to achieve the best results possible . Initially we reacted the YBCO powders at a temperature T ~ 950°C. These products were thoroughly ground, pelletized and again heated up to various temperatures in the range of 1050 to 1150°C, from which temperatures they were very slowly cooled down through their peritectic temperature. (1000°C) at the rate of 1-1.5°C/hr, till they reached about 950°C. From this point they were cooled at a relatively fast rate (100°C/hr) down to 400°C, where after they were furnace cooled. These steps were followed by oxygen annealing the samples so obtained. It was found that oxygen annealing in the temperature range 450 - 650°C was sufficient, however pressures in the range of 5-6 p.s.i. were required. We also discovered that along with the rate of cooling, the other important factor was the substrate on which the samples were melt texture grown. It was found that the best results, in terms of the

magnetic loop widths were obtained when the samples were placed on a curved Alumina substrates, making minimal contact with the substrate. These however did not yield the best anisotropic response. This feature viz. anisotropy, was quantified magnetically by measuring the magnetization with the applied field parallel to the c-axis and normal to it, respectively. The ratio of these two values provides a guide to the extent of anisotropic growth . On the width of the hysteresis loop widths provides a means to determine the critical current in that orientation and/or the sizes of the grains. We consistently found that in the conditions of our preparation the c-axis was found to lie normal to the surface of the pellet. Since the anisotropy factor usually did not rise above 3 in these materials we tried other substrates and crucibles. We obtained best results in flat bottomed Alumina crucibles with the pellets stacked one on top of the other. These provided us with the best results in terms of the anisotropy factor, i.e. the magnetic response was 4 to 5 times higher along the c-axis (H$\|\|$C) as compared to the transverse case, H$\perp$C. (Figure 1). The main features of the melt textured samples as compared to the untextured ones, are apparent from the figure (a) much larger magnetization, (b) much better defined anisotropy. Another characteristic which further corresponds to the reported behavior is the relatively rapid decrease of M for H parallel to the c axis while the decrease is slow for H perpendicular to the same. All the experiments to be described in this report utilized, similarly self made superconductors. The texturing of the materials was checked also by electron microscopy (performed at the A.Q. Khan Research Lab. K.R.L). The large uninterrupted grain growth was evident from the micrographs (Fig.2). The samples were cut up into suitable sizes 1 x 4 x 4 mm^3, and the critical temperatures were ascertained. The T_c (zero resistance) was typically ~ 89.90°K. While the onset was at 93°K. The magnetization values for the best samples reached (for H$\|\|$C) $\cong$ 23(emu/cc) at low fields, while the lower critical fields were in the region of 170-220 Oe at 77K.

DC Magnetization Measurements:

a) The dc magnetization was measured using our vibrating sample magneto-meter and lock in amplifier system. In addition to the usual, commercially provided pick-up coils, which enabled us to measure the sample moment parallel to the magnetic field we also developed a set of

coils to pick up the transverse component of magnetization. This has been outlined in Ref. [1]. A special feature of this effort was that it provided us an ability *to measure both components of magnetization simultaneously* . i.e. the component of M parallel to the applied field H ,as well as the one transverse to H .In particular one could monitor the rigidity with which the magnetic moment rotated when the sample was rotated. Our dc magnetization measurements included the studies of anisotropic response M(θ) ,(θ being the angle between the c axis and the applied field); the effects of field sweep rate on magnetization and magnetic relaxation effects.

Studies on Anisotropy of magnetization.

The effects of anisotropy were explored by the following method. Samples were either cooled in field or without field, down to the required temperature. The magnetization was then recorded continuously as the sample was rotated in situ, with respect to the field. This generated a typical M(θ) pattern at a fixed field. These patterns were studied as a function of temperature and field. Alternatively, the sample was cooled in field and then the field was turned off. This result in the flux remaining trapped at the defect site, the so called pinning centers. The amount of flux remaining trapped is called the 'remnant moment', and varies with T, H, and equally importantly with θ. This anisotropy of flux pinning is an important parameter, being related to the strength of shielding currents which flow in either orientation. It is understood that remnant moment is maximum at H//c and decreases as H is rotated away from this direction. The angle and field dependence of the remanence were studied by us in detail and reported in Refs. [1,2,3]. Figs.3 & 4 illustrate typical behavior. The maximum (ϕ=0, H//c), and saturation and decrease with field are evident line.

In the other type of measurements, the zero-field -cooled moment was rotated with respect to the field. Typical patterns are shown in Figs. 5 and 6. As can be seen the moment varies harmonically with peaks occurring at $\theta = n\pi/2$; i.e. maximum diamagnetic signal for H$||$c ($\theta = n\pi$) and minima for $\theta = (2n + 1)\pi/2$, i.e for (H$\perp$c). It is also to be noted that the pattern remains unchanged on reversal of θ. The up going and down going peaks coincide. These features however change drastically when the field is increased. (Fig.6). We found that the peak positions

shifted from multiples of $\pi/2$, and the angular span in going from maxima to minima was no longer $\pi/2$. It was found that the moment decreased very rapidly on going away from the c-axis while it took a larger θ interval to reach the maximum away from the ab-planes. These features are detailed in Ref.3 . We also found a marked hysteresis between up and down going data i.e. between increasing and decreasing angles. These features were explained by us using two conceptual models. These were as follows:

(a) Anisotropy of flux line energies (self-energy and rotational energy).

(b) Existence of "shoulder" and "core" regions of flux line distributions in the sample.

The former effect (a) implies that while it is easier to form a flux line parallel to the ab planes as compared to the c axis, it is difficult to rotate the flux lines away from the ab planes. On the basis of detailed measurements in the field range $10< H < 5000$ Oe we demonstrated how the development of various features in the $M(\theta)$ were a consequence of these anisotropy of relevant energies. e.g. these effects contribute to the vary rapid decrease in M as θ is moved away from the c-axis and delay the ability of the flux to be oriented away from the ab planes when the sample is rotated away from the ab planes. These features relate to the rotation of the sample in one sense only The latter effect, (b), on the other hand relate to the orientational gradient of the flux lines. In other words as the sample is rotated against a field it divides into two regions . One region close to the surface where the flux gradually rotates away from the surface field direction on rotation ,and hence develops an orientational gradient. While deeper within the flux is rigidly fixed to the original direction and rotates as such. We have shown how this effect determines the variation of M on the reversal of the sense of rotation. For a given field there is a certain minimum angle of rotation for which the change in orientation penetrates to the center of the sample. Until this angular rotation is achieved the "core" region survives with its unchanged magnetization. This leads to the hysterectic behavior on reversal.

We developed the concepts of "core" and "shoulder" region to describe the magnetization behavior on rotation (Fig.7). When a sample is rotated with respect to the field the flux near the surface is able to change its orientation while that lying deeper within can not do so, till the field is large enough. The area near the surface where the flux changes its direction with rotation is called the "shoulder" while that lying deeper, where the flux remains essentially fixed in orientation, and rotates rigidly with the sample, is called the "core". As the sample is rotated the flux develops an orientation gradient in the "shoulder". The net M(θ) behavior is a superposition of the "core" and "shoulder" responses. The "shoulder" region would generate an essentially angle dependent response (for isotropic materials) while the core generates a $\cos\theta$ type behavior.

Typically the core survives on field cooling of the sample, and on rotation in low fields, while the shoulder extends deeper as the rotation is increased. For low fields (Fig.6a) the fit of the data to $M = -(M_A \cos^2\theta + M_B \sin^2\theta)$ was very good, as expected theoretically for reversible (Meissner) response, while in large fields the core and shoulder concepts were employed to explain further anomalies. In particular the irreversible feature on reversing the sense of rotation, (Fig.6c,6d) where the response is altered in the region $270 < \theta < 360$, while it reproduces the up going behavior for $\theta < 270$, was also explained along the same lines. The results and discussion are detailed in Ref.2 and 3.

b) <u>Field sweep rate effects</u>:

The effects of field sweep rate $\dot{H}$ on the magnetization M in a superconductor are understood to yield some fundamental information regarding the dissipation law in superconductors in the vortex state. e.g. the variation of the exponent n in a typical form

$$E = a J^n \qquad (1).$$

It is understood that the variation of magnetization with the dc field sweep rate H generally yields a logarithmic form

$$(\partial \ln M)/\partial \ln \dot{H}) = C \quad (2)$$

where C is a constant depending on the field and temperature. Furthermore , this constant C can be shown to be approximately equal to 1/n, where n is defined in Eqtn(1). The effects of sweep rate on magnetization can be described in simple form as follows. The sweep $\dot{H}$,

generates an electric field E, according to Maxwell's equation $\nabla \times E = -\partial H/\partial t$. In response to this field E, shielding currents J begin to flow according to the dissipation law e.g. $E = aJ^n$. The currents in turn generate a magnetic moment M which becomes a function of sweep rate i.e. M (J(E ($\dot{H}$)). Since both, the magnetization changes with time M(t) and the effect M($\dot{H}$) depend on J(E) the effects dlnM/dlnH and dlnM/dlnt are expected to be related. This feature has been tested in our work.

Increasing the sweep rate yields increasing width of the hysteresis loops (see fig.8) which follows from the above discussion. (note that larger loop widths imply larger shielding currents and magnetization). From the logarithmic fits of the data (Eqtn. 2) we obtained the values of C at various fields. (Fig.9). We also studied the anisotropy of the sweep rate effects. These are reported in Ref.4. A major finding in this respect was that there exists a pronounced anisotropy to these effects, being larger for H$||$C and less for H$\perp$C.(See Fig.10) These effects were explained on the basis of comparisons between the flux creep and dynamic magnetization models. We also compared the values of C obtained from the above technique to the value of the flux creep or magnetic relaxation rate

$$S = \partial(\ln M)/\partial(\ln t) \qquad (3).$$

(The magnetic relaxation method will be described in a separate section.) A comparison showed that the two rates S and C appeared to converge at low fields as predicted theoretically but differ for larger fields. We found values for C to be in the range while values for S lie usually in the range 0.02 to 0.04. In addition to the variation of M with lnH we compared the effects of sweep rate on the *ac magnetization* χ_{ac} , in superposed dc fields. The basic idea of the experiment was that since the ac magnetization values depend on the dc flux present in the sample at any instant i.e. χ_{ac} (B_{dc}); and B_{dc}(H), this would suggests that the ac response would itself be a function of the sweep rate , $\chi_{ac} = f(B(\dot{H}))$. This was tested by monitoring the ac susceptibility of our melt textures samples using a conventional ac susceptibility setup. This consists of a balanced pair of secondary coils , with the sample inserted into one of them. The ac field of the primary coil acts on the sample and output of the secondaries is fed to a lock-in amplifier. The whole assembly of the coils was placed inside the liquid nitrogen cryostat to keep the coils

cooled , and finally the cryostat was placed within the pole pieces of the magnet. The ac response could be measured as the dc field was rammed up and down at different rates. It was clearly evident that the ac response varied with the sweep rate, become larger (i.e. more diamagnetic) for higher sweep rates. It was also evident that the response was *instantaneous* to our degree of resolution and was perfectly reversible . i.e. as the field sweep rate was varied χ_{ac} curves immediately retraced the loops corresponding to that sweep rate. There were no hysterectic or time lag effects involved. These data were found to be inconsistent with the classic critical state or flux creep picture. According to the flux creep picture, the system moves towards equilibrium by homogenizing the flux distribution via the flux creep process.. Thus it should not move away from it, if the rate of sweep is increased. These aspects are discussed in detail in Ref.4. While values for S lie usually in the range 0.02 to 0.04. In addition to the variation of m with lnH we compared the effects of sweep rate on the ac magnetization, in superposed dc fields. The basic idea of the experiment was that since the ac magnetization values depend on the dc flux at any instant i.e. χ_{ac} (B_{dc}); and B_{dc} ($\dot{H}$). This clearly suggests that $\chi_{ac} = f(B(\dot{H}))$ implying a rate dependence to the ac susceptibility as well. This was tested by monitoring the ac susceptibility of using a balanced coil set, and with the sample inserted in one of the secondary coils. Then the field was swept and χ_{ac} monitored as the output of the lock-in amplified. It was clearly evident that the ac response varied with the sweep rate become larger for higher sweep rates. It was also evident that the response was instantaneous to our degree of resolution and perfectly reversible. This latter observation is inconsistent with the prediction of the flux creep model which predicts a finite time for the sweep rate changes to effect the flux density and hence the ac response. In a similar vein the reversibility on changing the sweep rates is inconsistent with a flux creep picture. This would imply a movement of the system away from a more uniform to a less uniform state. In light of these observations we suggested that a dynamic magnetization model proposed earlier by Delin etal.[5]was more appropriate to describe these effects.

Magnetic Relaxation Studies:

A major part of our effort was directed towards studying the time variation of dc magnetization, i.e. the magnetic relaxation of high T_c superconductors. In these studies the field is ramped up to a certain

value and then held steady. The magnetization is then recorded as a function of time. Changes occur with time as the flux penetrates (creeps) in to the sample over defect centers , called *pinning centers* and an inhomogenous distribution of flux occurs within the material From the usual logarithmic variation,

$$M = M_0 (1- S \ln (1 + t /\tau) \qquad (4),$$

the value of the relaxation rate parameter S can be determined , as can be seenin Eqtn .3. Fig. 11 shows atypical fit of the M(t) data to the log function. We found that for our samples in the time window of $t<1500$ sec., the log fit yielded good results and with reasonable values for the parameters. A further significance of these studies is that they enable the determination of an important physical quantity, *the activation potential barrier U.* To realize this we recall that the relaxation rate can be related to the height of the energy barriers *U* opposing the vortex motion via the relation,

$$S = KT/U \qquad (5)$$

where KT is the thermal energy. It is also understood that in the simplest (linear) approximation, the activation barrier depends on the field and current as $U = U_0 - JBVX$. (Here U_0 is some intrinsic pinning potential, V is volume of flux bundle and X the jump distance of the flux bundle.

We studied the effects of field in both textured and untextured high T_c superconductors and found that the rate of relaxation $S = (KT/U)$ varies in a non-monotonic way with field. Initially the effect of the field was observed to decrease the rate of relaxation while at higher fields the rate increased with H. This has been understood in terms of the value of the field H^*, required for full penetration of the sample. For fields below and above it , the behavior of the relaxation rate is different. These effects were studied in single crystals, polycrystals and melt textured samples. Melt texture grown samples with their characteristically wide loops implying a large shielding current and critical state (non-homogenous) magnetization , provided ideal opportunity to study the magnetic relaxation.

There has been a great deal of discussion in the literature on the logarithmic time dependence, and the scale of the logarithmic time constant. We pave found in our measurements that, at least at relatively short times $t \leq 1500$ sec., the variation is logarithmic $M = M_0 (1-S \ln (1 + t/\tau)$ and the *time constants* τ *are macroscopic.* These two major

observations were found to hold consistently in a variety of samples. This may also be due to the limited field range of our observations. The point to emphasize is that as long as the activation potentials U, remains linear in J, (i.e. M), the time variation of M remains log like. Secondly, the time constants τ obtained from the fit do not reflect the intrinsic or microscopic attempt times, (e.g. the typical time required by a pinned vortex to overcome a potential barrier.) Rather τ is a reflection of the *macroscopic* conditions such as sample size, sweep rate H and the E(J) relationship of the system. Typically we found τ to lie in the range 0.1 - 1 msec. The time constant was found to vary with sweep rate, becoming larger for slow sweep rates prior to holding of field and vice versa. This effect is consistent with the analysis of Gurevich and Kupfer [6]and that of Caplin etal.[7]. Further details will be discussed in the section on crossed flux studies.

Crossed Flux Studies:

A large part of our experimental studies during the latter part of the reporting period was directed towards performing experiments in a crossed flux configuration. In this mode there is an applied field H_l (longitudinal field) along which the magnetization is being measured. In addition there is a field H_t applied transverse to H_l . The rationale behind these studies was that due to the very pronounced anisotropy of these samples, the effect of a transverse field would be quite different from that of the longitudinal one . There are at present few studies in this configuration and there appears to be a lack of consensus on the role of the transverse flux in either inhibiting or facilitating the entry of longitudinal flux. The question assumes importance in view of the many varied applications of superconductors where in addition to the ambient field there are strong parasitic transverse fields present. Furthermore, there are certain basic questions which relate to the presence of transverse families of flux lines. One of these is the issue of how two mutually orthogonal flux lines cross each other and under what conditions can they do so. Under certain conditions e.g. at low temperatures and strong pinning it is argued that. no cross flow may occur . While in other cases e.g. in the case of Bismuth based superconductors cross flow of vortices has been observed in magneto-optical measurements. We addressed this cross question in the context of the relatively stronger pinning YBCO compounds albeit at the high

temperature side of the phase diagram where pinning and coherence of vortices are understood to be weaker.

The effect of the transverse field on the longitudinal moment M_l was studied as a function of H_l and H_t. Furthermore, the effect of the crossed fields on the critical current (J_c $\alpha\Delta m$) was studied from the changes in the hysteresis loop widths while the effects on the dynamics (flux line motion) were studied by comparing the magnetic relaxation with and without the transverse fields and the effects of the sweep rates in the same mode .

In Fig.12 we display the effects of transverse fields of different magnitudes on the magnetization curves of a melt textured sample. In these data instead of applying another field, the transverse field was generated by cooling in a field in one direction, then rotating the sample to a transverse position and applying a field perpendicular to the initial direction. This has the effect of creating two mutually orthogonal families of flux lines. As the figure shows the effect of successively larger cooling fields is to decrease the loop widths in the longitudinal direction. In the present case, the longitudinal field direction corresponds to H//ab planes while the transverse is parallel to the c-axis. The loops shown are for the ab plane moment. For low fields the decrease in the moment was seen to be quite linear with the magnitude of the field cooled (transverse) moment. Thus our data showed (in contrast to some other studies at very low temperatures) that the effect of a transverse moment was to decrease the loop width and shielding currents, at low fields in particular. For higher fields the differences between the crossed and uncrossed hysteresis loops appears to diminish suggesting the expulsion of the cooled flux. Expulsion of the trapped flux was monitored using the double coil arrangement described previously. Similar studies were later conducted in the mode where both the fields are applied externally. No qualitative difference was seen compared to that described above. i.e. the longitudinal moment decreases rapidly as the transverse field is applied. This was interpreted by us as showing that even in the relatively stronger pinning system like YBCO at elevated temperatures the cross flow of vortices is possible. W e also noted (see Fig.) that there was a certain flattening of the hysteresis loops at high fields in the crossed field configuration. This would indicate that for higher flux densities there is an inhibiting tendency of the transverse field.

In addition to the magnetization studies we also investigated the change in the dynamics due to the crossed fields. The rationale for these was that if the transverse flux is affecting the movement of longitudinal flux, as evident from the hysteresis loops, then this should also reflect itself in the dynamics as well as the dissipation behavior. Hence magnetic relaxation studies were also conducted in the crossed field configuration. These magnetic relaxation studies, where M is measured as a function of time M(t) at a fixed field have been described above. As mentioned, the rate of relaxation $S = (\partial \ln m/\partial \ln t)$ yields the activation barriers via: the relation $S = (KT/U)$. Hence the objective of these studies in the crossed flux mode was to ascertain how the presence of the transverse flux effected the movement of the vortices in so far as it is reflected in the relaxation rate. If the transverse flux decreases the flux pinning energies i.e. lowers the activation barriers U, then
$S = (KT/U)$ should increase. In other words the relaxation rate should increase if the crossed flux has decreased the activation barriers.

The results of the these experiments were reported in Ref.8 and some of the data are displayed in Figure11, which shows the magnetization on a log scale. The linear fit is evident over the entire time range $t \leq 900$ sec. The different lines correspond to data at various transverse fields. We find the relaxation rate S increases from 0.023 (uncrossed), to 0.083 (field cooled in 1000 Oe). This corresponds to a decrease in U from 280 mev to 80 mev. We find that the decrease in U is linear with the quantity M^c_{rem} where M^c_{rem} indicates the quantity of flux trapped during field cooling

Similarly, experiments were conducted to observe how the sweep rate effect changed under the conditions of crossed flux. The underlying idea was that the lowered activation barriers apparent from the results of the previous section would imply that flux line can move with more ease in crossed flux condition. (Lowered activation potential barriers.) This should manifest itself as a change in the exponent n of the dissipation law

$$E = a J^n ,$$

and consequently in the values of the sweep rate constant C obtained from

$$(\partial \ln M)/\partial \ln \dot{H}) = C = 1/n.$$

This is expected because smaller values of n indicate flux flow with lowered activation barriers. The experiments confirmed this trend. There was a pronounced decrease in the values of n obtained in the crossed configuration.(Fig.13).

Thus the measurements of the dynamical features confirm the findings of the static measurements that crossed flux configuration leads to a lowering of the activation barriers.

Conclusions:

The studies conducted in this project provided us with a deeper understanding of the effects of the highly anisotropic, layered structure of the high T_c compounds. We have been able to explain the differences that we observe in the reversible and irreversible components of magnetization, as a function of the orientation, in terms of the differences of self energy and pinning energies of the vortices respectively. We were also able to explain the shapes of the M(H) loops and variations of the critical currents on the basis of the critical state model. We also found that the behavior of the dynamics could be studied in the conventional magnetic relaxation and swept field experiments and the pinning potentials for various orientations and fields determined. Our crossed field studies on these compounds showed that the effect of a crossed field is to lower the barriers to activation of vortex motion and thereby increase dissipation. This latter behavior was reported for the first time and was related by us to the differences in the vortex coherence between low and high temperatures.

References:

1. *Magnetization and Hysteresis of Melt textured Y1Ba2Cu3O7-x in a crossed Flux Configuration.* S.K.Hasanain, SadiaManzoor,A.Amirabadizadeh,Supercond.Sci. and Technol. 8 (1995) 519-524

2. *Anisotropy of Magnetization and Flux Pinning at 77K in Melt Textured YBCO.* S.K.Hasanain, G.H. Khosa, A. Kayani, Supercond. Sci. and Technol. 8 (1995) 534-539.

3. Peak *Shifts in Magnetization Rotation - Effects of Anisotropy and Pinning.* S.K.Hasanain, Sadia Manzoor and M. Aftab, Physica C 272 (1996) 43.

4. *Field Sweep Rate Dependence of dc and ac Magnetization: Comparison with Flux Creep and Dynamic Magnetization Models.* S.K.Hasanain, A. Mumtaz, upercond. Sci. Technol. 7, 944-948 (1994).

5. A.K.Delin, T.P.Orlando, E.J.Jr. McNiff, S.Foner, R.B.Van Dover, L.F.Schn - eemayer and J.V.Waszczak, Phys.Rev. B 46 (1992) 11092

6. A.Curevich, H.Kupfer, Phys.Rev. B 48 (1993) 6477

7. A.D.Caplin, L.F.Cohen, G.K.Perkins, and A.A.Zhukov Semicond. Sci. Technol. 7 (1994) 412

8. *Effects of Crossed Flux on Magnetic Relaxation and Magnetization Dynamics in Y1Ba2Cu3O7-X.*: S. Manzoor , S.K.Hasanain , J. Phys. Condens. Matter, 8, (1996) 8339.

Publications of Principal Investigator based on this project:

1. Effects of Crossed Flux on Magnetic Relaxation and Magnetization Dynamics in Y1Ba2Cu3O7-X. Co-author: S. Manzoor , J. Phys. Condens. Matter, 8, (1996) 8339.

2. Field Sweep Rate Dependence of dc and ac Magnetization: Comparison with Flux Creep and Dynamic Magnetization Models. Co-author A. Mumtaz, Supercond. Sci. Technol. 7, 944-948 (1994).

3. Anisotropy of Magnetization and Flux Pinning at 77K in Melt Textured YBCO. Co-authors: G.H. Khosa, A. Kayani, Supercond. Sci. and Technol. 8 (1995) 534-539.

4. Magnetization and Hysteresis of Melt textured Y1Ba2Cu3O7-x in a crossed Flux Configuration. Co-authors: Sadia Manzoor, A. Amirabadizadeh, Supercond. Sci. and Technol. 8 (1995) 519-524

5. Peak Shifts in Magnetization Rotation - Effects of Anisotropy and Pinning. Co-authors: Sadia Manzoor and M. Aftab, Physica C 272 (1996) 43.

6. Effects of Crossed Flux on Magnetization and Dynamics in Melt-Textured YBCO. Co-author: S. Manzoor, Proceedings of the 8th International Workshop on Critical Currents in Superconductors, Kitakyushu, Japan 1996 (Publishers: World Scientifi

7. Modified Flux Flow in Polycrystalline YBCO: Temperature and Current Dependence Coauthor: M.M. Asim - Supercond. Sci. and Technol. 9 (1996) 461.

Theses produced during the period 1994-1997 :

Ph.D. Theses:

1. ***Magnetic Relaxation and Dynamic studies in high T_c superconductors.*** **1995, Arif Mumtaz. (Research Fellow on this P.S.F project.)**
2. ***Effects of flux motion on the electrical conductivity in granular high T_c superconductors. 1996,*** **Mohammed Muneeb Asim.**

M.Phil. Theses

1. ***Fabrication and Characterization of Melt Grown High T_c Superconductors.*** **A. Kayani, 1994.**
2. ***Analysis of harmonic response in high T_c materials.*** **A. Noman, 1994.**
3. ***Application of critical state model to high T_c superconductors.*** **Majeed Anwar, 1994.**
4. ***AC susceptibility studies in high T_c superconductors.*** **Javed ahmed, 1994.**
5. ***Field dependent broadening of superconducting transitions.*** **Zehra Abbas, 1995.**
6. ***Investigations on anisotropy of magnetization in high T_c superconductors.*** **A.Amirabadizadeh, 1995.**
7. ***Design and calibration of ac susceptibility bridge.*** **Mubarik Ahmed Minhas, 1996.**
8. ***Rotational vortex flux characteristics in melt textured 123 samples.*** **Muhammad Aftab, 1996.**
9. ***Irreversibility line determination in high T_c superconductors*** **Mohammad Asif, 1995.**
10. ***Field sweep rate dependence of ac response in high T_c*** **superconductors S.A.Satti, 1997.**
11. ***Superconducting characteristics of some bismuth based high T_c materials.*** **M. Jehangir, 1997.**

List of scientists participating in the project:

1. Dr.S.K.Hasanain,

   Principal Investigator. (30% of total time spent on the project).

2. Arif Mumtaz ,

   Research Associate with this Project. (100 % of total time time spent on Research project.)

3. All the students whose M.Phil and PhD theses have been listed ,particapated in various ways in the project, in particular Mr.Muneeb Asim, Ms.Sadia Manzoor and Ms.Shaista Shahzada.

M(H) loop of MT5, parallel and perpendicular to c-axis.

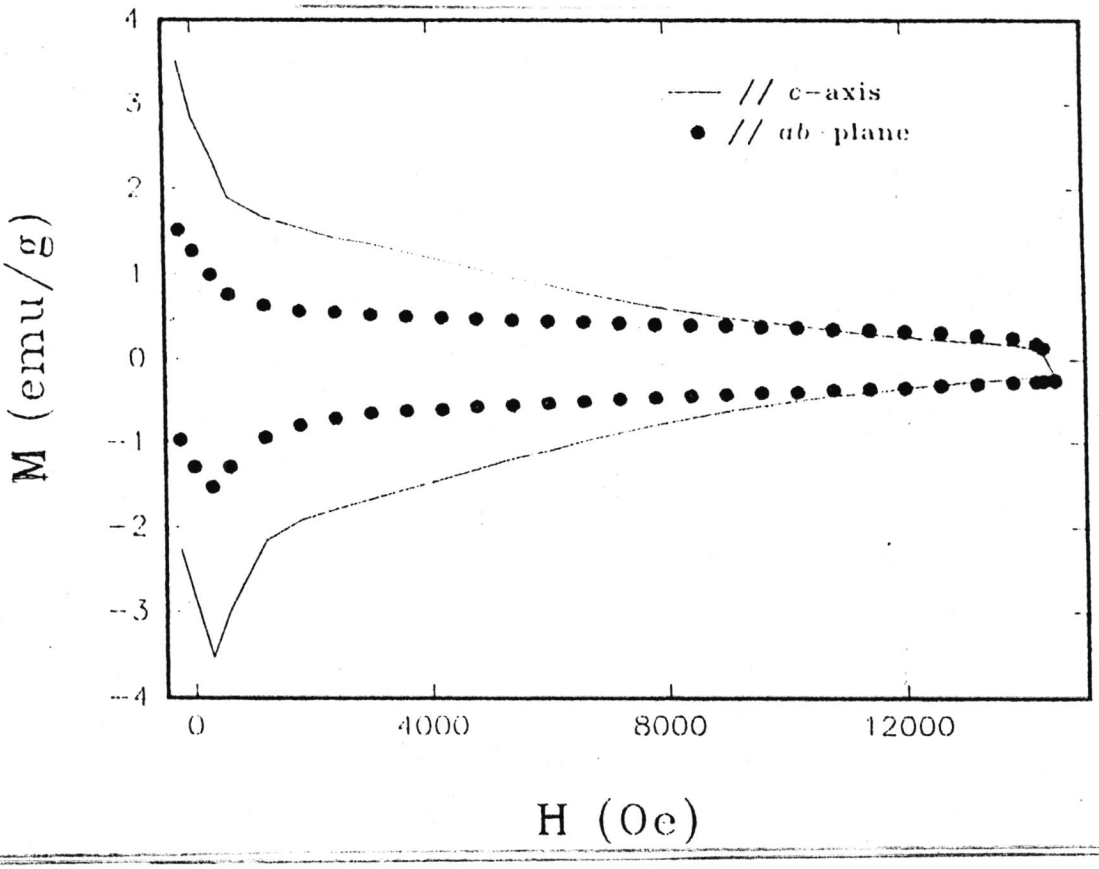

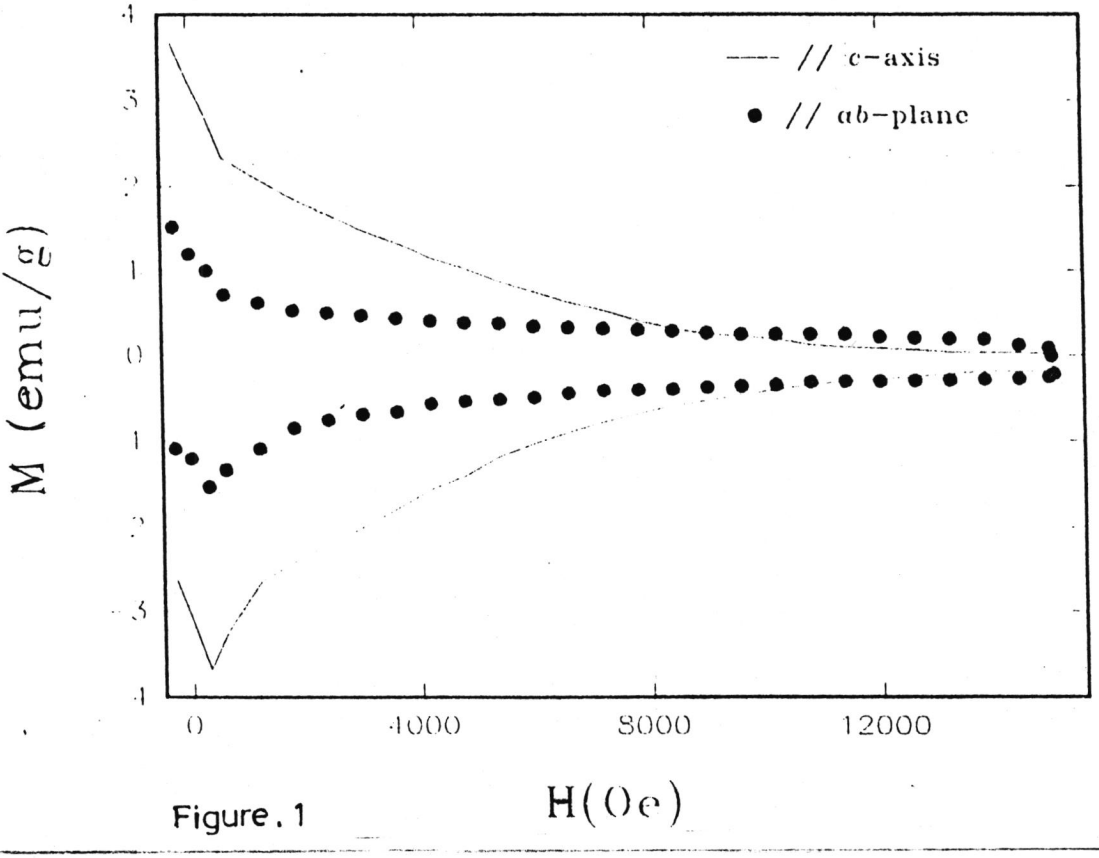

Figure. 1

M(H) loop of MT12, parallel and perpendicular to c-axis.

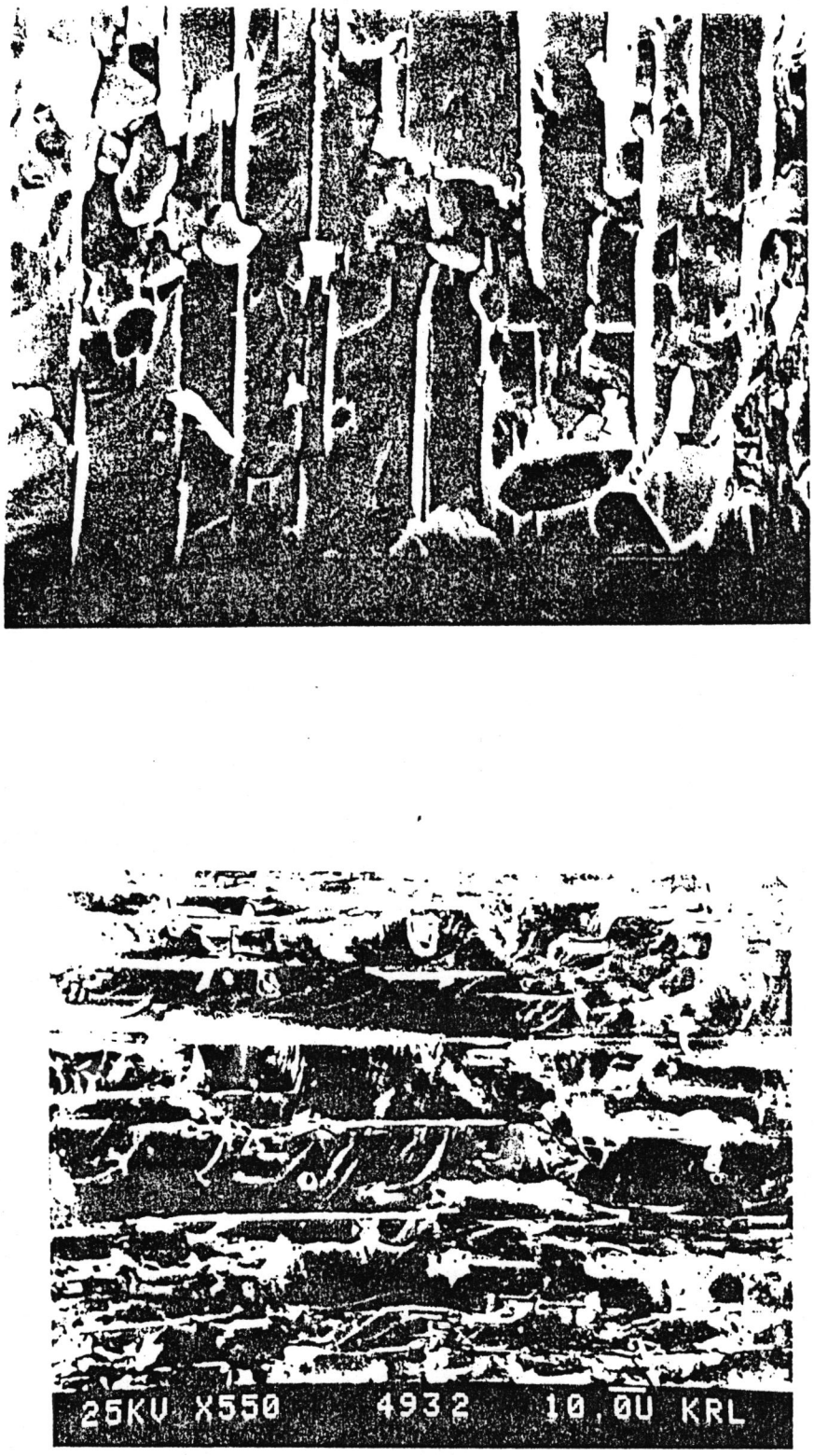

Fig. 2. Electrons micrographs of melt texture grown samples.

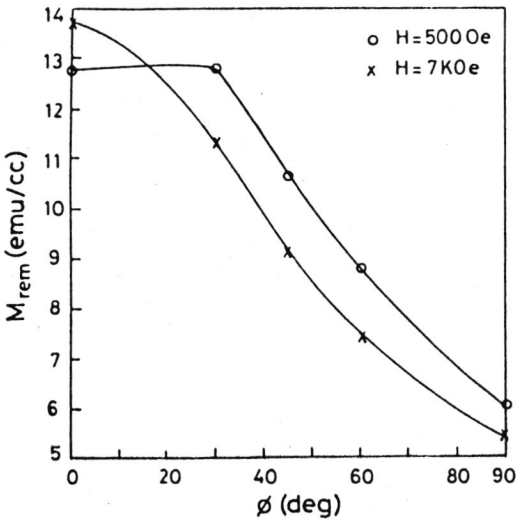

Figure 3a The variation of remanent magnetization with cooling angle ϕ for the different indicated fields. The solid line serves as a guide to the eye.

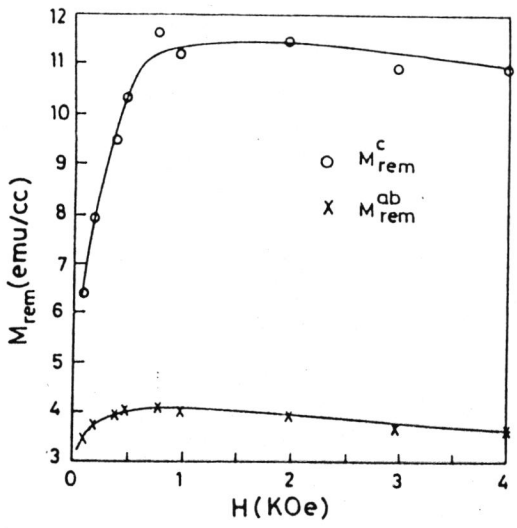

Figure 3b Dependence of remanent magnetization on the cooling field for $H \parallel c$ and $H \perp c$ of the YBCO sample at 77 K. The solid line serves as a guide to the eye.

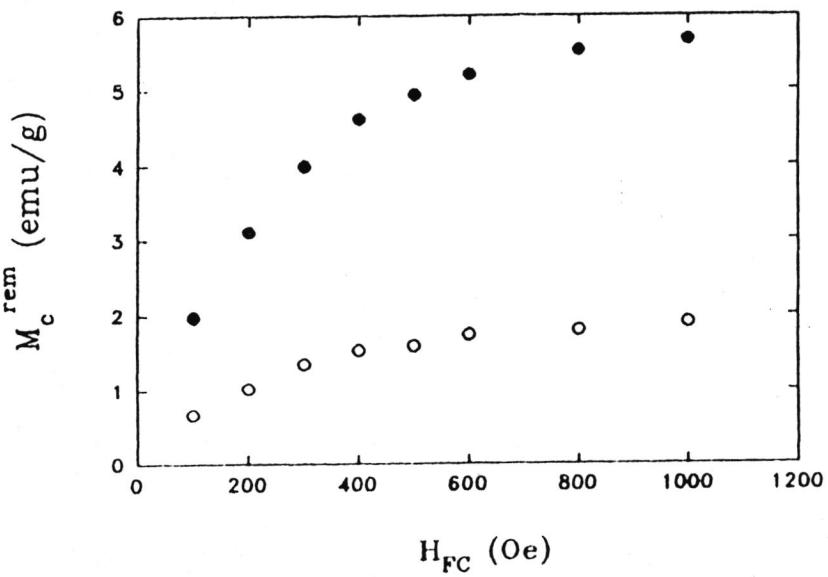

Figure 4 Remnant moment M_c^{rem} along the c axis (●) and the remnant moment M_{ab}^{rem} along the a–b planes (○) against cooling field H_{FC}.

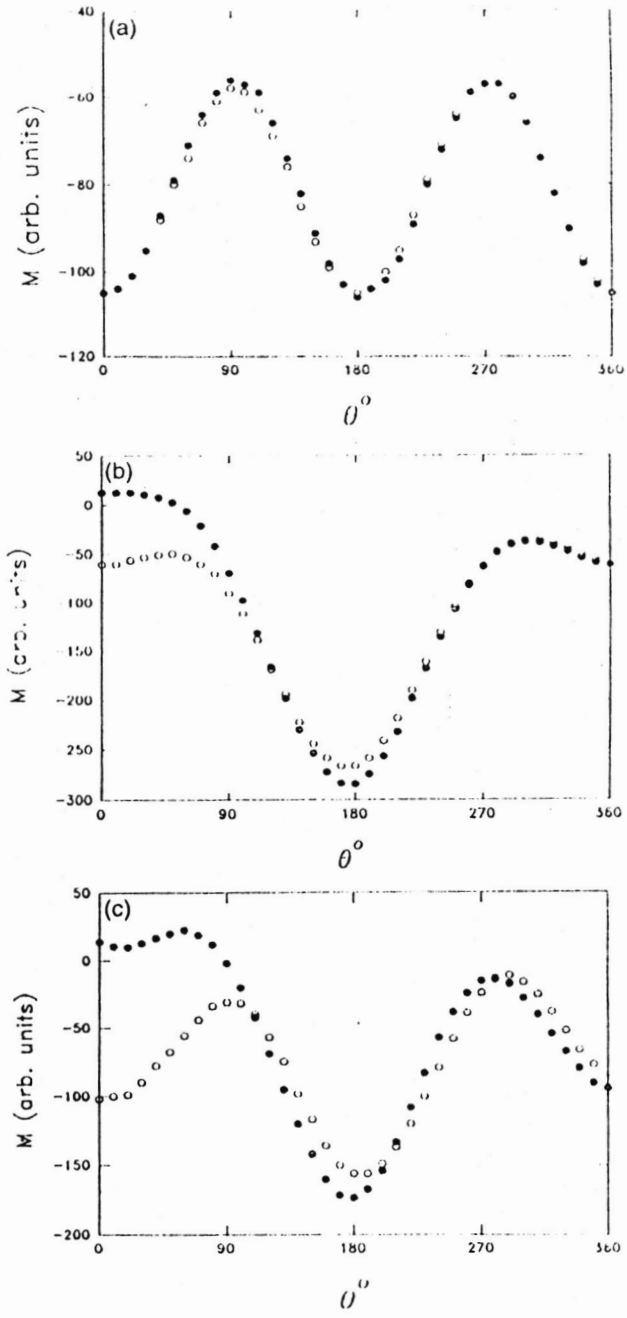

Fig. 5. Variation of the field cooled magnetization M with angle for applied field parallel to the c-axis H_{app} = (a) 23 Oe, (b) 100 Oe (c) 200 Oe. Data is shown for increasing angles (●) and upon reversal of rotation (○).

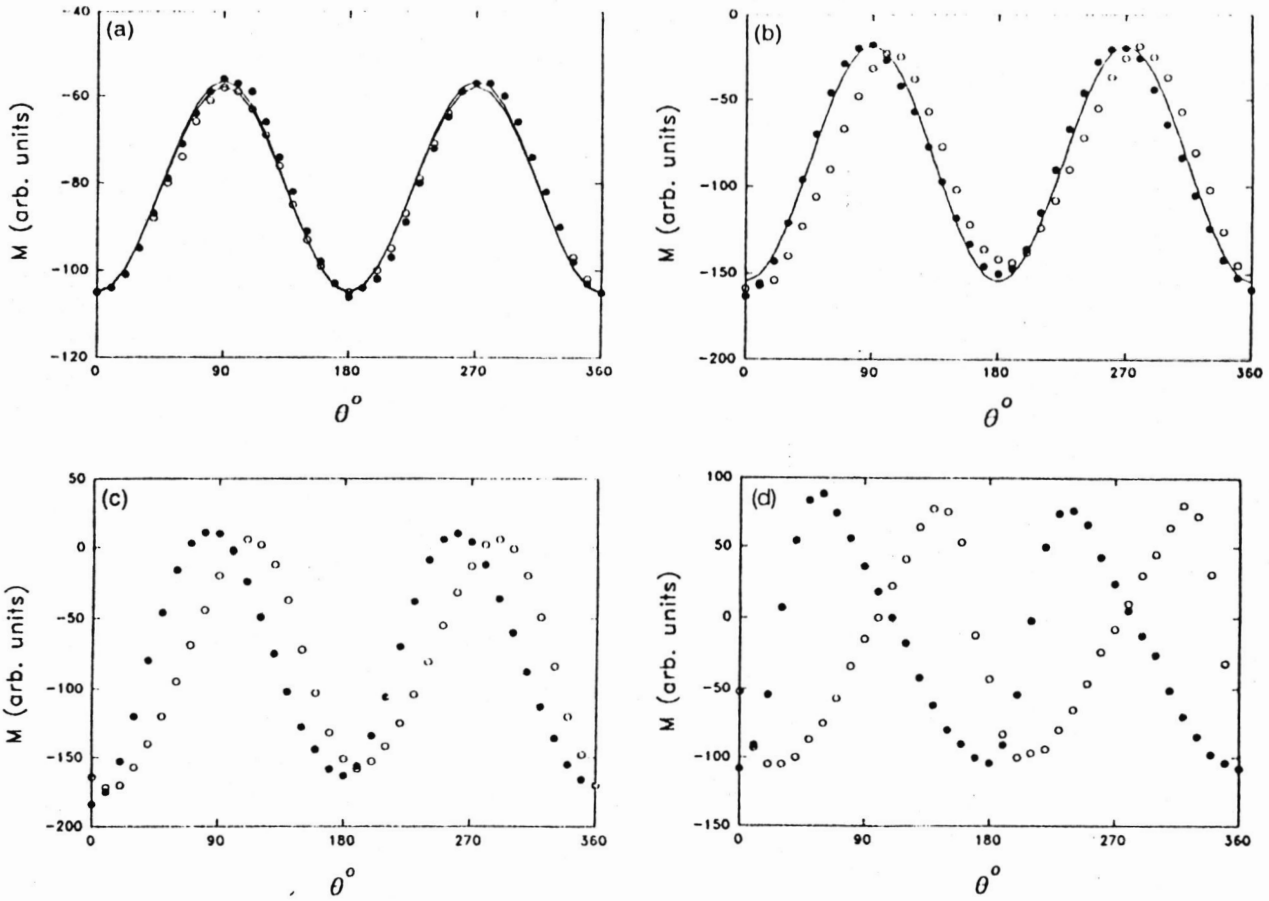

Fig. 6. Zero field cooled magnetization as a function of angle for H_{app} parallel to the c-axis equal to (a) 23 Oe, (b) 300 Oe, (c) 500 Oe, and (d) 3 kOe. Filled circles (●) denote the data for increasing angles, and hollow circles (○) are for the data taken on reversal of rotation. Solid lines are fits to $M = -(M_A \cos^2\theta + M_B \sin^2\theta)$. In (a) the data could be fit to this equation for both increasing and decreasing angles. In (b) however, a good fit is obtained only for increasing angles.

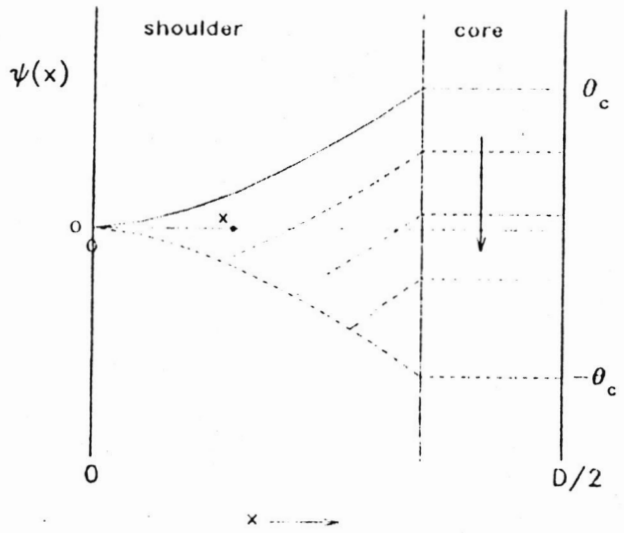

Fig. 7. Flux orientation profiles $\psi(x)$ in the generalized critical state model for increasing angles (—), and upon reversal of rotation (- - - - -).

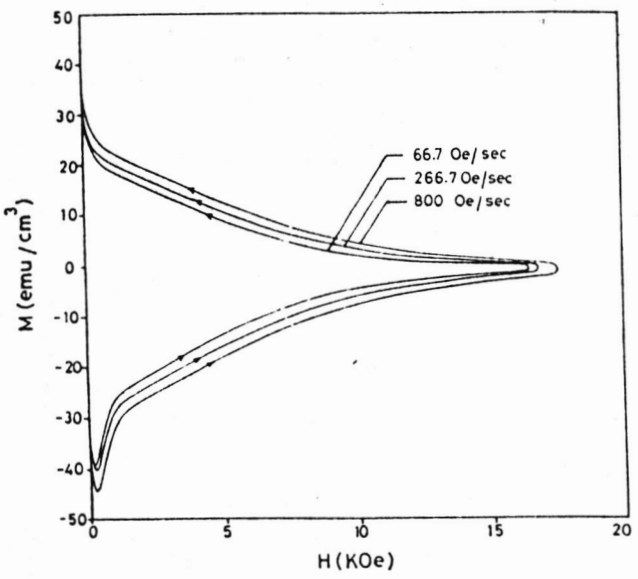

Figure 8. Representative $M(H)$ loops for one of the Y(123) samples, (for $H \parallel c$ orientation) at various sweep rates. Arrows indicate direction of sweep of field. Progressive broadening of the loops with increasing sweep rate is evident.

Field sweep rate dependence of DC and AC magnetization

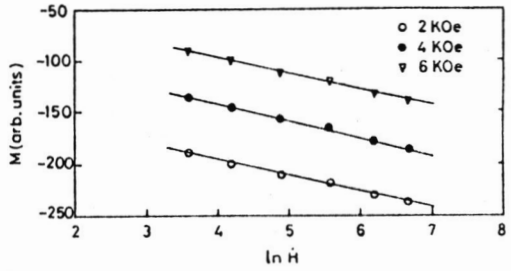

Figure 9. The magnetization values as in figure 1 at three different fields, as a function of $\ln(\dot{H})$, indicating linear dependence $M \propto \ln(\dot{H})$. Straight lines are guides to the eye.

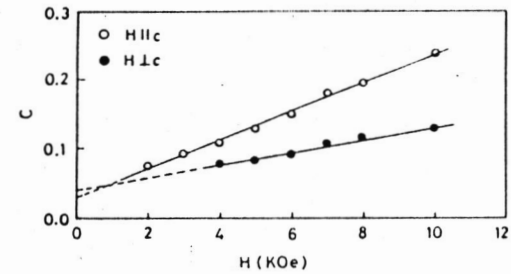

Figure 10. The normalized slope $C = (1/m_0)(dm/d \ln \dot{H})$ of the data as a function of field. Data for both $H \parallel c$ and $H \perp c$ orientations are given. Note the larger values for $H \parallel c$. The broken line represents extrapolated values of C for $H \simeq 0$.

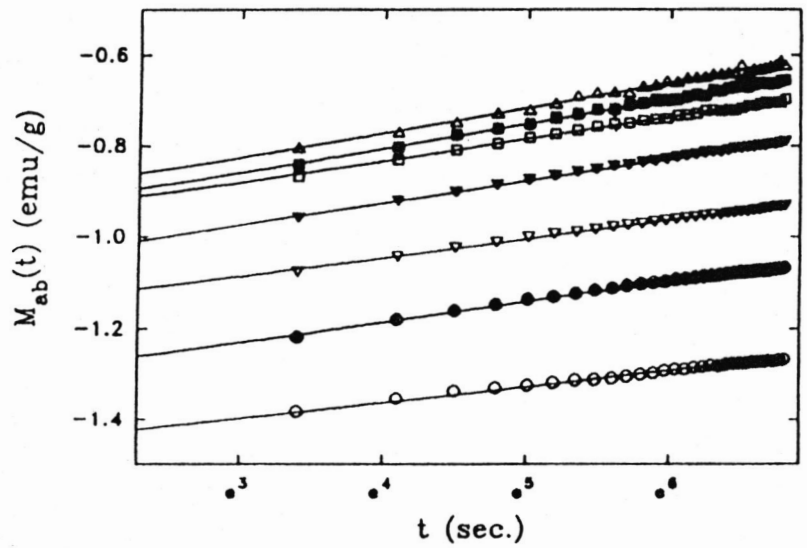

Figure 11. Magnetization relaxation data taken after a field ramp to $H_{ab} = 600$ Oe for the SFC (○), as well as for the CFC with $H_{FC} = 100$ Oe (●), $H_{FC} = 200$ Oe (▽), $H_{FC} = 400$ Oe (▼), $H_{FC} = 600$ Oe (□), $H_{FC} = 800$ Oe (■) and $H_{FC} = 1000$ Oe (△). The straight lines are fits to equation (1).

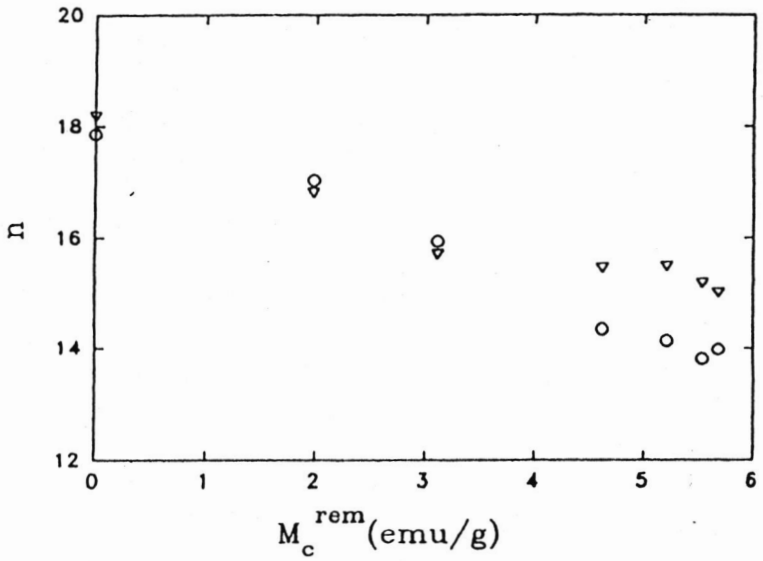

Figure 13 Variation in the exponent n obtained from figure 8 as a function of the c-axis remanence for two different values of the a–b-plane field: ○, $H_{ab} = 600$ Oe; ▽, $H_{ab} = 1000$ Oe.

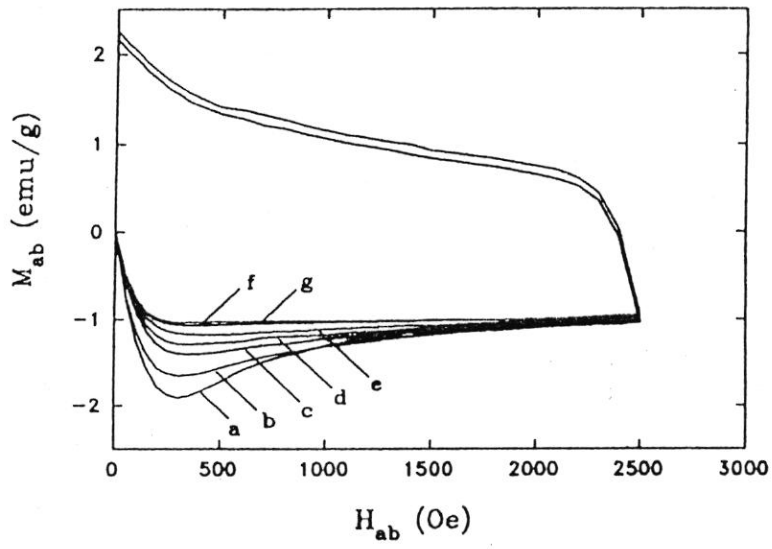

Figure 12a $M(H)$ loops of the a–b plane for the single-flux case (curve a), as well as for different cooling fields parallel to the c axis: curve b, $H_{FC} = 100$ Oe; curve c, $H_{FC} = 200$ Oe; curve d, $H_{FC} = 300$ Oe; curve e, $H_{FC} = 400$ Oe; curve f, $H_{FC} = 500$ Oe; curve g, $H_{FC} = 600$ Oe. The loop for $H_{FC} = 800$ Oe has been measured but is not shown in the figure for clarity. The outer curve for the field-decreasing branch corresponds to the single-flux loop (curve a), while the inner curve corresponds to $H_{FC} = 600$ Oe (curve g). The other curves on the field decreasing branch lie between these two but are not shown for clarity.

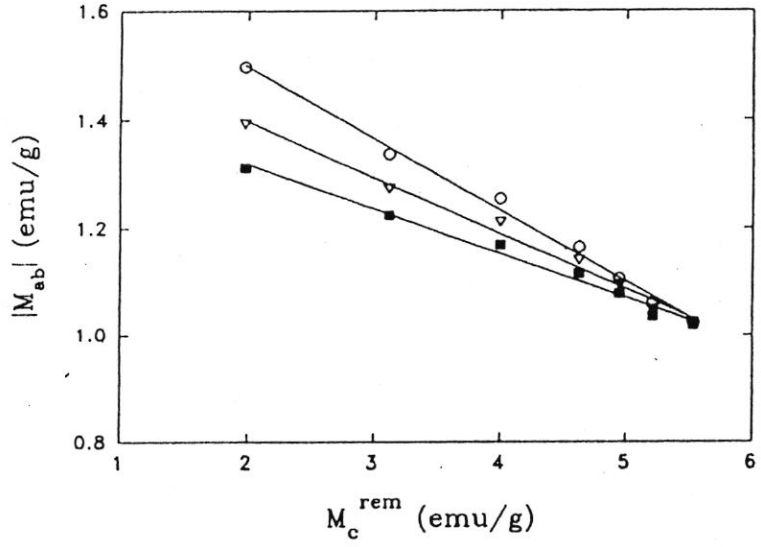

Figure 12b Magnitude of the diamagnetic response $|M_{ab}|$ of the a–b planes as a function of the remanence M_c^{rem} along the c axis. $|M_{ab}|$ has been extracted from figure 2 at three values of the a–b-plane field: ○, $H_{ab} = 600$ Oe; ▽, $H_{ab} = 800$ Oe; ■, $H_{ab} = 1000$ Oe. The straight lines serve as a guide to the eye.

Supercond. Sci. Technol. 8 (1995) 519–524. Printed in the UK

Magnetization and hysteresis of melt-textured $YBa_2Cu_3O_{7-x}$ in a crossed flux configuration

S K Hasanain, Sadia Manzoor and A Amirabadizadeh†

Department of Physics, Quaid-i-Azam University, Islamabad, Pakistan

Received 16 March 1995, in final form 27 April 1995

Abstract. We report on the measurement of magnetization in melt-textured $YBa_2Cu_3O_{7-x}$ samples, in the presence of a crossed remnant flux along the *c* axis. The *ab* plane magnetization curves become progressively flatter as the magnitude of the remanence increases. The remanence along the *c* axis decreases as the field in the *ab* plane increases, and with decreasing remanence the crossed flux magnetization curves merge with the uncrossed one. The *c* axis remanence is observed to help in both the entry and exit of the *ab* plane flux by effectively reducing the pinning barriers. The decrease of the remanence and flux pinning along the *ab* plane are discussed in terms of rotation and expulsion of flux, and the possibility of flux cutting.

1. Introduction

The use of the critical state model in analysing and explaining irreversible magnetization and critical currents in superconductors is a well established procedure [1–3]. Most such work has however been in the context of unidirectional applied fields where the development of a magnetization and critical currents in response to a flux density gradient are determined. Of much interest and considerably more complexity is the matter of the distribution and mutual interactions amongst non-collinear families of vortices [4–8]. Such studies were initiated in the context of rotational viscosity and flux cutting [7,9] in the low-T_c superconductors. In [10] and [11] it has been shown that the behaviour of remnant flux rotated against an external field could be explained in terms of a generalized critical state model [7] with a gradient of the flux orientation angle $\psi(x)$. While there is a large body of data on magnetization rotation experiments [12, 13] in high-T_c materials, this has been in the context of anisotropy of magnetization, and has generally not addressed the questions regarding interactions or effects of non-collinear flux densities. Contrasting views have been expressed in the literature, regarding the possibilities of flux line cutting in the high-T_c materials in the above situations. In some cases it has been argued [14, 15] that the barriers to flux line cutting are too high to make the process energetically feasible. Others however have observed [5, 6] that the possibility of curvature and twisting of flux lines strongly reduces these barriers. LeBlanc *et al* [16] have shown that flux cutting processes occur at least in the intergrain region of high-T_c superconductors, when helical flux is made to transverse axial flux. The effect of simultaneously present crossed flux densities in high-T_c materials obviously contains an additional parameter, viz. the effects of anisotropy, e.g. the remanence and pinning along the *c* axis are much larger than for the *ab* planes [17, 18]. Park *et al* [19, 20] have shown that the presence of *c* axis remnant flux helps to stabilize flux pinning along the *ab* planes. This was manifested in the increased width of the *ab* plane hysteresis loops when a remanence was present along the *c* axis.

It is the purpose of this study to observe the effects of crossed remnant flux on the magnetization and hysteresis in a transverse direction using bulk-textured high-T_c material. The study is carried out at $T = 77$ K, a temperature much higher than that in [19] and [20]. Thus we may expect drastic differences in the behaviour of crossed flux, due to the weakening of flux pinning and smaller elastic moduli of the vortex lattice at elevated temperatures [6, 21]. Using a two-coil arrangement we monitor the changes in both the longitudinal ($M \parallel H$) and transverse ($M \perp H$) components as the field is varied, and compare the hysteresis loop widths in the crossed and uncrossed conditions.

2. Experiment

The experiments were performed on a family of melt-texture-grown $YBa_2Cu_3O_{7-x}$ samples. The samples were prepared by the standard method [22] of very slow cooling ($\leq 2\,^{\circ}C\,h^{-1}$) through the peritectic temperature, after partial melting at 1100 °C, for about 30–40 min. After oxygen

† Present address: Department of Physics, Birjand University, Birjand, Iran.

0953-2048/95/070519+06$19.50

annealing at 600 °C for 48 h, the samples were cut out in suitable sizes, typically $1 \times 4 \times 4$ mm^3. The texturing was checked by electron microscopy and large clear grain growth was visible. The best samples were selected on the basis of electron microscopy and magnetization anisotropy tests. The samples had a zero-resistance temperature close to 89 K, and a sharp diamagnetic transition between 90 and 88 K. All d.c. magnetization measurements were made at $T = 77$ K using a commercial vibrating sample magnetometer (VSM). While the longitudinal moment (M_y) was measured with the commercially obtained set of pickup coils, the transverse moment (M_y) was measured with a self-wound set of coils, designed according to [23]. Details are given elsewhere [24]. Each component was measured using a separate lock-in amplifier. The sample vibration was along the z direction, while the field was applied along the x direction. By rotating the sample about the z axis, the c or ab directions can be made parallel to the applied field. The rotational head of the VSM allowed a 1° resolution of orientation.

In our experimental set-up the crossed flux configuration was obtained using only one magnetic field always applied along the x direction. Initially, the sample was field cooled at a particular angle ϕ with respect to the c axis. The field was then turned off and the sample and remnant moment were rotated by $\pi/2$ so that the y coil now read the remnant moment. The field (along x) was turned on again, but now at $\pi/2$ to the initial crystallographic direction, e.g. if field cooling was along the c axis ($\phi = 0$), the field was finally applied along the ab plane. The subsequent variations of M_x and M_y are then recorded simultaneously. In this way the remnant and longitudinal flux densities act as two crossed flux families, one along the c axis and the other in the ab plane. The magnitude of the initial remanence could be varied by changing the magnitude of the cooling field H_{FC}.

The following discussion is divided into three parts. The first, 2.1, describes the basic anisotropy effects which characterize the sample, the second, 2.2, discusses the effects of crossed remnant flux on the hysteresis of the longitudinal flux while the third, 2.3, describes the magnetization curves obtained in the crossed flux condition.

2.1. Anisotropy determination: uncrossed flux

A series of important background tests was conducted to enable the characterization of the sample, and the extent of generation of transverse moments in the samples in the absence of a crossed flux. As regards the former of these tests, we have made systematic studies of field-cooled, zero-field-cooled and remnant moments and their angular dependence, which are reported elsewhere [25]. For the present discussion the data which are relevant are the variation of the remnant moment with cooling field H_{FC}, for H both parallel and perpendicular to the c axis, and these are shown in figure 1. As reported by other authors [18], the remanence along both axes initially increases and then attains saturation at a field characteristics of the orientation. It is obvious that the c axis remanence saturates to a much higher value and at a significantly higher field.

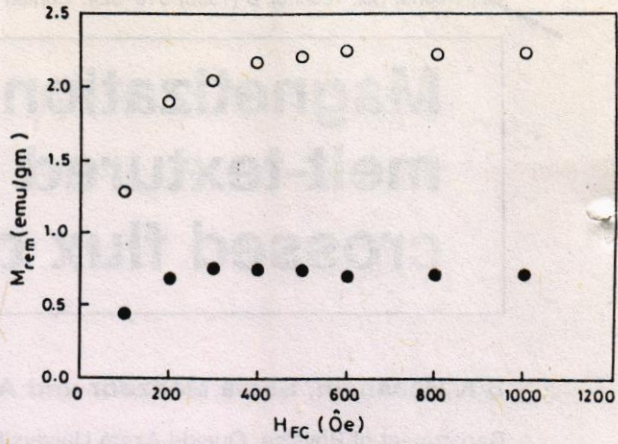

Figure 1. Remanent moment M^{rem} against cooling field H_{FC}, for the field along the c axis (o; M_c^{rem}) or along the a planes (●; M_{ab}^{rem}).

We obtain values for $(M_c^{rem})_s/(M_{ab}^{rem})_s \cong 3$ for most of th samples studied. Here $(M_c^{rem})_s$ represents the value of the axis remanence at saturation, while $(M_{ab}^{rem})_s$ represents th saturation value of the ab plane remanence. This clearl indicates stronger pinning for the $H \parallel c$ case. Also, th field required for saturating the remanence along the c axi is $H_{FC} \cong 500$ Oe, while for H_{ab} we obtain saturation a about 200 Oe. The remnant moment when rotated (again zero external field) shows no depinning and generates $M(\theta$ oscillations of fixed amplitudes as expected for a fixe moment whose projection on the pickup coils varies a $M \cos\theta$. By varying the angle ϕ (between H_{FC} and th c axis) and studying $M_{rem}(\theta, \phi)$ [25], we determined quit clearly that the remanence is strictly along the c axis fo $\phi = 0$ and normal to it for $\phi = \pi/2$, but at intermediat angles it is neither strictly along the field nor along the axis.

Finally, in this context, we note that we carefull checked for the presence of any transverse moments whe a field is applied along either the ab plane or the c axi This has to be ascertained so that the crossed flux studie can be analysed unambiguously; otherwise, variation of th remanence along a transverse direction could be attribute [26] to a simple generation of transverse moments by th field along x. The effects of transverse moment generatic were found to lie within 10% of the longitudinal mome and less than 2% of the remnant moment, at most. The were carefully corrected for in the $M(H)$ loop analysis the crossed flux configuration.

2.2. Hysteresis effects in crossed flux configuration

In these measurements we determined the effect of t remnant flux on the shielding currents and hysteresis in t direction transverse to the remanence itself. As discussed the beginning, the idea is to ascertain whether the remna flux helps stabilize or decreases the transverse pinning. T remnant flux (along c or ab) is rotated to the y directio The field along x is raised to a certain value H and $M_x($ is noted. Then the field is reduced to zero, and the value the remanence along x, $M_x(0)$, is noted. According to t critical state model, the change $\Delta M_x = M_x(0) - M_x(H$ is a measure of the shielding, and is related to the char

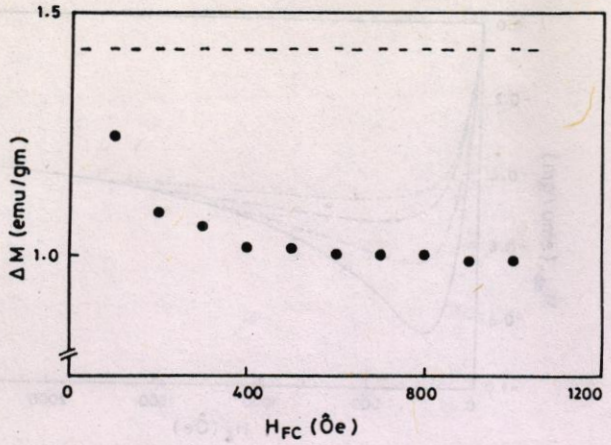

Figure 2. ΔM against H_{FC}. ΔM is the change in M_{ab} as $H_x = 200$ Oe is turned off (see the text for details). The crossed flux is along the c axis. Note the higher value of ΔM for the single-flux case indicated by the dashed line.

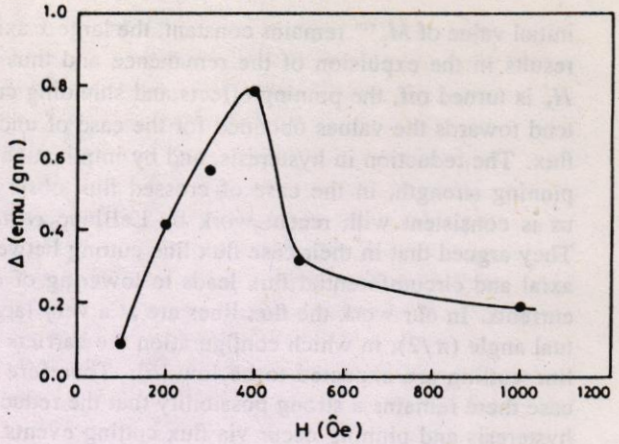

Figure 3. The variation of Δ with H (see the text for details). Δ represents the difference of ΔM (as defined in figure 2) between crossed and uncrossed flux data for various cooling fields (H_{FC}) and initial values of H_x. (Note $H = H_{FC} = (H_i)_x$, for all points.) The solid line serves as a guide to the eye.

in the flux density ΔB_x. The larger ΔM is, the smaller ΔB is and the greater the shielding currents preventing a change in B on field suppression. This can be seen easily from the following equation for the flux change on field going to zero:

$$\Delta B_x = 4\pi\,\Delta M_x + \Delta H_x \qquad (1)$$

where $\Delta M_x = M_{xf} - M_{xi}$ and ΔB_x and ΔH_x are defined similarly. Here the subscripts f and i denote the final and initial values respectively. Since $H_f = 0$, $\Delta M_x > 0$ and $\Delta B_x < 0$ in this part of the cycle, it follows that

$$4\pi|\Delta M_x| = (H_i)_x - |\Delta B_x|. \qquad (2)$$

A larger ΔM_x, according to (2), obviously implies a smaller $|\Delta B_x|$ and a greater degree of pinning of the remanence. Hence a comparison of ΔM_x values for a fixed value of H_i, but different values of H_{FC} (i.e. different transverse remanences) would depict the effect of the initial remnant flux (e.g. along c) on the longitudinal moments (e.g. along ab) and their shielding current.

In figure 2 we show the data for the case where $\phi = 0$, i.e. the remanence is established along the c axis, and its effect on the ab plane ΔM_x (defined above) is studied as a function of H_{FC}. The value of the initial field applied along the ab planes, $(H_i)_x$ in (2), is fixed at 200 Oe. Also shown in the figure is the comparable value for the ab plane ΔM_x for the case of no crossed remanence (i.e. the single-flux case) denoted by ΔM_{SF}.

It is apparent that in the crossed flux mode ΔM_x is smaller, and by implication (2) $|\Delta B_x|$ is larger, than for the case of no crossed remanence, i.e. the effect of the c axis crossed flux is to reduce the remanence along the ab plane. Thus, in our case, we do not find the c axis moment stabilizing the ab plane pinning or increasing the shielding currents. It is also apparent that ΔM_x decreases up to the field $H_{FC} \cong 600$ Oe, which is just about the field where the c axis remanence is shown to saturate (see figure 1). Increasing H_{FC} beyond this value apparently makes no difference, since the magnitude of the c axis remanence remains constant. Thus it is clearly the magnitude of the c axis remanence which determines the decrease of the ab plane pinning or critical state currents. It would appear that even though these shielding currents for the two remanences must ideally flow in transverse planes, the presence of one leads to a reduction in the other.

Further insight into the interaction of these crossed fluxes and the connection with the subsequent magnetization loops is obtained by considering the data of figure 3. Here we have plotted the data for the case where both the cooling field H_{FC} and the initial field along the ab plane $(H_i)_x$ are being varied. Indeed $|H_{FC}| = |(H_i)_x| = H$. As previously, $\phi = 0$ and $H_{FC} \parallel c$.

The quantity plotted in figure 3 is the difference between the ΔM for the crossed and uncrossed flux cases, i.e.

$$\Delta \equiv \Delta M_{SF} - \Delta M_{CF}$$

where $\Delta M_{SF} = [M_x(0) - M_x(H_i)_x]$ represents magnetization changes in the uncrossed flux mode (SF), while $\Delta M_{CF} = [M_x(0) - M_x(H_i)_x]$ represents the same for the case of crossed flux (CF). The physical significance of the ΔM is the same as discussed earlier, except that $(H_i)_x$, the initial field, is no longer a constant. Hence it is the difference of the ΔM, viz. Δ, which yields the physically interesting behaviour. From figure 3 it is clear that Δ increases and goes through a maximum at about 400 Oe, and tends towards zero at higher fields. Since Δ is now the measure of the influence of the c axis remanence on ΔB_x, we may interpret the peak in Δ as that arising from two competing effects. The first is the increase in initial value of M_c^{rem} as H_{FC} is being increased (see figure 1). This tends to increase Δ up to some maximum field. At the same time, the increase in H_x tends to decrease the value of the c axis remanence. (This latter point will be displayed clearly in the following data.) Thus these two competing tendencies in M_c^{rem} lead to a field where the effect of the crossed remanence is maximal. For higher fields, while the

initial value of M_c^{rem} remains constant, the large x axis field results in the expulsion of the remanence and thus, when H_x is turned off, the pinning effects and shielding currents tend towards the values obtained for the case of uncrossed flux. The reduction in hysteresis, and by implication in the pinning strength, in the case of crossed flux observed by us is consistent with recent work by LeBlanc *et al* [16]. They argued that in their case flux line cutting between the axial and circumferential flux leads to lowering of critical currents. In our work the flux lines are at a very large mutual angle ($\pi/2$), in which configuration the barriers to flux line cutting are expected to be low [6]. Therefore in our case there remains a strong possibility that the reduction of hysteresis and pinning occur via flux cutting events.

2.3. $M(H)$ loops in the crossed flux configuration

The method for measurement of these data has already been defined. The field cooling is performed along the c axis, and the remnant moment is designated as M_c^{rem}. After turning off the field the remanence is rotated to the y direction. The remanence turns rigidly and there is no projection along the x coil. The field is now applied along the x axis, and both M_x and M_y are noted. It is reiterated that before making these tests the background effects, such as transverse moment generation by the field H_x, have been checked and minimized by very careful alignment of the sample.

The study has been conducted for four different fields, H_{FC} = 150, 300, 500 and 800 Oe. However since the results for 500 and 800 Oe are almost the same, data for only three fields are being shown. It will be noticed that these low fields lie below or up to the maximum in M_c^{rem}.

Thus with increasing H_{FC} in this range we expect to observe the effects of increasing c axis remanence on the $M(H)$ loops of the ab plane. Figure 4(a) and (b) comprises three sets of magnetization data recorded simultaneously along the x and y directions respectively for three different cooling fields. While the x axis data are, as mentioned earlier, for the ab plane moment $M_{ab}(H_x)$, the y axis data are for the variation of the c axis remanence $M_c^{rem}(H_x)$, where H_x represents the longitudinal (x axis) field being applied. Also shown in the figure are the $M_{ab}(H_x)$ data for the case of no remnant flux (single-flux case). The data are reported here for one of the samples, but very similar results have been obtained for another sample of the same composition but almost three times the remnant moment value. This is mentioned so as to point out that the behaviour being reported is quite general and is not confined to weaker-pinning samples.

Several features are immediately apparent from the $M_{ab}(H_x)$ curves in the crossed flux mode. The curves deviate systematically from the uncrossed flux data. With increasing values of H_{FC} and M_c^{rem}, the curves show a lowered value of the initial slope (see also figure 5), a smaller value of the maximum diamagnetic signal and an increasingly pronounced flatness of the $M_{ab}(H_x)$ curves beyond the diamagnetic maximum. These features clearly indicate the ease of flux entry along the ab planes in the presence of a remnant flux along the c axis. As further

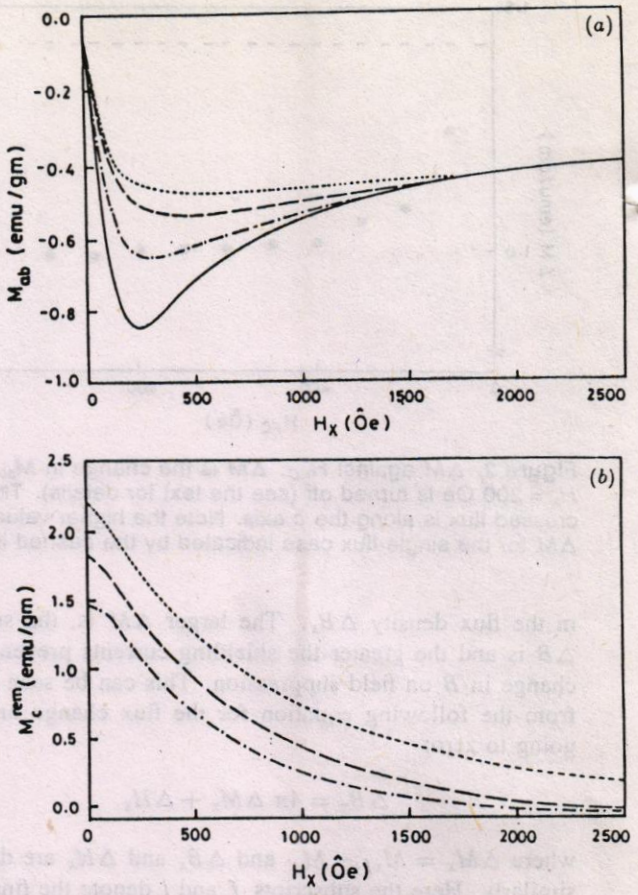

Figure 4. (a) Magnetization curves $M_{ab}(H_x)$ in uncrossed and crossed flux conditions for various cooling fields parallel to the c axis: ——, single-flux data; — · —, H_{FC} = 150 Oe; – – –, H_{FC} = 300 Oe; · · · · · ·, H_{FC} = 500 Oe. (b) The decrease in c axis remanence M_c^{rem} as H_x is increased: — · —, H_{FC} = 150 Oe; – – –, H_{FC} = 300 Oe; · · · · · ·, H_{FC} = 500 Oe (these data are taken simultaneously with those of (a)).

evidence of this phenomenon, we note that not only are the initial slopes of the $M_{ab}(H_x)$ curves in increasing H_{FC} lower, but so also is the extent of the linear portions. This can be seen in figure 5, where the low-field ($H_x \leq 350$ Oe) part of the data has been plotted on an expanded scale. We find that flux entry along the ab planes begins at lower and lower fields as M_c^{rem} is increased. Going back to figure 4(a) we observe the crossed flux curves eventually merging with the uncrossed flux (single-flux) data. This merging takes place at increasingly higher values of H_x, as H_{FC} is increased. It shifts from H_x = 1250 to 1500 and 1700 Oe as H_{FC} is increased from 150 to 300 and 500 Oe. Both the flatness of the crossed flux curves and the shift of their merging point with the single-flux data indicate that the larger amount of flux entering the ab planes in the presence of a c axis remanence causes the differences between the crossed flux and single-flux data to persist up to higher fields.

In figure 4(b), we note that the increase of H_x is also accompanied by the continual decrease of the c axis remanence. This rapid decrease which we observe is again in contrast to the low-temperature data of Park *et al* [19, 20], where the remanence decays to zero after several

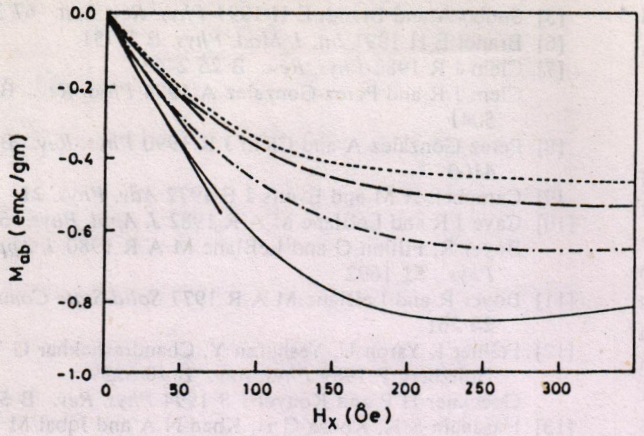

Figure 5. The low-field part of figure 4(a), M_{ab} against H_x, shown on an expanded scale: ——, single-flux data; — · —, H_{FC} = 150 Oe; – – –, H_{FC} = 300 Oe; · · · · · ·, H_{FC} = 500 Oe. Tangents indicate the decreasing extent of the linear segments of the $M(H)$ curve as H_{FC} is increased.

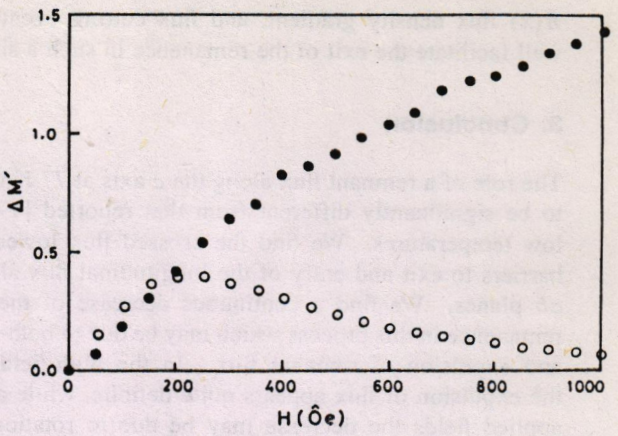

Figure 6. $\Delta M'$ against H_x for both c axis (●) and ab plane (○) data. $\Delta M'$ for the c axis indicates the change in remanence $\Delta M_c'^{rem} = |M_c^{rem}(0) - M_c^{rem}(H_x)|$, while $\Delta M_{ab}' = |M_{ab}^{SF}(H_x) - M_{ab}^{CF}(H_x)|$ gives the difference between M_{ab} for the uncrossed (SF) and crossed flux (CF) data. $\Delta M'$ is given in emu/gm.

cycles of H_x. For all three field-cooled curves it appears that the remanence remains non-zero up to a larger value than the field H_x where the crossed and uncrossed flux data merge; e.g. at H_{FC} = 150 Oe, the curves merge at 1250 Oe, while $M_c^{rem} = 0$ at $H \cong 1850$ Oe. A similar trend is seen for $H_{FC} = 300$ and 500 Oe. Thus it would appear that very small values of the transverse or crossed flux do not make any difference to the longitudinal magnetization (we note e.g. in the case of $H_{FC} = 500$ Oe that at $H_x \cong 1700$ Oe where merging occurs M_c^{rem} has decreased by only 80% of its initial value).

It could be conjectured that the decreased diamagnetism along the x direction and the decreasing positive remanence along y may indicate a rotation [10, 11] of the c axis flux towards the field direction. In the low-field region $H \leq 200$ Oe, we find on careful analysis that the difference between the crossed and uncrossed flux data, at given field H_x, is more than the corresponding change in M_c^{rem} (as H_x increases from zero to H). Thus even if all the decrease in the c axis moment were to be due to a rotation of this flux to the x direction, it could still not account for the full decrease of the moment along the x axis (i.e. the ab plane moment). Note that the x axis moment is negative; hence a rotation of the y axis moment towards the field would reduce the total M_x, i.e. make it less negative. In the higher-field region on the other hand the decrease in the c axis remanence is much more than the corresponding changes in $M_{ab}(H_x)$. This is true for all three values of the cooling field H_{FC}, and one of the representative sets of data is shown in figure 6. Shown in this figure are the changes in remanence M_c^{rem} (filled circles) as the field H_x is increased, $\Delta M_c' = |M_c^{rem}(0) - M_c^{rem}(H_x)|$ where $M_c^{rem}(0)$ is the initial value, while $M_c^{rem}(H_x)$ is the corresponding value at $H = H_x$. Similarly the open circles show the difference between values of M_{ab} in the crossed and uncrossed modes, i.e. $\Delta M_{ab}' = |M_{ab}^{SF}(H_x) - M_{ab}^{CF}(H_x)|$ (the superscripts SF and CF represent single flux and crossed flux). For the data shown here $H_{FC} = 500$ Oe, but very similar results have been obtained for $H_{FC} = 150$ and 300 Oe. In the lower-field region ($H_x < 200$ Oe) in figure 6, the differences between $\Delta M_c'$ and $\Delta M_{ab}'$ appear to be small, but we stress that these differences are outside our range of error (indicated by the size of the symbols in figure 6), and furthermore appear systematically in both the $H_{FC} = 150$ and 300 Oe data. In all these cases we find changes in M_{ab} in the lower-field region to be slightly higher than the corresponding changes in M_c^{rem}. Hence although the closeness of the $\Delta M_c'$ and $\Delta M_{ab}'$ values implies that a rotation of the c axis remanence towards the ab plane is the main phenomenon in the low-field regime, the presence of non-negligible and consistent differences between $\Delta M_c'$ and $\Delta M_{ab}'$ suggests that there may be a further ease of flux entry along the ab planes in the crossed flux mode. This latter point appears consistent with the lowered values of the shielding currents and hysteresis in the crossed flux mode, as has been discussed in the previous section.

Beyond a field of 200 Oe however, the differences between the changes in M_c^{rem} and M_{ab} become very significant and increase with increasing field. In this case there must be an expulsion of the trapped flux to account for the large changes in M_c^{rem} which are not accompanied by corresponding changes in M_{ab}. We note that there is a change in slope of the $M_c^{rem}(H_x)$ data of figure 4(b) which also suggests that there are at least two different mechanisms effective in its decrease. The above discussion leads us to speculate that in the low-field region, where the x axis field is confined close to the surface, the boundary condition [10, 11] $B(x = 0) = H_{ext}$ (the externally applied field) probably ensures rotation of flux to the field (x direction), while on deeper penetration, where the remnant flux is expected have a higher density according to the critical state models, the field causes an expulsion of the remanence. Note that in the higher-field region of figure 4 the continued decrease of M_c^{rem} is accompanied by the usual (uncrossed flux) behaviour of M_x, clearly showing the expulsion of the remanence.

It is interesting that the y axis flux on being expelled would have to traverse the crossed x axis flux against the

$B(x)$ flux density gradient, and flux cutting events could well facilitate the exit of the remanence in such a situation.

3. Conclusion

The role of a remnant flux along the c axis at 77 K is found to be significantly different from that reported [19, 20] at low temperatures. We find the crossed flux lowering the barriers to exit and entry of the longitudinal flux along the ab planes. We find a continuous decrease of the c axis remanence in this process which may be due to both rotation and expulsion of remnant flux. In the high-field region the expulsion of flux appears quite definite, while at lower applied fields the decrease may be due to rotation. It is important to note that the fields up to which we have worked ($H_x \leq 2.5$ kOe) are well above the penetration field H_{c1} of the grains, and hence the effects are intragrain effects. Since flux cutting in high-T_c materials has already been conclusively demonstrated [16] in the intergrain regions, we speculate that such events could be also effective in the intragrain region in our samples at the relatively elevated temperature of 77 K, and could play an important role in the ability of the remanence to cut through the longitudinal flux.

Acknowledgment

This work was supported by the Pakistan Science Foundation grant PSF/C-QU/PHYS(90).

References

[1] Bean C P 1962 *Phys. Rev. Lett.* **8** 250; 1964 *Rev. Mod. Phys.* **36** 31
[2] Fietz W A, Beasley M R, Silcox J and Webb W W 1964 *Phys. Rev.* **136** 335
[3] Kim Y B, Hempstead C F and Strnad A R 1962 *Phys. Rev. Lett.* **9** 306
[4] Brandt E H 1990 *Physica* B **165 & 166** 1129
[5] Sudbo A and Brandt E H 1991 *Phys. Rev. Lett.* **67** 3176
[6] Brandt E H 1991 *Int. J. Mod. Phys.* B **5** 751
[7] Clem J R 1982 *Phys. Rev.* B **26** 2463
Clem J R and Perez-Gonzalez A 1984 *Phys. Rev.* B **30** 5041
[8] Perez-Gonzalez A and Clem J R 1990 *Phys. Rev.* B **42** 4100
[9] Campbell A M and Evetts J E 1972 *Adv. Phys.* **21**
[10] Cave J R and LeBlanc M A R 1982 *J. Appl. Phys.* **53** 163
Boyer R, Fillion G and LeBlanc M A R 1980 *J. Appl. Phys.* **51** 1692
[11] Boyer R and LeBlanc M A R 1977 *Solid State Commun.* **24** 261
[12] Fellner I, Yaron U, Yeshuran Y, Chandrashekhar G V and Holtzberg F 1989 *Phys. Rev.* B **40** 5239
Goeckner H P and Kouvel J S 1994 *Phys. Rev.* B **50** 343
[13] Hasanain S K, Khosa G H, Khan N A and Iqbal M Z 199 *Supercond. Sci. Technol.* **6** 691
[14] Nelson D R 1988 *Phys. Rev. Lett.* **60** 1973
Nelson D R and Seung H S 1989 *Phys. Rev.* B **39** 9153
Marchetti M C and Nelson D R 1990 *Phys. Rev.* B **41** 1910
[15] Obukhov S P and Rubinstein M 1990 *Phys. Rev. Lett.* **65** 1279
Obukhov S P and Seung H S 1991 *Phys. Rev. Lett.* **66** 2279
[16] LeBlanc M A R, Celebi S, Wang S X and Plechacek V 1993 *Phys. Rev. Lett.* **71** 3367
[17] Yaron U, Fellner I and Yeshuran Y 1991 *Phys. Rev.* B **44** 12 531
[18] Song Y, Helesley C E, Misra A and Gaines J R 1993 *Phys Lett.* **173A** 489
[19] Park S J and Kouvel J S 1993 *Phys. Rev.* B **48** 13 995
[20] Park S J, Kouvel J S, Radousky H B and Lin J Z 1993 *Phys. Rev.* B **48** 13 998
[21] Ullmaier H 1975 *Irreversible Properties of Type II Superconductors* (Berlin: Springer)
[22] Salama K, Selvamanickam V, Gao L and Sun K 1989 *Appl. Phys. Lett.* **54** 2354
[23] Mallinson J 1966 *J. Appl. Phys.* **37** 2514
[24] Amirabadizadeh A 1995 *MPhil Dissertation* Quaid-i-Azam University
[25] Khosa G H, Hasanain S K and Kayani A N *Supercond. Sc. Technol.* submitted
[26] Farrel D E, Williams C M, Wolf S A, Bansal N P and Kogan V G 1988 *Phys. Rev. Lett.* **61** 2805

Supercond. Sci. Technol. 8 (1995) 534–539. Printed in the UK

Anisotropy of magnetization and flux pinning at 77 K in melt textured YBCO

G H Khosa†, S K Hasanain‡ and A N Kayani§

† Department of Physics, Government College, Jampur, Pakistan
‡ Department of Physics, Quaid-i-Azam University, Islamabad, Pakistan
§ GIK Institute of Science and Technology, Topi, NWFP, Pakistan

Received 13 January 1995, in final form 21 April 1995

Abstract. We have studied the zero-field cooled (M_{ZFC}), field cooled (M_{FC}) and remanent magnetization (M_{REM}) variations as a function of orientation and field at 77 K in melt textured $Y_1Ba_2Cu_3O_{7-x}$ superconductors. We find a lesser preference of the remanent flux for the *c*-axis, as compared with low temperatures, which is interpreted as being due to more three-dimensional behaviour of vortices. The three-dimensional behaviour is more pronounced at higher fields. Field cooled magnetization does not in general satisfy the relation $M_{FC} = M_{ZFC} + M_{REM}$, indicative of lack of rigidity and continued depinning of vortices during the (field cooled) magnetization rotation process. The differences between M_{FC} and $M_{ZFC} + M_{REM}$ are discussed as a function of field and rotation angle. Data are explained in terms of weaker pinning and decreased effects of anisotropy as compared with low temperatures. We also find evidence for intergrain flux pinning at $H = 10$ Oe in zero-field cooled magnetization.

1. Introduction

The study of magnetic anisotropy of high-T_c superconductors has received considerable attention, particularly at low temperatures ($T \ll T_c$). At such low temperatures the vortex lattice is relatively stiff and the effects of fluctuations, entropic disturbances and topological excitations (kinks etc) are minimal [1, 2]. This leads to a simplification of the analysis. Magnetization rotation experiments [3] have shed considerable light on these aspects, and the picture that emerges, at least at low temperatures, is that the pinned flux shows a marked preference for the *c*-axis. Furthermore it was shown that the net field cooled magnetization when rotated against an applied field can be adequately represented by a simple equation [4]

$$M_{FC}(\theta) = M_{ZFC}(\theta) + M_{REM}(\theta). \qquad (1)$$

Here M_{FC}, M_{ZFC} and M_{REM} refer to the field cooled, zero-field cooled and remanent moments, whereas θ is the angle of rotation of the sample with respect to the applied field. Thus the above equation essentially implies a rigid field cooled moment, whose variation with angle consists of demagnetization factor and anisotropy effects, contained in $M_{ZFC}(\theta)$ and a $\cos\theta$ type term in $M_{REM}(\theta)$. The latter arises due to the change in the projection of the fixed moment on the pickup coils. This rigidity of the field cooled moment, being due to stronger pinning, is therefore expected to be weaker at elevated temperatures [5]. This is one of the main questions investigated in this work, i.e. the extent to which the field cooled magnetization can be represented by equation (1) at higher temperatures. Secondly we expect that at a higher temperature (T close to T_c) the change in the dimensionality of the vortex lattice system [1, 6, 7] should lead to significant differences compared with the low-temperature behaviour. It is well known [7] that at low temperatures ($T \ll T_c$) the very small coherence length normal to the *ab*-plane, ξ_c, leads to an effectively two-dimensional [8] behaviour of the vortices. At higher temperatures where ξ_c becomes greater than the Cu–O plane separation the system displays the characteristics of an anisotropic three-dimensional superconductor [6, 9]. The change in dimensionality can be expected in particular to effect the marked preference of the remanent flux for the *c*-axis which has been observed at low temperatures.

Since most applications of these superconductors become more practical for higher temperatures, e.g. $T =$ 77 K, it becomes important to understand the anisotropy of their response at these temperatures. With these features in mind we have investigated the magnetic anisotropy of melt texture grown superconductors at $T = 77$ K by the magnetization rotation method, and compared our results to those obtained at lower temperatures.

2. Experimental procedure

Samples of composition $Y_1Ba_2Cu_3O_{7-x}$ were grown by the standard melt texture growth procedure [10]. These samples were cooled slowly (2 °C h^{-1}) between 1040 °C and 950 °C in a uniform temperature environment, after heating up to 1140 °C in an alumina crucible. The samples were annealed for more than 60 h to replenish lost oxygen.

0953-2048/95/070534+06$19.50

Electron microscopy results showed the platelet-like growth of grains. Uninterrupted grain growth along the ab-plane extended in some parts of the sample up to almost 1 mm. Average grain sizes were about $0.1 \times 0.1 \times 0.01$ mm^3. The sample used in the $M(\theta)$ measurements was a small piece of volume $9.1 \times 3.2 \times 3.1$ mm^3. The critical temperature determined from DC resistivity and AC susceptibility was 89 K. Magnetic measurements reported were carried out on a vibrating sample magnetometer (VSM) which enabled a rotation of the sample relative to the external field. The accuracy of the rotational head of the VSM enabled a 1° resolution of position. The experimental procedures were as follows. The sample was cooled to a low temperature (77 K) either in field cooled (FC) or zero-field cooled (ZFC) conditions. In ZFC measurements the field was applied at 77 K and the sample was rotated relative to the applied field H. The moment was measured as a function of the angle θ between the applied field H and the c-axis and at different values of H. In the FC process the sample was cooled in a fixed applied field, and subsequently M_{FC} was measured as a function of θ. In the remanent moment measurements, the sample was cooled to low temperature in a fixed applied field which was then turned off and M_{REM} was measured as a function of θ for different values of H and ϕ, the angle of the c-axis with respect to the cooling field. In these particular measurements the remanent field of the magnet was not more than ± 1 Oe in all cases.

3. Results and discussion

We have divided our results into three major parts.

(1) Zero-field cooled magnetization (M_{ZFC}) measurements.

(2) Remanent magnetization (M_{REM}) measurements.

(3) Field cooled magnetization (M_{FC}) measurements.

The angular dependence for each case will now be discussed in turn.

3.1. Angular dependence of M_{ZFC}

Low-field ZFC measurements on the sample are shown in figure 1(a) for $H = 30$ Oe. As discussed in the literature [11, 12], the oscillatory behaviour of the magnetization is evident. Since H_{c1} for this sample, as determined from the onset of deviation from linearity of the M–H loop, is at least 80 Oe for $H \parallel c$ and 35 Oe for $H \perp c$ at 77 K, the applied field ($H = 30$ Oe) is below H_{c1}. For $H < H_{c1}$ the oscillatory behaviour is understood [4] to be due to variation in the demagnetization factor N, on rotation of the sample. The solid lines in figure 1(a) and (b) are fitted to

$$M_{ZFC} = -H\left(A\cos^2\theta + B\sin^2\theta\right) \qquad (2)$$

where

$$A = \frac{1}{4\pi(1-N_c)} \text{ and } B = \frac{1}{4\pi(1-N_b)}.$$

The values of the demagnetization factors are obtained from the fit to be $N_c = 0.48$ and $N_b = 0.26$. N_c is obviously larger than N_b due to the relatively small dimensions of the grains along the c-axis. There is some deviation from the fit for $\theta = \pi/2$ and $3\pi/2$ and $\theta = \pi$ and 2π, but otherwise the fit to equation (2) is quite good. The M_{ZFC} data for very low fields, namely $H = 10$ Oe (figure 1(b)), show an interesting feature. While at a relatively high field ($H = 30$ Oe) the variation $M(\theta)$ is described accurately by the M_{ZFC} equation yielding the above quoted values of N_c and N_b, the same is not observed for the 10 Oe case. Here the behaviour indicates the presence of pinned flux. This is apparent from the deeper minimum at $\theta = \pi$, and shallower extrema at $\theta = 0$ and 2π. As discussed elsewhere [5], this is a signature of pinned flux. This appears anomalous since $H < H_{c1}$. However we feel that an interpretation consistent with other data at higher H is possible. At very low H the flux penetrating the weak links or intergrains in the sample is pinned, and gives a contribution ($M_R(\theta) \sim \cos\theta$), which added to the demagnetization factor variations of M_{ZFC} gives the net curve in figure 1(b). At the higher field, $H = 30$ Oe, the weakened pinning strength of these regions allows for no intergrain trapped flux, and a smooth oscillation is observed. At intermediate fields, $H_{c1} < H <$ 200 Oe, we again see deviations from the M_{ZFC} equation which may also be attributed to the presence of intragrain

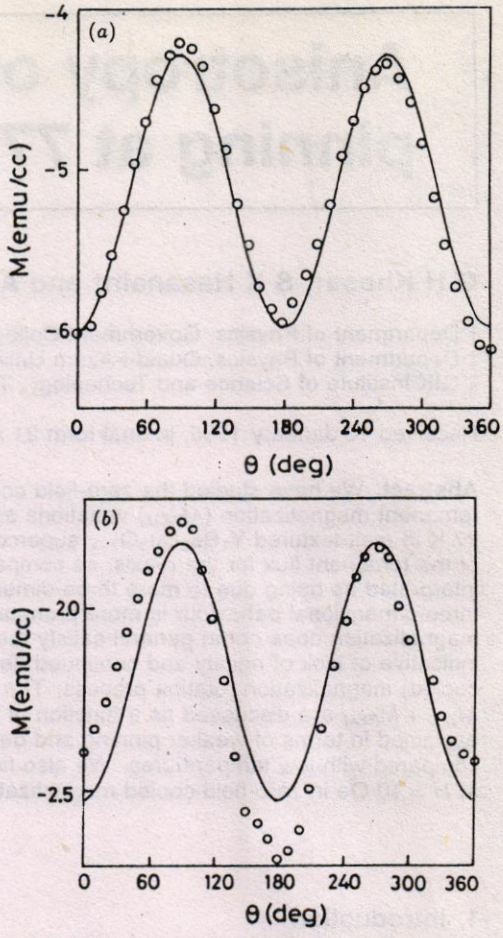

Figure 1. Angular dependence of zero-field cooled magnetization of a YBCO sample at 77 K for (a) $H = 30$ Oe (b) $H = 10$ Oe. The solid lines indicate the fit to equation (2).

Electron microscopy results showed the platelet-like growth of grains. Uninterrupted grain growth along the ab-plane extended in some parts of the sample up to almost 1 mm. Average grain sizes were about $0.1 \times 0.1 \times 0.01$ mm^3. The sample used in the $M(\theta)$ measurements was a small piece of volume $9.1 \times 3.2 \times 3.1$ mm^3. The critical temperature determined from DC resistivity and AC susceptibility was 89 K. Magnetic measurements reported were carried out on a vibrating sample magnetometer (VSM) which enabled a rotation of the sample relative to the external field. The accuracy of the rotational head of the VSM enabled a 1° resolution of position. The experimental procedures were as follows. The sample was cooled to a low temperature (77 K) either in field cooled (FC) or zero-field cooled (ZFC) conditions. In ZFC measurements the field was applied at 77 K and the sample was rotated relative to the applied field H. The moment was measured as a function of the angle θ between the applied field H and the c-axis and at different values of H. In the FC process the sample was cooled in a fixed applied field, and subsequently M_{FC} was measured as a function of θ. In the remanent moment measurements, the sample was cooled to low temperature in a fixed applied field which was then turned off and M_{REM} was measured as a function of θ for different values of H and ϕ, the angle of the c-axis with respect to the cooling field. In these particular measurements the remanent field of the magnet was not more than ± 1 Oe in all cases.

3. Results and discussion

We have divided our results into three major parts.

(1) Zero-field cooled magnetization (M_{ZFC}) measurements.

(2) Remanent magnetization (M_{REM}) measurements.

(3) Field cooled magnetization (M_{FC}) measurements.

The angular dependence for each case will now be discussed in turn.

3.1. Angular dependence of M_{ZFC}

Low-field ZFC measurements on the sample are shown in figure 1(a) for $H = 30$ Oe. As discussed in the literature [11, 12], the oscillatory behaviour of the magnetization is evident. Since H_{c1} for this sample, as determined from the onset of deviation from linearity of the M–H loop, is at least 80 Oe for $H \parallel c$ and 35 Oe for $H \perp c$ at 77 K, the applied field ($H = 30$ Oe) is below H_{c1}. For $H < H_{c1}$ the oscillatory behaviour is understood [4] to be due to variation in the demagnetization factor N, on rotation of the sample. The solid lines in figure 1(a) and (b) are fitted to

$$M_{ZFC} = -H\left(A\cos^2\theta + B\sin^2\theta\right) \qquad (2)$$

where

$$A = \frac{1}{4\pi(1-N_c)} \text{ and } B = \frac{1}{4\pi(1-N_b)}.$$

The values of the demagnetization factors are obtained from the fit to be $N_c = 0.48$ and $N_b = 0.26$. N_c is obviously larger than N_b due to the relatively small dimensions of the grains along the c-axis. There is some deviation from the fit for $\theta = \pi/2$ and $3\pi/2$ and $\theta = \pi$ and 2π, but otherwise the fit to equation (2) is quite good. The M_{ZFC} data for very low fields, namely $H = 10$ Oe (figure 1(b)), show an interesting feature. While at a relatively high field ($H = 30$ Oe) the variation $M(\theta)$ is described accurately by the M_{ZFC} equation yielding the above quoted values of N_c and N_b, the same is not observed for the 10 Oe case. Here the behaviour indicates the presence of pinned flux. This is apparent from the deeper minimum at $\theta = \pi$, and shallower extrema at $\theta = 0$ and 2π. As discussed elsewhere [5], this is a signature of pinned flux. This appears anomalous since $H < H_{c1}$. However we feel that an interpretation consistent with other data at higher H is possible. At very low H the flux penetrating the weak links or intergrains in the sample is pinned, and gives a contribution ($M_R(\theta) \sim \cos\theta$), which added to the demagnetization factor variations of M_{ZFC} gives the net curve in figure 1(b). At the higher field, $H = 30$ Oe, the weakened pinning strength of these regions allows for no intergrain trapped flux, and a smooth oscillation is observed. At intermediate fields, $H_{c1} < H <$ 200 Oe, we again see deviations from the M_{ZFC} equation, which may also be attributed to the presence of intragrain

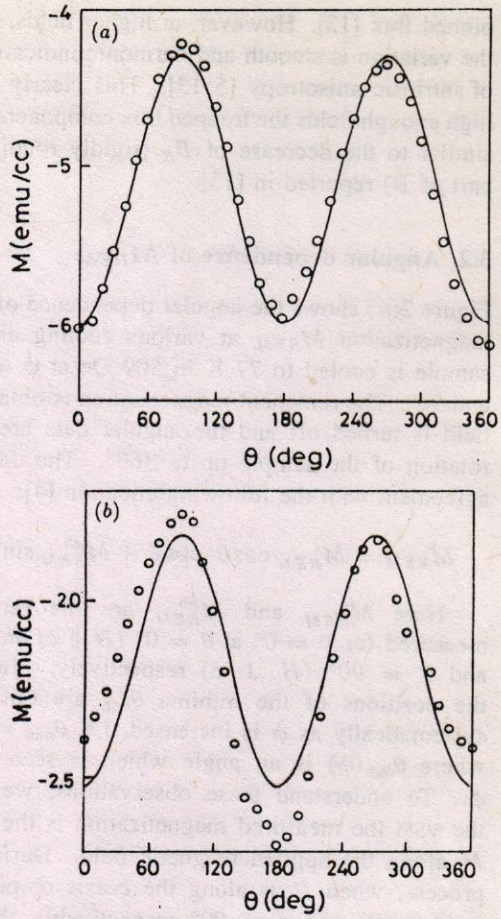

Figure 1. Angular dependence of zero-field cooled magnetization of a YBCO sample at 77 K for (a) $H = 30$ Oe (b) $H = 10$ Oe. The solid lines indicate the fit to equation (2).

pinned flux [13]. However, at higher fields, $H \geq 500$ Oe, the variation is smooth and harmonic indicating the effects of intrinsic anisotropy [5, 13]. This clearly shows that at high enough fields the trapped flux component is negligible, similar to the decrease of B_R (rigidly rotating or trapped part of B) reported in [13].

3.2. Angular dependence of M_{REM}

Figure 2(a) shows the angular dependence of the remanent magnetization M_{REM} at various cooling angles ϕ. The sample is cooled to 77 K in 500 Oe at $\phi = 0°$, 30°, 60° and 90°. The remanent magnetization is obtained when the field is turned off and the angular data are noted during rotation of the sample up to 360°. The data show good agreement with the following equation [4]:

$$M_{REM} = M^c_{REM} \cos\theta \cos\phi + M^{ab}_{REM} \sin\theta \sin\phi. \quad (3)$$

Here M^c_{REM} and M^{ab}_{REM} are the remanent values measured for $\phi = 0°$ at $\theta = 0°$ ($H \parallel c$) and for $\phi = 90°$ and $\theta = 90°$ ($H \perp c$) respectively. In these curves the positions of the minima θ_{min} are observed to shift systematically as ϕ is increased, i.e. $\theta_{min} = \pi + \theta_{min}(\phi)$, where $\theta_{min}(\phi)$ is an angle which is seen to depend on ϕ. To understand these observations, we recall that in the VSM the measured magnetization is the component of M along the applied magnetic field. During the cooling process, when H is along the c-axis or perpendicular to it ($\phi = 0°$ and $\phi = 90°$ respectively), the vortex lines are trapped and pinned parallel to the applied field. The obtained remanence is M^c_{REM} or M^{ab}_{REM}, and upon rotation we measure their components along the field direction $M^c_{REM} \cos\theta$ or $M^{ab}_{REM} \sin\theta$. If the initial orientation of the remanence depends on the initial cooling angle ϕ (between H and c), then the minima are expected to shift away from π ($\phi = 0$) towards 270° ($\phi = \pi/2$), i.e. the minimum corresponds to the angle θ when M_{REM} becomes opposite to the initial H direction. The fact that we observe a shift in the minimum with ϕ shows that the direction of flux trapping depends on the angle ϕ. In figure 2(b) we show the variation of the shift in the minimum $\theta_{min}(\phi)$ with ϕ. It is seen that this shift $\theta_{min}(\phi)$ is neither entirely linear (which would indicate the flux trapping strictly along the field direction) nor is it zero (as would be the case for flux trapping strictly along the c-axis, irrespective of ϕ). We observe that for ϕ as large as 60°, θ_{min} is only 30°, i.e. the flux is still tilted preferentially close to the c-axis. For $\phi = 90°$, the shift in the minimum is 90°, clearly indicating that the trapped flux now prefers to lie along the ab-plane. At intermediate angles ($0° < \phi < 90°$), the actual flux structure may be quite complex, for example as seen in decoration experiments [14, 15] where both vortex chains parallel to the field and a vortex lattice have been observed to coexist. The major noticeable feature of these data is that, unlike the low-temperature case, there is a shift in the position of θ_{min}, clearly indicating that the remanent flux is not entirely along the c-axis but is closer to the direction of applied field. As mentioned in the introduction, this may be expected due to the increased interplane coupling (as ξ

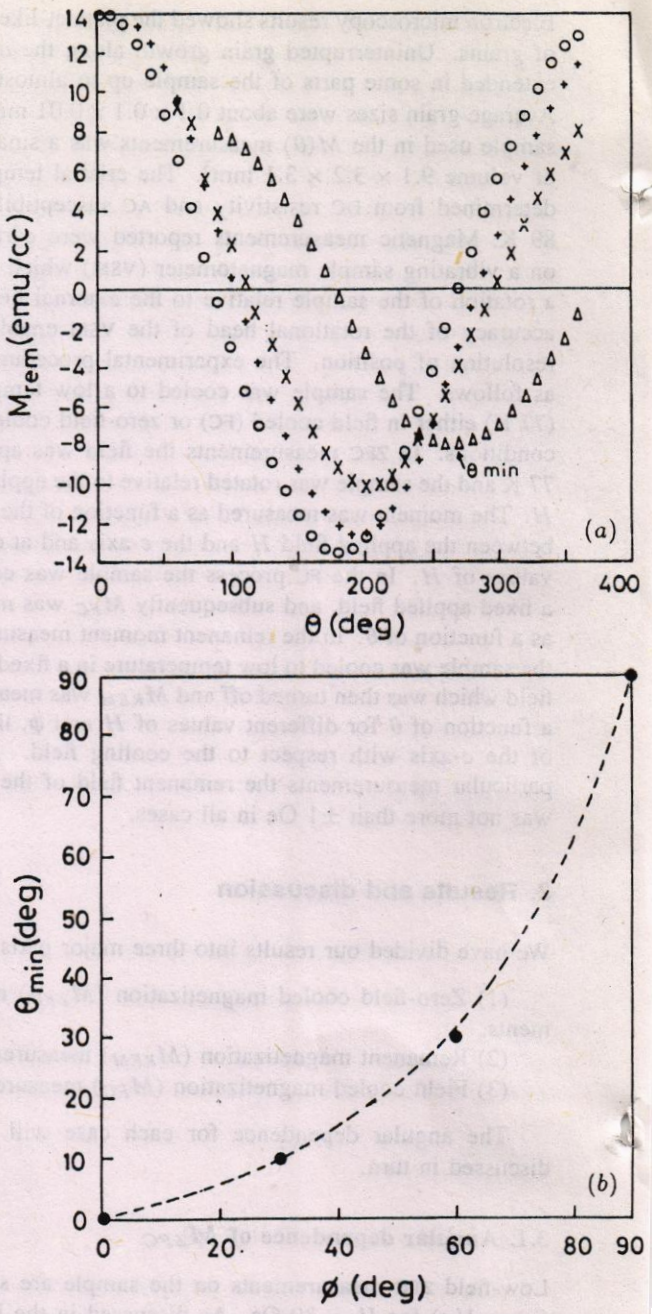

Figure 2. (a) Angular dependence of the remanent magnetization for various cooling angles at 77 K and a cooling field of 500 Oe (○, +, × and △ represent data for $\phi = 0°$, 30°, 60° and 90° respectively). (b) The variation of the shift in the minimum, $\theta_{min}(\phi)$, with cooling angle ϕ for $H = 500$ Oe ($\theta_{min}(\phi) = \theta_{min} - \pi$).

increases with temperature) and two-dimension to three dimension crossover, enabling flux orientation at angles intermediate between c-axis and ab-plane.

A similar trend is seen in figure 3, where M_{REM} i plotted as a function of ϕ. The change in the remanen magnetization is not linear with ϕ over the whole range For low H, M_{REM} is almost the same at 0° and 30°. The there is an almost linear decrease. For higher H (e.g 7 kOe), the decrease is evident even for $\phi = 30°$. Thu the preference for the c-axis is also field dependent, i.e. a higher H the flux is tending to align close to the directio

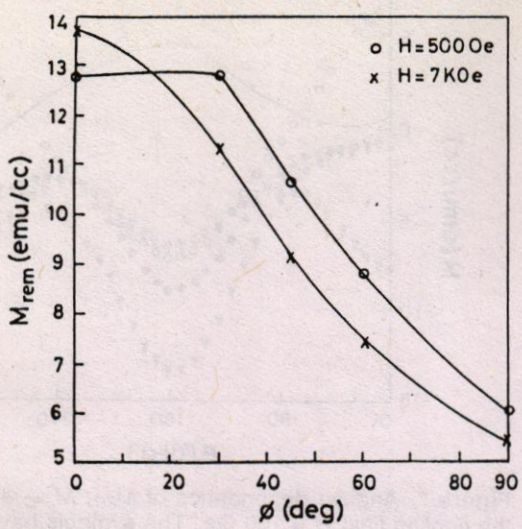

Figure 3. The variation of remanent magnetization with cooling angle ϕ for the different indicated fields. The solid line serves as a guide to the eye.

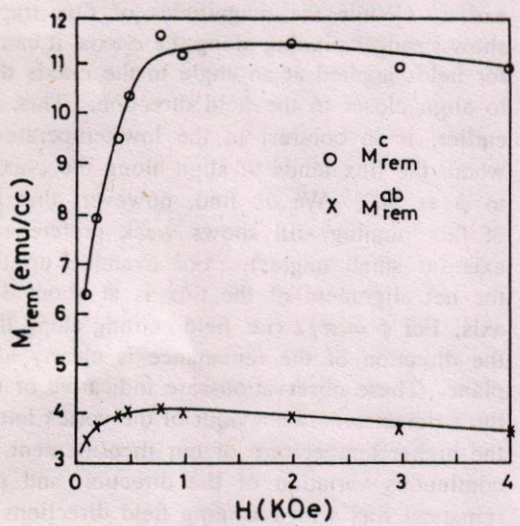

Figure 4. Dependence of remanent magnetization on the cooling field for $H \parallel c$ and $H \perp c$ of the YBCO sample at 77 K. The solid line serves as a guide to the eye.

of the field.

We obtain for our sample the anisotropy ratio $M^c_{REM}/M^{ab}_{REM} \sim 3$. Yaron *et al* [4] have quoted this ratio as being close to 5 for their low-temperature (4.2 K) data. Figure 4 shows the values of remanent moment, M^c_{REM} and M^{ab}_{REM} at 77 K, as a function of the applied cooling field. M^c_{REM} rapidly increases with the applied magnetic field until the saturation level is reached in the vicinity of 800 Oe. On the other hand M^{ab}_{REM} attains saturation at about 300 Oe. These observations reflect the differences between the pinning strengths along the c-axis and the ab-plane. According to [16], this behaviour can be due to the anisotropic nature of H_{c1} (lower critical field). We find that for our sample the ratio of H^c_{c1}/H^{ab}_{c1} is 2.3 and the ratio of the saturation fields is 2.67. Thus a good agreement is seen between the ratios of the saturating fields and of H_{c1} in the two orientations. This tendency has been verified

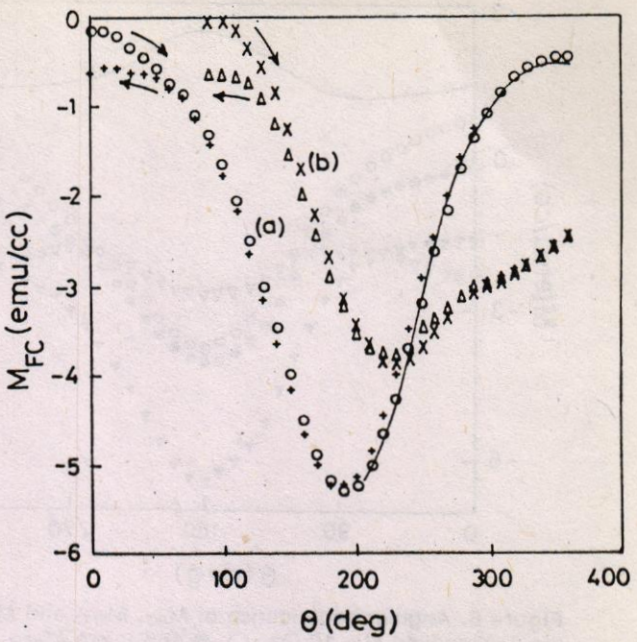

Figure 5. Angular dependence of field cooled magnetization for the cooling field of 20 Oe at cooling angle (*a*) $\phi = 0$ and (*b*) $\phi = \pi/2$ at 77 K.

by repeating the measurements on a number of similar samples.

3.3. Angular dependence of M_{FC}

We measure the field cooled magnetization M_{FC} at various cooling angles and different applied fields H. Figure 5 shows the M_{FC} data as a function of θ for $\phi = 0°$ and 90° at $H = 20$ Oe. This figure represents the data obtained when the sample was rotated from $\theta = 0°$ to 360° and back to $\theta = 0°$ for $\phi = 0°$; and for $\phi = 90°$, where the sample was rotated from $\theta = 90°$ to 360° and back to 90°. Figure 5 illustrates that different amounts of flux are trapped during cooling when the sample is cooled with $H \parallel c$ and $H \perp c$. This can be seen from the difference in the amplitudes of oscillations for the curves (*a*) and (*b*). We can analyse these curves with the help of equation (4), which is a combination of equations (2) and (3),

$$M_{FC} = -H\left[A\cos^2\theta + B\sin^2\theta\right] + M^c_{REM}\cos\theta\cos\phi + M^{ab}_{REM}\sin\theta\sin\phi. \quad (4)$$

The fit of the M_{FC} data in the range $\pi < \theta < 2\pi$ to equation (4) is indicated by the solid line in figure 5. The data from 0 to π are excluded for obvious reasons. Due to the depinning taking place in this region, and the transient behaviour as discussed in [9], we may not expect the data in this range to give a good fit. While we are able to fit the M_{FC} data in the higher-θ range with equation (4), the values of the coefficients do not coincide with those found independently from M_{ZFC} and M_{REM} measurements. Thus the relation $M_{FC} = M_{ZFC} + M_{REM}$ is not valid in our case at a temperature of 77 K even at a low field like $H = 10$ Oe, if one uses the values of M_{ZFC} and M_{REM} measured independently. Figure 6 illustrates the comparison of M_{FC}, M_{ZFC} and M_{REM} data as a function

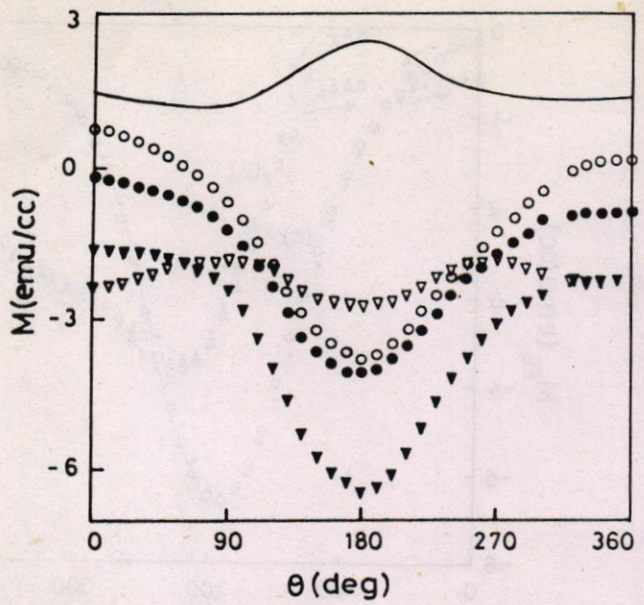

Figure 6. Angular dependence of M_{FC}, M_{ZFC} and M_{REM} for the cooling field H = 10 Oe. ○, ● and ▽ are M_{REM}, M_{FC} and M_{ZFC} respectively, while ▼ and the solid line indicate $M_{REM} + M_{ZFC}$ and $\Delta M = M_{FC} - (M_{ZFC} + M_{REM})$ respectively.

of θ for $\phi = 0°$ and $H = 10$ Oe. For the sake of comparison we have also plotted the difference $\Delta M = M_F - (M_{ZFC} + M_{REM})$. The difference between M_{FC} and M_{REM} is seen to be approximately constant for angles close to zero ($0 < \theta < \pi/2$) and 2π ($3\pi/2 < \theta < 2\pi$). We also note that ΔM is a maximum for $\theta = \pi$, while M_{FC} is close to M_{REM} for θ lying in the range $\pi/2 \leq \theta \leq 3\pi/2$. The difference for $\pi/2 < \theta < 3\pi/2$ and $H \ll H_{c1}$ is thus only due to M_{ZFC}. At $\theta = \pi$ the negative value of M_{ZFC} becomes large due to the demagnetization factor contribution. Hence the difference ΔM becomes more positive ($\Delta M = M_{FC} - (M_{ZFC} + M_{REM}) \approx -M_{ZFC}$). This leads to the observed maximum in ΔM at $\theta = \pi$. Figure 7 shows the angular behaviour of M_{FC}, M_{ZFC}, M_{REM} and ΔM for $\phi = 0$ and a higher field $H = 100$ Oe. (Very similar data are obtained for $H = 500$ Oe.) In contrast to figure 6, the M_{FC} curve here appears very close to the M_{ZFC} curve in most of the angular regime. The solid line represents ΔM. There is a large difference between M_{FC} and $(M_{ZFC} + M_{REM})$ which is due to very low remanence in the field cooled case. Indeed $M_{FC} \sim M_{ZFC}$ and $\Delta M \sim -M_{REM}$. As M_{REM} gives maximum negative projection for $\theta = \pi$, ΔM is maximum positive as is shown in the figure. In these curves it appears that in the presence of relatively high external fields, the direction of vortices during rotation could be very different from the direction of original trapping. During rotation, the field exercises a force on the flux lines which can rotate or expel some of the flux lines from the sample.

4. Conclusions

The main feature to emerge from the study is that at a temperature close to T_c ($T/T_c = 0.86$), while the effects of anisotropy of magnetization and pinning are clearly apparent, there are very significant systematic differences

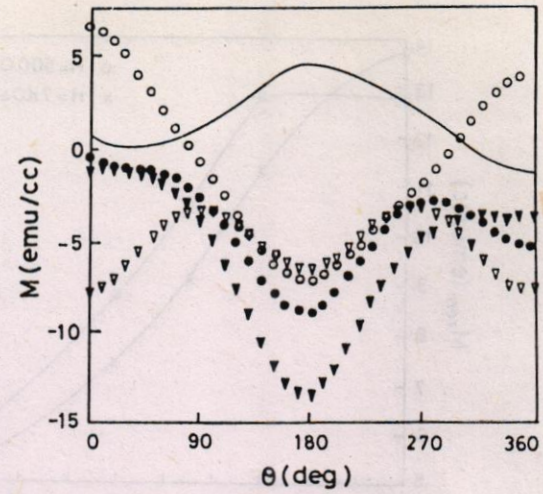

Figure 7. Angular dependence of M_{FC}, M_{ZFC} and M_{REM} for the cooling field H = 100 Oe. The symbols have the same meaning as in figure 6.

compared with the low-temperature behaviour referenced earlier. While the magnitudes of flux trapping clearly show stronger pinning along the c-axis, it can be seen that for fields applied at an angle to the c-axis the flux tends to align closer to the field direction. This, as discussed earlier, is in contrast to the low-temperature behaviour where the flux tends to align along the c-axis almost up to $\phi = 90°$. We do find, however, that the direction of flux pinning still shows weak preference for the c-axis (at small angles). For example up to $\phi = 60°$ the net alignment of the flux is at about 30° to the c-axis. For $\phi = \pi/2$ (i.e. field cooling along the ab-plane), the direction of the remanence is clearly along the ab-plane. These observations are indicative of the enhanced three-dimensional behaviour of the vortex lattice system at the higher temperature of our measurement. The almost continuous variation of the direction and magnitude of remanent flux with changing field directions is indicative of the ability of flux lines to align at angles intermediate between the c-axis and the ab-plane. This is in turn consistent with the three-dimensional behaviour of vortex lines expected at the elevated temperature of this study, and also shown in [7]. Furthermore our observations are in accordance with the work of Kogan *et al* [17], where it has been shown that the application of a field along directions other than ab and c leads in general to the presence of a transverse moment ($M \perp H$). Part of this transverse moment along c remains trapped when the field is turned off, giving a net remanence aligned away from the original H direction.

We also observe that in the field region $H \ll H_{c1}$ the zero-field cooled data show deviations from the pure demagnetization factor oscillation of $M(\theta)$ which can be explained in terms of flux pinning. Since fields are below H_{c1} and the state is zero field cooled, this can only be due to the intergrain penetrated flux. Thus such measurement can also be used to identify the existence of intergrain flux pinning.

The variation of the field cooled magnetization shows that it does not satisfy the low-temperature equality

$M_{FC} = M_{ZFC} + M_{REM}$. We understand this as occurring due to increased depinning when the sample is rotated against the applied field for the field cooled rotation $M_{FC}(\theta)$. We observe that while the data can be fitted to equation (4), the coefficients are not the same as those obtained independently from the M_{ZFC} and $M_{REM}(\theta)$ measurements. Thus it is clear that the field cooled moment cannot be described by the simple picture useful at low temperatures. Recent data by Goeckner and Kouvel [13] show that, in general, the magnetization rotation data exhibit both a frictional (M_F) and rotating component (M_R). While the former follows the field, the latter rotates with the sample. The magnitude of the frictional part increases with increasing H while M_R decreases with H. This appears to be true in our case as well, where the higher-field data (FC) show no evidence of any pinned moments (after $\theta = \pi$) while the low-field data clearly show its presence.

Finally we would like to comment that in magnetization rotation experiments, in general, one may actually have a generalized critical state with a gradient of the flux orientation, as originally discussed by Cave and LeBlanc [18]. This implies an outer region of the sample with flux direction closer to the applied field direction, and a central core region with flux still pinned along the original direction. While these ideas may not be directly applicable to the strong-pinning and highly anisotropic low-temperature situation, they may be quite useful at higher temperatures. At present we are attempting an analysis of the transient region ($\theta < \pi$), along these lines.

Acknowledgment

This work has been supported by a grant from the Pakistan Science Foundation (PSF/C/QU-Phys-90).

References

[1] Brandt E H 1991 *Int. J. Mod. Phys.* B **5** 571; 1992 *Physica* C **195** 1
[2] Feinberg D and Villard C 1990 *Phys. Rev. Lett.* **65** 919
[3] Felner I, Yaron U, Yeshurun Y, Chandrashekhar G V and Holtzberg F 1989 *Phys. Rev.* B **40** 5239
[4] Yaron U, Felner I and Yeshurun Y 1991 *Phys. Rev.* B **44** 12 531
[5] Hasanain S K, Khosa G H, Iqbal M Z and Khan N A 1993 *Supercond. Sci. Technol.* **6** 691
[6] Doniach S 1990 The phenomenology of flux motion in high temperature superconductors *Proc. Los Alamos Symp. 1989* ed K S Bedell, Coffey, D E Meltzer, D Pines and J R Schrieffer (Reading, MA: Addison-Wesley) p 406
[7] Fastampa R, Giura M, Marcon R and Silva E 1991 *Phys. Rev. Lett.* **67** 1795
[8] Tinkham M 1963 *Phys. Rev.* **129** 2413
Harper P E and Tinkham M 1968 *Phys. Rev.* **172** 441
[9] Lawrence W E and Doniach S 1971 *Proc. 12th Int. Conf. on Low Temperature Physics (Kyoto)* ed E Kanda (Tokyo: Kiegaku) p 361
[10] Salama K, Solvamanicham V, Gao L and Sun K 1989 *Appl. Phys. Lett.* **55** 2352
[11] Kolesnik S, Skoshiewicz T, Igalson J and Korczak Z 1992 *Phys. Rev.* B **45** 10 158
[12] Zhang Hong, Chen Tong, Sun Yanxi, Ren Hongtao, Xiao Ling, He Qing and Yan Shousheng 1991 *Physica* C **174** 355
[13] Goeckner H P and Kouvel J S 1994 *Phys. Rev.* B **50** 3435
[14] Palstra T T M, Batlogg B, Schneemeyer L F, Van Dover R B and Waszczak J V 1988 *Phys. Rev.* B **38** 5102
[15] Dolan G J, Holtzberg F, Field C and Dinger T 1989 *Phys. Rev. Lett.* **32** 2184
[16] Song Yi, Heleley C E, Misra A and Gaines J R 1993 *Phys. Lett.* **1173A** 489
[17] Kogan V G, Fang M M and Mitra S 1988 *Phys. Rev.* B **38** 11 958
[18] Cave J R and LeBlanc M A R 1982 *J. Appl. Phys.* **53** 1631

J. Phys.: Condens. Matter 8 (1996) 8339–8350. Printed in the UK

Effects of crossed flux on magnetization dynamics and magnetic relaxation of melt-textured $Y_1Ba_2Cu_3O_{7-x}$

Sadia Manzoor and S K Hasanain

Department of Physics, Quaid-i-Azam University, Islamabad 45320, Pakistan

Received 12 March 1996, in final form 28 May 1996

Abstract. We report magnetization measurements of melt-textured $Y_1Ba_2Cu_3O_{7-x}$ in a crossed-flux configuration (CFC), i.e. in the presence of two mutually perpendicular flux components. We have measured the $M(H)$ loops of the a–b planes and their dependence on the field sweep rate in the presence of various remnant fluxes along the c axis. Furthermore, we have carried out magnetic relaxation studies of the a–b plane moment in the CFC, and compared the results with those obtained in the single-flux configuration (SFC), i.e. when there is no c-axis remanence. Our results in three different experiments show enhanced flux entry along the a–b planes in the CFC. We interpret this in terms of a suppression of the shielding currents and discuss flux cutting as a possible mechanism which can lead to it.

1. Introduction

Recently interest has revived in the vortex dynamics of high-T_c superconductors in the crossed-flux configuration (CFC). By this we mean the simultaneous presence of two non-parallel families of flux lines, which in most cases are taken to be mutually orthogonal. Such situations had been discussed [1] in the context of the low-T_c materials for the analysis of the force-free configuration ($J_\parallel \times B = 0$), where $J_\parallel$ is the component of the current parallel to the magnetic induction B. In a CFC the current shielding one flux component is, over part of its path, parallel to the other component of flux. If $J_\parallel$ is larger than a critical value $J_{C\parallel}$, flux-cutting events can occur, leading to a breakdown of the force-free configuration [1–3]. The concept of flux cutting and reconnection leading to dissipative processes in such configurations had been invoked. An associated discussion has had to do with the effect of the transverse flux density on the critical state currents of the longitudinal flux [1]. More recently this debate has focused on the possibility of flux cutting in the high-T_c materials, and the effects of anisotropy and flux line curving on the flux-cutting barriers [4, 5]. These ideas have obvious implications for the stability of an entangled glass or liquid of flux lines. The CFC is not purely of academic interest but is also important to understand because, in many magnetomechanical applications of superconductors, similar situations may be encountered. That is, there is an applied field and there are parasitic or remnant fields in some other direction, which affect the overall response.

There exists considerable controversy regarding the role of transverse flux on the motion of flux in a longitudinal direction. Magnetic studies by Park and co-workers [6, 7] on $YBa_2Cu_3O_{7-x}$ (YBCO) single crystals [6, 7] show that a strongly pinned remanence along the c axis inhibits flux entry along the a–b planes. These results are in direct contrast with those obtained by LeBlanc and co-workers [8, 9] on sintered tubes of (YBCO) material,

0953-8984/96/438339+12$19.50

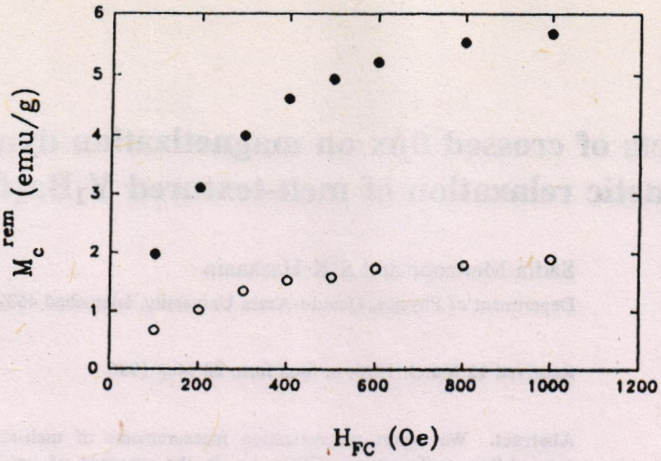

Figure 1. Remnant moment M_c^{rem} along the c axis (●) and the remnant moment M_{ab}^{rem} along the a–b planes (○) against cooling field H_{FC}.

and by us [10] on melt textured samples of YBCO. LeBlanc and co-workers showed that flux-cutting events take place in a CFC, and the presence of a toroidal field suppressed the shielding currents for the axial field. Our studies also showed that the presence of a transverse flux along the c axis actually enhances flux entry in a longitudinal direction (i.e. along the a–b planes), by suppressing the shielding currents associated with the a–b plane moment. This apparent discrepancy will be discussed in detail in the conclusions.

Recent magneto-optical investigations by Indenbom *et al* [11] show that, in a strongly correlated 3D system, the force-free configuration of current and vortices can be very stable, and a perpendicular field component does not penetrate through an array of longitudinal flux lines. In a weakly coupled 2D system such as BSCCO on the other hand, the transverse flux does not appear to influence the motion of the longitudinal flux lines. As pointed out in [11], a breakdown of the force-free configuration can occur in vortex systems with weak internal connections, such as 2D systems, or even in anisotropic 3D superconductors in which the transverse flux can penetrate from the ends, where the force-free configuration is locally not realized. In such a situation, vortex lattice cutting and reconnection appear to be an important mechanism, particularly when large intervortex angles can be established, since cutting barriers are minimal for mutually perpendicular flux lines [4].

In a previous experiment we measured the magnetization M_{ab} of melt-textured samples along the a–b planes, in the presence of a field-cooled remnant flux along the c axis [10]. We clearly observed a decreased diamagnetic signal for M_{ab} as the magnitude of the remnant flux along the c axis was increased. Since the ease of flux entry in such a measurement can be related to a decrease in the effective activation barriers for flux movement, we have performed experiments which can give more quantitative results on the decrease in the activation barriers with increasing transverse flux density. In the present paper, we extend our previous investigations to include magnetic relaxation studies of the a–b plane moment in the presence of a remnant flux along the c axis and obtain the relaxation rate $S = (1/M_0)[\partial M/\partial(\ln t)]$.

Additionally we have investigated the effects of various field sweep rates on the $M(H)$ loops in the CFC, and compared the results with the single-flux case, i.e. in the absence

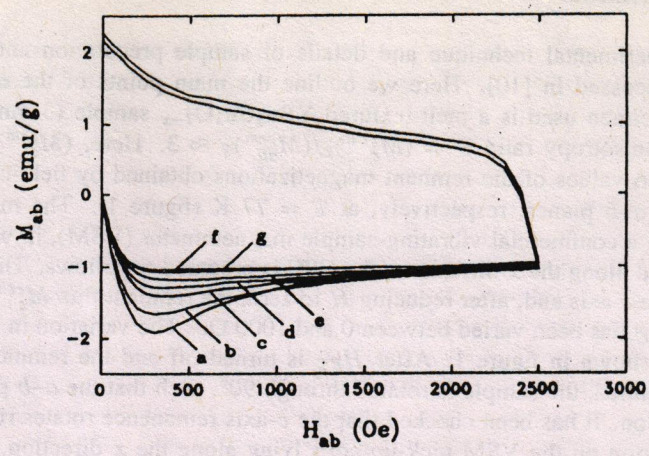

Figure 2. $M(H)$ loops of the a–b plane for the single-flux case (curve a), as well as for different cooling fields parallel to the c axis: curve b, $H_{FC} = 100$ Oe; curve c, $H_{FC} = 200$ Oe; curve d, $H_{FC} = 300$ Oe; curve e, $H_{FC} = 400$ Oe; curve f, $H_{FC} = 500$ Oe; curve g, $H_{FC} = 600$ Oe. The loop for $H_{FC} = 800$ Oe has been measured but is not shown in the figure for clarity. The outer curve for the field-decreasing branch corresponds to the single-flux loop (curve a), while the inner curve corresponds to $H_{FC} = 600$ Oe (curve g). The other curves on the field decreasing branch lie between these two but are not shown for clarity.

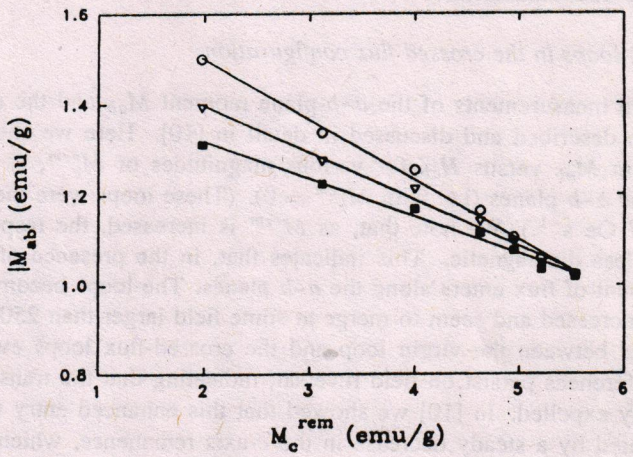

Figure 3. Magnitude of the diamagnetic response $|M_{ab}|$ of the a–b planes as a function of the remanence M_c^{rem} along the c axis. $|M_{ab}|$ has been extracted from figure 2 at three values of the a–b-plane field: ○, $H_{ab} = 600$ Oe; ▽, $H_{ab} = 800$ Oe; ■, $H_{ab} = 1000$ Oe. The straight lines serve as a guide to the eye.

of a c-axis remanence. These experiments yield valuable information on the dynamics of vortex motion in the CFC and have been used to extract the so-called sweep creep rate $C = (1/M)[\partial M/\partial(\ln \dot{H})]$, as well as the $E(J)$ behaviour in the crossed-flux mode for various remnant flux densities.

2. Experiments

The experimental technique and details of sample preparation and characterization have been discussed in [10]. Here we outline the main points of the experimental procedure. The specimen used is a melt-textured $YBa_2Cu_3O_{7-x}$ sample (3 mm × 3 mm × 3 mm). It has an anisotropy ratio $\Gamma = (M_c^{rem})_s/(M_{ab}^{rem})_S \approx 3$. Here, $(M_c^{rem})_S$ and $(M_{ab}^{rem})_s$ are the saturation values of the remnant magnetizations obtained by field-cooling along the c axis and the a–b planes, respectively, at $T = 77$ K (figure 1). The measurements have been made on a commercial vibrating-sample magnetometer (VSM), in which the magnetic field is applied along the x direction. The CFC is prepared as follows. The sample is field cooled along the c axis and, after reducing H to zero, the remnant flux M_c^{rem} obtained. The cooling field H_{FC} has been varied between 0 and 1000 Oe. The variation in M_c^{rem} with cooling field H_{FC} is shown in figure 1. After H_{FC} is turned off and the remnant flux parallel to the c axis obtained, the sample is rotated through 90°, such that the a–b plane now lies along the x direction. It has been checked that the c-axis remanence rotates rigidly and does not give a projection on the VSM pick-up coils lying along the x direction. Following the rotation of M_c^{rem}, a magnetic field is applied along the a–b planes, and the magnetization $M_{ab}(H_{ab})$ is measured. In the magnetic relaxation experiments, the a–b-plane field is ramped up to 600 Oe at the rate of 5 Oe s^{-1}, and the relaxation data are taken at this value of H_{ab}. In the $M(H, \dot{H})$ experiments, H_{ab} is swept around a half-loop ($0 \rightarrow H_{max} \rightarrow 0$), the maximum field being 2500 Oe. These latter experiments have been performed at five different sweep rates varying between 8 and 187 Oe s^{-1}. All studies have been carried out at 77 K.

3. Results and discussion

3.1. M(H) loops in the crossed-flux configuration

The *in-situ* measurements of the a–b-plane moment M_{ab} and the c-axis remanence M_c^{rem} have been described and discussed in detail in [10]. Here we show in figure 2 only the variation in M_{ab} versus H_{ab} for various magnitudes of M_c^{rem}, as well as the single-flux loop of the a–b planes (i.e. with $M_c^{rem} = 0$). (These loops were measured at a field sweep rate of 17 Oe s^{-1}.) We note that, as M_c^{rem} is increased, the response of the a–b planes becomes less diamagnetic. This indicates that, in the presence of a c-axis remanence, a large amount of flux enters along the a–b planes. The loops become increasingly flatter as M_c^{rem} is increased and seem to merge at some field larger than 2500 Oe. There exist finite differences between the virgin loop and the crossed-flux loops even at $H_{ab} = 2500$ Oe. These differences persist on field reversal, indicating that the transverse flux has not been completely expelled. In [10] we showed that this enhanced entry of the a–b-plane flux is accompanied by a steady decrease in the c-axis remanence, which we argued was due to its expulsion following cutting. It has been shown in [10] that the differences between the $M_{ab}(H)$ loops in the crossed and uncrossed configurations could not be explained away by assuming a rotation of the c-axis flux towards the a–b planes. At low fields ($H_{ab} \leqslant 200$ Oe), the changes in M_c^{rem} with field were too small to account for the difference between the a–b-plane magnetizations in the crossed and uncrossed modes. At higher fields, however, the change in M_c^{rem} increases steadily, while the differences between the a–b-plane loops in the crossed and uncrossed modes diminish towards zero. M_c^{rem} does not appear to rotate towards the a–b planes, as this would be reflected in persisting differences between the uncrossed- and crossed-flux loops. This leads one to believe that the c-axis flux is being expelled as the a–b-plane field increases to large values.

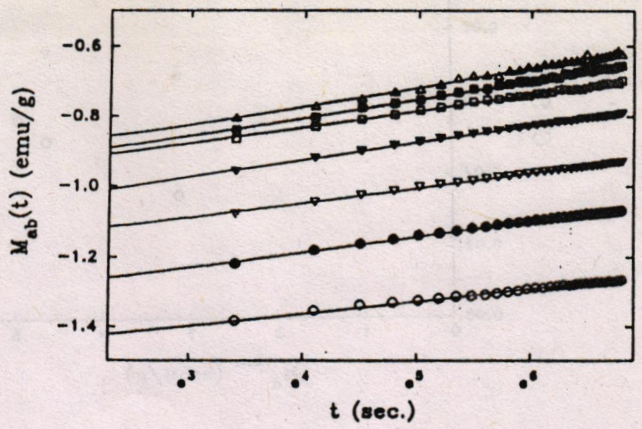

Figure 4. Magnetization relaxation data taken after a field ramp to $H_{ab} = 600$ Oe for the SFC (○), as well as for the CFC with $H_{FC} = 100$ Oe (●), $H_{FC} = 200$ Oe (▽), $H_{FC} = 400$ Oe (▼), $H_{FC} = 600$ Oe (□), $H_{FC} = 800$ Oe (■) and $H_{FC} = 1000$ Oe (△). The straight lines are fits to equation (1).

From figure 2 the values of M_{ab} have been extracted at $H_{ab} = 600$, 800 and 1000 Oe. In figure 3 these have been plotted as a function of M_c^{rem}, the c-axis remanence at the start of the hysteresis loop. We do not use the width ΔM_{ab} of the hysteresis loop for our analysis, rather only the value of $|M_{ab}|$ on the ascending field branch. This choice is motivated by the fact that the crossed flux leaves its signature primarily on the magnetization in the ascending field branch. In figure 3 we find that, for all three values of H_{ab}, M_{ab} decreases linearly with increasing M_c^{rem}, its rate of change (with M_c^{rem}) being smaller for higher values of H_{ab}. The convergence of the lines is reflective of the flatness of the $M(H)$ loops for large remanences. According to the critical state model, M_{ab} is a measure of the appropriate shielding currents. Thus figure 3 indicates a continuous linear decrease in the shielding currents as the transverse remnant flux is increased.

3.2. Magnetic relaxation studies in the crossed-flux configuration

Although there exist extensive data on relaxation in the single-flux configuration (SFC) (both parallel and perpendicular to the c axis) [12–14], we have not come across studies of relaxation effects in a CFC. The relaxation or creep process is understood to take place over current-dependent activation energy barriers $U_{eff}(J)$ [15, 16]. A suppression of the critical currents in the presence of crossed flux (as can be seen from figure 3) would obviously affect the height of these activation energy barriers. The detailed dependence would vary with the particular $U_{eff}(J)$ relationship which is valid in the temperature and field regimes under consideration.

We have measured the temporal decay of the a–b-plane moment in a short time window of 900 s with a sampling time of 1 s, following a field ramp of 600 Oe at the rate of about 5 Oe s^{-1}. Figure 4 shows the $M_{ab}(t)$ curves for the single-flux case ($M_c^{rem} = 0$), as well as for six values of the crossed flux. (The closeness of the curves at high remanences is again only an artefact of the saturation of M_c^{rem} with H_{FC}.) We find a logarithmic time

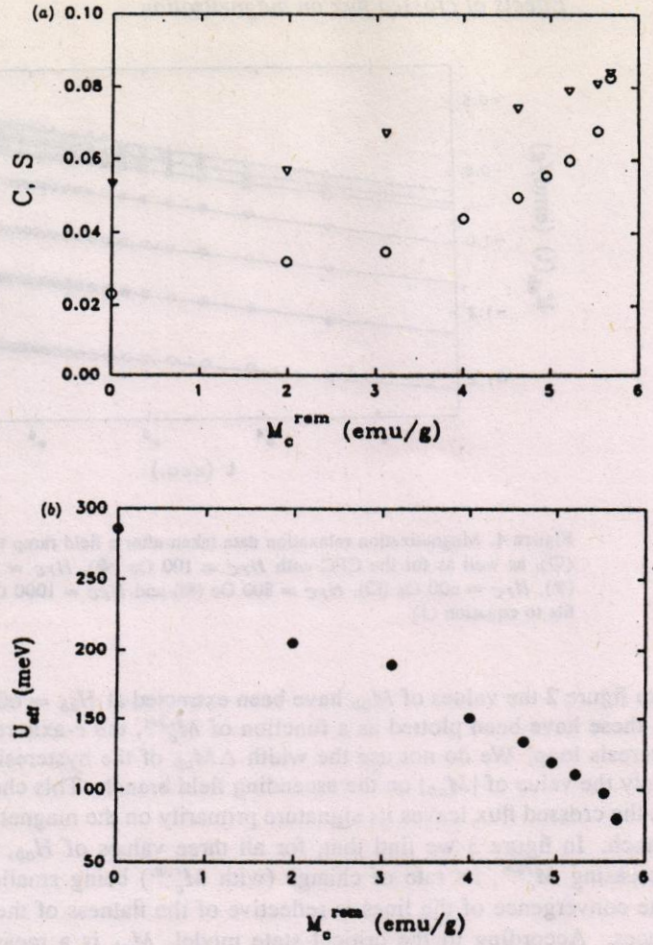

Figure 5. (*a*) Dependences of the relaxation rate S (O), and sweep creep rate C (∇) on M_c^{rem}. The values of C and S have been obtained for $H_{ab} = 600$ Oe. (*b*) Effective activation energy U_{eff} for the motion of the a–b-plane flux as a function of M_c^{rem}. U_{eff} has been obtained from the values of S according to $S = kT/U_{eff}$.

dependence of the a–b-plane magnetization, with the data fitting the expression

$$M(t) = M_0[1 + S\ln(1 + t/\tau)]. \tag{1}$$

well. Here S is the normalized relaxation rate and τ is some macroscopic relaxation time. For relatively small time windows the collective creep model can be approximated to give a logarithmic time dependence for $M(t)$ [17]. In this approximation, the rate $S = (1/M_0)[\partial M/\partial(\ln t)]$ yields the activation barrier $S = kT/U_{eff}(J)$. Typical forms for $U_{eff}(J)$ are the classical linear (Anderson) form $U_{eff}(J) = U_0[1 - (J/J_c)]$, and the non-linear dependence $U_{eff}(J) \sim U_0(J_c/J)^{\mu}$. With increasing field, one usually obtains a decrease in $U_{eff}(J)$, reflecting the decreased value of the critical current J_c.

We find that the presence of crossed flux does not change the functional form of the $M(t)$ dependence at least in the short time window. Its only effect seems to lie in an

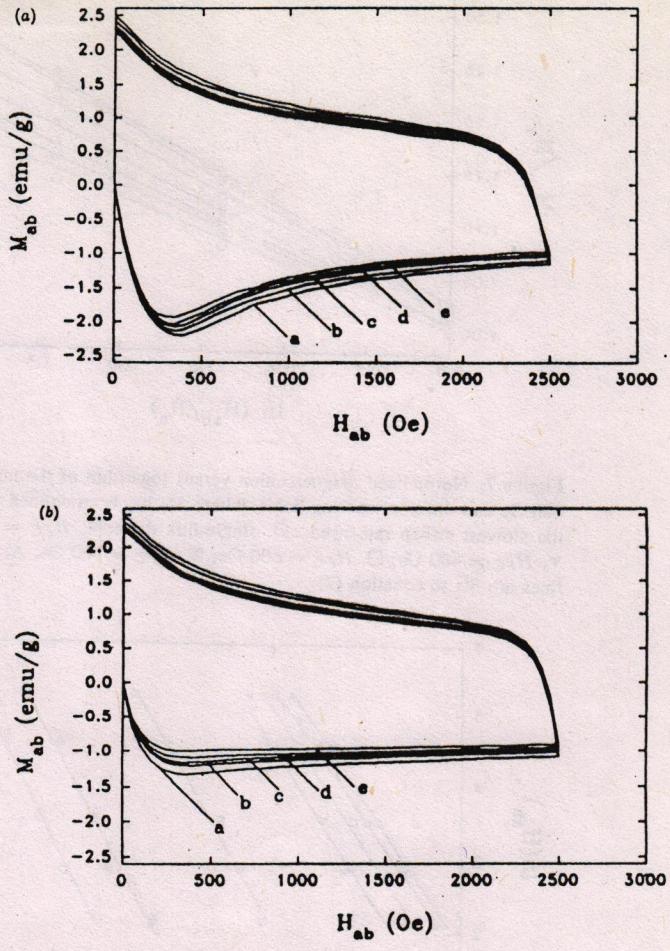

Figure 6. (*a*) $M_{ab}(H_{ab}, \dot{H}_{ab})$ loops for the single-flux configuration with $\dot{H}_{ab} = 187$ Oe s^{-1} (curve a), 92 Oe s^{-1} (curve b), 33 Oe s^{-1} (curve c), 17 Oe s^{-1} (curve d) and 8 Oe s^{-1} (curve e). (*b*) $M_{ab}(H_{ab}, \dot{H}_{ab})$ loops measured in the crossed-flux configuration with $H_{FC} = 800$ Oe and $\dot{H}_{ab} = 187$ Oe s^{-1} (curve a), 92 Oe s^{-1} (curve b), 33 Oe s^{-1} (curve c), 17 Oe s^{-1} (curve d) and 8 Oe s^{-1} (curve e).

enhancement of the relaxation rate, from $S = 0.023$ in the single-flux mode to $S = 0.083$ in the presence of a transverse remanence of 5.7 emu g^{-1} (corresponding to a cooling field of 1000 Oe). This corresponds to a decrease in U_{eff} from 280 to 80 meV. It is physically more relevant to represent S and U_{eff} as functions of the flux trapped along the c axis (figure 5). Here we can see that the variation in U_{eff} with M_c^{rem} is reasonably linear and is reminiscent of the linear behaviour of $M_{ab}(\propto J)$ with M_c^{rem}. The relaxation rate on the other hand increases very strongly with increasing M_c^{rem} at higher values of the remnant flux. The relaxation data have been taken at $H_{ab} = 600$ Oe, a field at which there is a significant amount of c-axis flux present in the sample, as can be seen from the differences between the single-flux loop and the crossed-flux loops in figure 2.

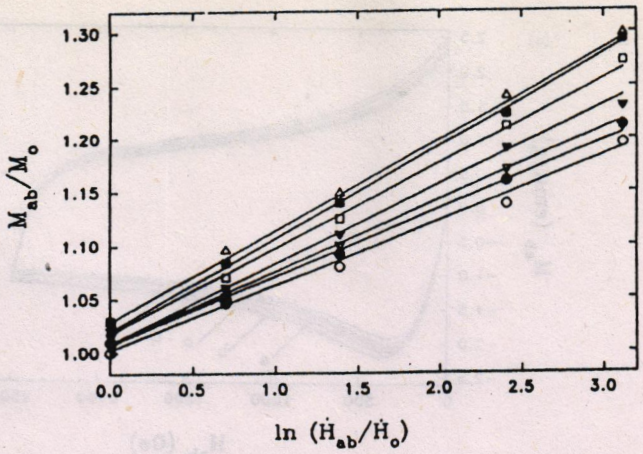

Figure 7. Normalized magnetization versus logarithm of the normalized sweep rate at H_{ab} = 600 Oe and different cooling fields, where M_0 has been defined in the text and $\dot{H}_0 = 8$ Oe s^{-1}, the slowest sweep rate used: ○, single-flux data; ●, H_{FC} = 100 Oe; ▽, H_{FC} = 200 Oe; ▼, H_{FC} = 400 Oe; □, H_{FC} = 600 Oe; ■, H_{FC} = 800 Oe; △, H_{FC} = 1000 Oe. The straight lines are fits to equation (2).

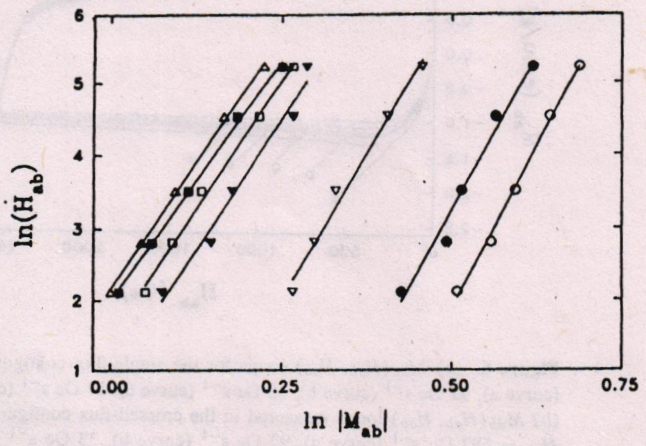

Figure 8. The log–log plot of sweep rate $\dot{H}_{ab}$ and magnetization $|M_{ab}|$ at H_{ab} = 600 Oe for different cooling fields. Data are shown for the single-flux case (○), H_{FC} = 100 Oe (●), H_{FC} = 200 Oe (▽), H_{FC} = 400 Oe (▼), H_{FC} = 600 Oe (□), H_{FC} = 800 Oe (■) and H_{FC} = 1000 Oe (△). The straight lines are fits to a linear equation of the form $\ln \dot{H}_{ab} = n \ln |M_{ab}| + C$ where C is a constant and n the slope of the lines. n is thus the exponent of the power law $\dot{H}_{ab} = A|M_{ab}|^n$.

At a cooling field of 1000 Oe, S increases by about 300% of its value in the single-flux mode. The very rapid increase in S (and related decrease in U_{eff}) due to the crossed flux motivates the obvious question as to the mechanism whereby the transverse flux facilitates the entry of the longitudinal flux. The most plausible explanation seems to be that the transverse flux enables the longitudinal flux to cut through and then to rejoin within the

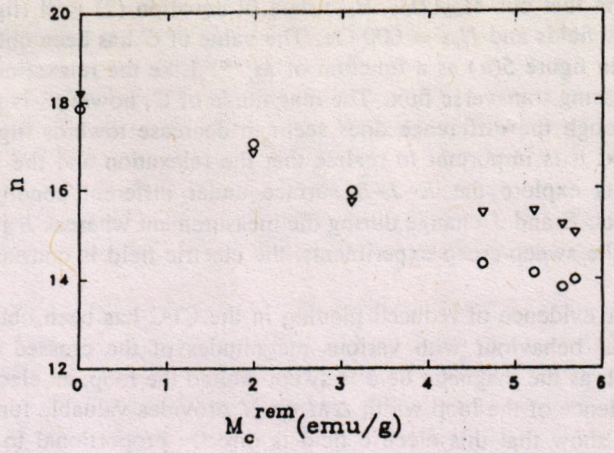

Figure 9. Variation in the exponent n obtained from figure 8 as a function of the c-axis remanence for two different values of the a–b-plane field: ○, H_{ab} = 600 Oe; ▽, H_{ab} = 1000 Oe.

sample. The angle ($\theta = \pi/2$) which nominally exists between the two flux families, and the relatively low degree of correlation or coherence of the lines also help to realize the process of cutting. While the former ensures that repulsive effects between vortex cores are minimized, the latter, as discussed in [2], makes it possible for transverse vortex segments to curve and tilt without entailing large displacements of the vortex elements at extended distances.

3.3. Sweep rate dependence of magnetization in a crossed-flux configuration

The effect of field sweep rate on the magnetization of high-T_c superconductors has been well established [18–21]. Basically, the effect of ramping a magnetic field is to generate an electric field proportional to the sweep rate $\dot{H}$, which in turn generates currents according to the particular $E(J)$ dependence in that part of the phase space. The currents thus generated are manifested as additional magnetization.

Various models which invoke flux diffusion and drift dynamics have been proposed to explain this dependence of the magnetization on the sweep rate of the applied field. It has been shown that the width of the hysteresis loop increases with increasing sweep rate. M is found to be logarithmically dependent on $\dot{H}$:

$$M = M_0(H, T)[1 + C \ln(\dot{H}/\dot{H}_0)] \tag{2}$$

where $\dot{H}$ is the sweep rate of the applied field and M_0 is the magnetization associated with the rate $\dot{H}_0$.

To investigate the effect of the crossed flux on the above relationship and the E–J dependence, we have carried out experiments in the CFC at five different sweep rates from 8 to 187 Oe s^{-1}. Each set of five $M_{ab}(H_{ab}, \dot{H}_{ab})$ loops has been obtained for a given value of M_c^{rem}. There was a total of seven such sets measured, corresponding to cooling fields H_{FC} = 0, 100, 200, 400, 600, 800 and 1000 Oe. In figure 6(a), the broadening of the $M_{ab}(H_{ab})$ loops with increasing sweep rates in the SFC is evident. Figure 6(b) shows the $M_{ab}(H_{ab}, \dot{H}_{ab})$ loops in the CFC for a cooling field of 800 Oe, corresponding to a remnant flux of 5.5 emu g^{-1}.

We find that our $M_{ab}(H_{ab}, \dot{H}_{ab})$ data fit equation (2) well (figure 7), for all values of the cooling fields and $H_{ab} = 600$ Oe. The value of C has been obtained from these fits and is shown in figure 5(a) as a function of M_c^{rem}. Like the relaxation rate S, C too increases with increasing transverse flux. The magnitude of C, however, is generally larger than that of S, although the difference does seem to decrease towards higher values of M_c^{rem}. In this context it is important to realize that the relaxation and the sweep-creep ($M(H, \dot{H})$) experiments explore the E–J–B surface under different conditions. In the relaxation experiments, E and J change during the measurement whereas B is approximately constant while, in the sweep-creep experiments, the electric field is constant, being proportional to $\dot{H}$ [22].

Further evidence of reduced pinning in the CFC has been obtained from the variation in the E–J behaviour with various magnitudes of the crossed flux. In a sweep-creep experiment, as the magnetic field is swept around the loop, an electric field is induced, and the dependence of the loop width ΔM on $\dot{H}$ provides valuable further information. Caplin *et al* [22] show that this electric field is directly proportional to the applied sweep rate. Taking $\Delta M_{ab} \propto J$, the $M_{ab}(H_{ab}, \dot{H}_{ab})$ loops can be translated into the E–J relationship at constant values of B. To do this we have plotted $\ln \dot{H}_{ab}$ versus $\ln |M_{ab}|$ obtained from the $M_{ab}(H_{ab}, \dot{H}_{ab})$ loops at $H_{ab} = 600$ and 1000 Oe for all six values of the transverse flux. The data for $H_{ab} = 600$ Oe are shown in figure 8. Note that we have again used $|M_{ab}|$ instead of $|\Delta M_{ab}|$ for reasons previously given. All data points can be fitted by a straight line, indicating a power-law relationship between $\dot{H}_{ab}$ and M_{ab}. Since $\dot{H} \propto E$ and $M_{ab} \propto J$, the curves in figure 8 can be used to derive an E–J relationship of the form $E = AJ^n$. Clearly, the absolute magnitudes of E and J are undefined within multiplicative factors, but we are interested only in the values of n which is the physically relevant parameter. (Note that, because of the logarithmic scales, the proportionality factors between $\dot{H}$ and E and M_{ab} and J do not affect the value of n.)

Figure 9 shows the variation in the exponent n with increasing transverse flux for two values of the a–b-plane field $H_{ab} = 600$ and 1000 Oe. We find a steady decrease of n with increasing M_c^{rem}. The relatively large values of n are in keeping with the fact that n can be shown to be approximately equal to $1/C$ [22], and C as determined by us is typically much smaller than unity (see figure 5(a)). The flattening off of n at higher M_c^{rem} for $H_{ab} = 1000$ Oe is most probably due to the lower effect of the remanence when the a–b-plane field becomes large. It is well known [23] that, in the limit where flux-pinning barriers become negligible to vortex motion (flux flow), n goes towards unity. Hence a decrease in n in the presence of crossed flux again suggests a reduction in the effective pinning barriers to the motion of the a–b-plane flux.

4. Conclusions

We find in three different experiments that a remnant flux pinned along the c axis facilitates flux entry along the a–b planes. This is due to suppression of the critical currents shielding the a–b-plane flux in the presence of transverse flux. We also measure a drastic enhancement in the relaxation rate of the a–b-plane moment which, as indicated by our results, is due to a reduction in the current-dependent activation energy barriers. U_{eff} decreases linearly with increasing transverse flux, as does the critical current $J \propto M$. The measurements using the sweep-creep technique also provide evidence of reduced pinning in the CFC. The increasing creep rate C as well as the decrease in the exponent n both indicate that in the CFC the barriers to the entry of longitudinal flux are lowered.

There is a basis of similarity between our results and those obtained by LeBlanc and co-workers [8,9], both studies being carried out on polycrystalline YBCO at $T = 77$ K. Both these results disagree, however, with the work of Park and co-workers [6,7] on YBCO single crystals and melt-textured samples at $T = 4.2$ K.

In YBCO there exists evidence of a correlated hexagonal flux line lattice at 4.2 K, and an uncorrelated flux line lattice at 77 K [24]. We argue along the lines of [5,11] that it is the degree of coherence of the flux lines, which enhances or inhibits the entry (or exit) of a transverse flux component. For weaker coherence of the flux lines (e.g. due to increased thermal fluctuations), the possibilities of cutting are enhanced. It has been argued that, while for rigid flux lines (i.e. at lower temperatures) the barriers to flux cutting are too high, weakly correlated flux lines, on the other hand, can locally reduce these barriers owing to their ability to twist and curve, without causing large displacements of the entire flux line lattice [5]. As obtained in [5], the barriers to flux cutting are drastically reduced by even a small amount of twist of the vortices. Hence, we believe that temperature and its effect on the morphology of flux lines may be the reason for the discrepancy between our results and those of Park and co-workers.

We explain the suppression of the critical currents (and hence the energy barriers $U_{eff}(J)$) measured in our experiments in the context of flux cutting and reconnection. It has been reported earlier [8,9] that flux line cutting depresses the critical currents in the intergrain region of sintered YBCO samples. In our present experimental situation, the mutually perpendicular configuration of flux lines, as well as the relatively high temperatures ($T = 0.87T_c$) are favourable for flux-cutting events.

Acknowledgment

S Manzoor is grateful to the Akhter Ali Memorial Fellowship Fund for financial assistance.

References

[1] Campbell A M and Evetts J E 1972 *Adv. Phys.* **21** 199
[2] Brandt E H 1995 *Rep. Prog. Phys.* **58** 1465
[3] Clem J R 1982 *Phys. Rev.* B **26** 2463
[4] Brandt E H 1991 *Int. J. Mod. Phys.* B **5** 751
[5] Sudbo A and Brandt E H 1991 *Phys. Rev. Lett.* **67** 3176
[6] Park S J and Kouvel J S 1993 *Phys. Rev.* B **48** 13995
[7] Park S J, Kouvel J S, Radousky H B and Lin J Z 1993 *Phys. Rev.* B **48** 13998
[8] LeBlanc M A R, Celebi S, Wang S X and Plechácek V 1993 *Phys. Rev. Lett.* **71** 3367
[9] Celebi S and LeBlanc M A R 1994 *Phys. Rev.* B **49** 16009
[10] Hasanain S K, Manzoor S and Amirabadizadeh A 1995 *Supercond. Sci. Technol.* **8** 519
[11] Indenbom M V, Forkl A, Ludescher B, Kronmüller H, Habermeier H-U, Leibold B, D'Anna G, Li T W, Kes P H and Menovsky A A 1994 *Physica* C **226** 325
[12] Matsushita T, Funaba S, Nagamatsu Y, Ni B, Funaki K and Yamafuji K 1989 *Japan. J. Appl. Phys.* **28** L1508
[13] Zhang L, Liu J Z, Lan M D, Klavins P and Shelton R N 1991 *Phys. Rev.* B **44** 10190
[14] Gurevich A and Küpfer H 1993 *Phys. Rev.* B **48** 6477
[15] Anderson P W 1962 *Phys. Rev. Lett.* **9** 309
[16] Anderson P W and Kim Y B 1964 *Rev. Mod. Phys.* **36** 39
[17] Hagen C W and Griessen R 1989 *Phys. Rev. Lett.* **62** 2857
[18] Griessen R 1991 *Physica* C **172** 441
[19] Gurevich A, Küpfer H, Runtsch B, Meier-Hirmer R, Lee D and Salama K 1991 *Phys. Rev.* B **44** 12090
[20] Sun Y R, Thompson J R, Christen D K, Ossandon J G, Chen Y J and Goyal K 1992 *Phys. Rev.* B **46** 8480
[21] Delin K A, Orlando T P, Mc Niff E J, Foner S, Van Dover R B, Schneemeyer L F and Waszcak J V 1992 *Phys. Rev.* B **46** 11092

[22] Caplin A D, Cohen L F, Perkins G K and Zhukov A A 1994 *Semicond. Sci. Technol.* 7 412
[23] Blatter G, Feigel'man M V, Geshkenbein V B, Larkin A I and Vinokur V M 1994 *Rev. Mod. Phys.* 66 1125
[24] Gammel P L, Schneemeyer L F, Waszczak J V and Bishop D J 1988 *Phys. Rev. Lett.* 61 1666

Supercond. Sci. Technol. 9 (1996) 461–466. Printed in the UK

Modified flux flow in polycrystalline YBCO: temperature and current dependence

M M Asim and S K Hasanain

Department of Physics, Quaid-i-Azam University, Islamabad 45320, Pakistan

Received 12 February 1996

Abstract. DC resistivity of a zero-field-cooled granular YBCO sample has been studied as a function of angle between the applied field and transport current, at various fields, currents and temperatures. In addition to the large angle-independent dissipation, a small angle-dependent part has been observed which has a $\sin^2\theta$ behaviour. This part varies with increasing fields according to a modified flux flow expression, in line with the reported microwave surface resistance data. Interestingly, the exponent, n, of the field dependence obtained from a modified flux flow expression gives values close to the one at low currents and low temperatures, whereas it reduces towards 0.5 for large values of currents and temperatures close to T_c. With increasing current and temperature, the behaviour of the flux flow in YBCO approaches that which has been reported for BSCCO. The behaviour is considered to be due to a decrease of the coherence of vortex segments at higher currents and temperatures. Furthermore, the deviation of the voltage from $\sin^2\theta$ at low angles has also been studied at different currents and temperatures, which further supports our previous conjecture of Lorentz-force-mediated flux redistribution between inter- and intragrain regions.

1. Introduction

The granular network of high-T_c superconductors has invariably made the transport properties quite complex. The network consists of superconducting grains embedded in a background of depressed superconductivity caused by weak links between the grains. The grains themselves have large critical currents and fields, while the intergrain region has much smaller values of the same. The low values of critical current and field have limited the valuable applications of oxide superconductors despite their high critical temperatures. The mechanism of dissipation in inter- and intragrain regions is still not completely understood [1–4]. Dissipation due to weak links [5, 6], fluctuations effects [7] and Kosterlitz–Thouless-type vortex depairing effects [8] are some of the commonly discussed mechanisms in addition to the conventional flux flow resistivity [9]. There are reports both in favour of [10–14] and against [15, 16] the role of flux flow in high-T_c materials. Therefore the role of flux flow as a dissipative process in granular semiconductors remains a topic of much interest. The typical signature of flux flow, namely a $\sin^2\theta$ dependence of the electric fields (where θ is the angle between J and B) has been observed both in DC resistivity [14, 17] and microwave surface resistance experiments [10–12]. However there is a large part of the dissipation which is independent of angle between the field and current. For fields below H_{c1}, this contribution originates from the motion of fluxons in the weak-link region for fields belo H_{c1}. This so-called phase slip dissipation is understood t occur due to the time variation of the phase difference [1 between the adjacent superconducting regions due to th motion of a vortex. A number of theories [16] have bee proposed to explain the existence of the angle-independer dissipation in the high-field region. In addition to the angle independent part (ρ_{ps}) it is also evident that there is Lorentz-force-dependent part which varies as $V \propto \sin^2\theta$ Blackstead and coworkers [10–12] have shown in the experiments using microwave techniques that the resistanc in both YBCO and BSCCO polycrystalline materials ha a small flux flow component (ρ_{ff}) in addition to a larg isotropic background. They showed [10–12] that th dissipation fitted a modified flux flow expression of th form

$$\rho_{ff} = (\rho_n - \rho_{ps})\left(\frac{H}{H_{c2}}\right)^n \qquad (1$$

where ρ_n is the normal state resistivity and H_{c2} is th higher critical field. They found using equation (1) tha the exponent $n = 1$ for the case of YBCO while it wa equal to 0.5 for BSCCO. This difference was explaine by them as originating in the two-dimensional nature o the BSCCO vortex lattice. The effective decoupling o the BSCCO vortex along the c-axis leading to a formatio of pancake vortices was suggested as a possible reaso why the exponent n in the two cases is different. In th

0953-2048/96/060461+06$19.50

case of weaker c-axis coherence (the case of BSCCO), the movement of one almost decoupled vortex may not lead to the motion of the remaining segment of the vortex, thereby suppressing the field dependence ($n < 1$). However, in the case of a coherent vortex along the c-axis a larger segment is able to move, generating larger dissipation i.e. $n \rightarrow 1$. In our previous work [14] we have reported results for the DC resistivity in the low and moderate field range which were in accordance with (1). However, we found that our data at 77 K fitted better to $n = 0.5$, even for YBCO. To understand the reason for the difference between the value of the exponent n, as determined by Blackstead's group [12] and ourselves for the same (YBCO) type of samples, is the basic motivation for the current work. To determine the conditions in which the modified flux flow in our YBCO samples begins to approach the form of [12], namely $n = 1$, we performed the resistivity measurements over a range of temperatures and currents. The underlying idea is that at higher temperatures and currents the disorder and consequent decoupling of the vortex segments should become more pronounced, possible leading to $n \rightarrow 0.5$, while for lower temperatures and currents the enhanced coherence could lead to $n \rightarrow 1$. If this is so it would clearly indicate the dependence of the modified flux flow on the degree of coherence of the vortex lines. Secondly, we note that in the microwave experiments in BSCCO [10], the modified flux flow exhibited a maximum as a function of field H. This is clearly an artifact of the functional form of the modified flux flow form. Since this form was observed in the more two-dimensional, low-coherence samples, we speculate that in YBCO samples when the experimental conditions, e.g. higher temperatures and higher current density, reduce the coherence, a maximum may again be observed.

We have also shown in our earlier work [14, 19] that at low field $H_{c1} < H \leq 4$ kOe, there was an anomalous variation in the $V(\theta)$ behaviour. As the angle θ was increased from 0, the total dissipation initially decreased up to an angle which depended on the applied field. This effect has also been investigated as functions of temperature and current. Our previous conjecture, that the effect arises from a flux redistribution between inter- and intragrain regions finds further support.

2. Experimental details

We have used the same sample as was previously [14] studied i.e. $YBa_2Cu_3O_{7-x}$. T_c was 91 K. The dimensions of the sample were $2.4 \times 1.5 \times 12$ mm^3. As mentioned previously [14] this sample showed a predominance of the 123 phase and typical magnetization loops at 77 K showed hysteresis in fields even in excess of 15 kOe. The deviation of the $M(H)$ loop from linearity was at 75 Oe, while the cusp in the $M(H)$ loop was at ≈ 225 Oe. We have carried our $V(I)_T$ and $V(\theta)_{I,T}$ measurements in the temperature range 77 to 86 K. The fluctuations in temperature were of ± 0.2 K. The maximum current applied to the sample was 500 mA. The standard four-probe method was used for all types of transport properties. The contacts were made with silver paste. The contact resistance at room temperature was 3 mΩ.

3. Results

The $V(I)$ characteristics of this sample have been studied in the low-field region 20 Oe $\leq H \leq$ 800 Oe at 80 K, 83 K and 86 K. Typical data at 86 K are shown in figure 1. The data were fit to the expression

$$V = \alpha(I - I_c)^x \tag{2}$$

where I_c is the current for the first measurable voltage recorded, typically 0.5 μV. The value of x lies in the range 3.93 and 1.37 ± 0.03 for this temperature in the above field range. As is clear from figure 2, there is a very rapid drop in x in the low-field region which decreases very slowly after about 200 Oe, a value which lies above H_{c1}. Similar trends were observed at lower temperatures, except that the decrease in x with H is slightly slower e.g. at 80 K, x decreases to about 2.1 at 800 Oe. It is noticeable particularly at $T = 86$ K, that as H increases beyond H_{c1}, the exponent x tends towards one. This trend is clearly noticeable as a function of temperature where the exponent x at $H = 800$ Oe decreases from 2.25 to 1.4 as T increases from 80 to 86 K. The decrease in x with increasing temperature for $H > H_{c1}$ is indicative of a decrease of the effect of flux pinning and increasing tendency of vortices to flow with the flux flow exponent i.e. $n = 1$. Values of x between four and two have been commonly reported [20–22] for the field region where the dissipation is mainly within the intergrain Josephson junction network. The phase slip dissipation derived on the basis of Ambegaokar an Halperin (AH) [23] theory predicts

$$V \propto V_o[I_o[aH^{-y}]]^{-2} \tag{3}$$

where I_o is the zeroth-order Bessel's function and a is a current- and temperature-dependent constant. Fitting our $V(H)$ data at $T = 86$ K and $I = 20$ mA to the above expression, approximated for a small value of the argument, we obtained $y = 0.32 \pm 0.01$. This is consistent with the results of reference [24] where the authors also find that γ, the argument of the Bessel's function, has a $H^{-1/3}$ dependence in the low-field region, and with the discussion in reference [25] where the field dependence of the exponent is shown to vary between zero and one. The latter work reports a $y^{-1/2}$ dependence and suggests that the change from $y = 0$ to $y = 1$ is indicative of increasing interaction between vortices and change of the appropriate correlated volume of vortices. Thus it is clear that a value of $y = 0.33$ is consistent with the discussion in reference [25] for the lower-field regions, or smaller correlated volumes.

3.1. Low-angle anomaly

The second feature investigated is the low-angle anomaly in $V(\theta)$, which we have reported earlier [14, 19]. As the zero-field-cooled (ZFC) sample is rotated with respect to the field, we noticed an initial decrease in voltage (figure 3) before it follows a $\sin^2\theta$ pattern. As previously reported, this dip is not observable in field-cooled (FC) specimens nor does it appear when the angular rotation is reversed ($2\pi \rightarrow 0$). Furthermore this minimum vanishes at large

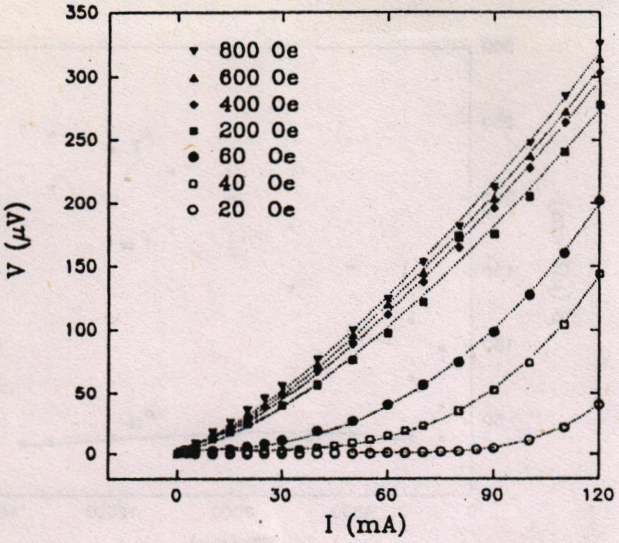

Figure 1. Voltage as a function of current for the YBCO sample at 86 K in different fields. Dotted lines are for the fit to power law (2). The values of x are 3.93, 3, 2.35, 1.45, 1.4 and 1.37 for fields increasing from 20 Oe to 800 Oe.

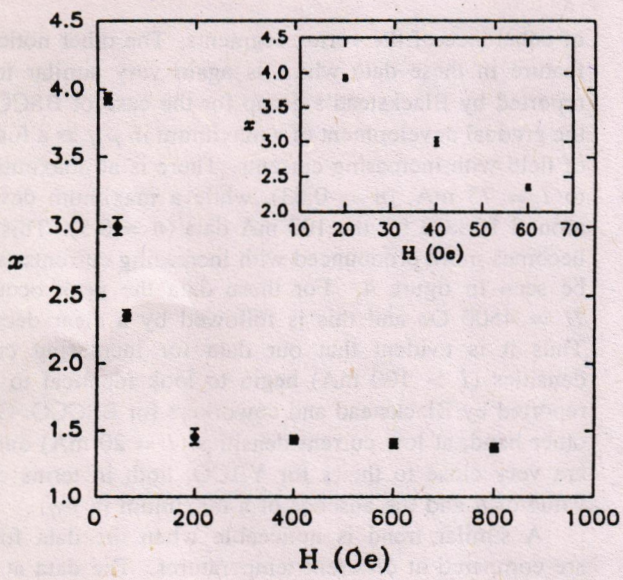

Figure 2. Typical variation of the exponent x (where $V \propto (I - I_0)^x$) as a function of applied field, for $T = 86$ K. The low-field behaviour is shown in the inset.

fields $H \cong 4$ kOe at 77 K. Furthermore there was no such effect for $H < H_{c1}$. All these observations led us to the conclusion that the effect was due to redistribution of flux between inter- and intragrain regions. Immediately after ZFC, the field is highly concentrated in the intergrain region, which on rotation, due to a finite $J \times B$ force ($\theta \neq 0$), drives the flux into the grains. We have extended our experiments to higher temperatures and also varied the currents. In the temperature-dependent data the current was fixed at 50 mA, while the field was 2 kOe. The voltage decreased up to $\theta = 15°$ for $T = 77$ K, and up to 10° for 80 K, while there was a continuous increase, i.e. no minimum, in $V(\theta)$ at 86 K. This clearly

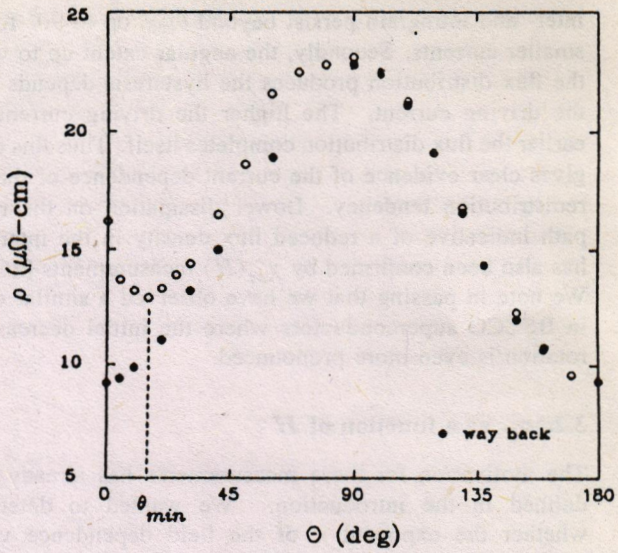

Figure 3. The angular dependence of resistivity at 77 K and $I = 50$ mA in an applied field of 2 kOe. Note the local minimum in ρ at θ_{min}, and the hysteresis between increasing and decreasing angles.

shows that the occurrence of a minimum depends upon temperature. This behaviour is understandable in the sense that with increasing temperature, the flux increasingly enters the grains. This is enhanced by virtue of both low shielding currents and reduced pinning. Hence the inter- and intragrain flux densities tend to become uniform and no redistribution of flux occurs at higher temperatures, e.g. at 86 K and $H = 2$ kOe.

We have also investigated the current dependence of this effect. The temperature was fixed at 77 K while the field was kept at 2 kOe. $V(\theta)$ curves were taken for 20 mA $\leq I \leq$ 150 mA. It was clear from the data that θ_{min} (the angle up to which the voltage decreased) changes with increasing current. θ_{min} was as large as 20° for $I = 20$ mA, became 15° for 50 mA and was finally reduced to 10° for 100 mA. However, beyond 100 mA, up to 150 mA, there appeared to be no change in θ_{min}. The decrease in θ_{min} with increasing J implies that the driving force $J \times B = JB \sin\theta$ becomes large enough at relatively small angles, so as to move the vortices into the grains. The constancy of the angle θ_{min} (at $\approx 10°$) for higher currents ($I > 100$ mA) is not surprising since the flux redistribution requires a finite $J \times B$ force, i.e. a significant angle θ.

The next point about the $V(\theta)$ behaviour is the hysteresis between increasing and decreasing angles. Here we compare the data for θ increased up to 2π and then decreased back from 2π to zero. The data for 50 mA current (figure 3) shows hysteresis between zero and 90°. For higher currents, $I = 75$ mA, this range is reduced to about 45° while for $I = 150$ mA this hysteresis extends only up to 20°. Thus the irreversible behaviour of $V(\theta)$ diminishes as we move towards higher currents. In all cases, the hysteresis follows the same pattern namely the dissipation in decreasing angle is less than the corresponding values in increasing angles. The hysteresis indicates that flux distribution effects between

inter- and intragrain persist beyond θ_{min}, up to 90° for the smaller currents. Secondly, the angular extent up to which the flux distribution produces the hysteresis depends upon the driving current. The higher the driving current, the earlier the flux distribution completes itself. Thus this effect gives clear evidence of the current dependence of the flux redistribution tendency. Lower dissipation on the return path indicative of a reduced flux density in the intergrain has also been confirmed by $\chi'_{ac}(H)$ measurements [26, 27]. We note in passing that we have observed a similar effect in BSCCO superconductors where the initial decrease on rotation is even more pronounced.

3.2. ρ_{ff} as a function of H

The motivation for these measurements has already been defined in the introduction. We wanted to determine whether the exponent n of the field dependence varied in any systematic way with temperature and measuring currents. In particular could we reconcile the value of $n = 0.57$ at 77 K and $I = 100$ mA for our YBCO sample, with those reported by Blackstead and coworkers ($n = 1$) for the same system?

In the measurements to be described, $V(H)$ data were initially taken for $\theta = 0°(J \| B)$ as a function of field between $H = 0$ to 16 kOe. Subsequently, we warmed up and again zero-field cooled the sample to the same temperature, reset θ at 90° and finally measured the voltage in an increasing field. Data were taken at 79.3, 80.7 and 86 K. First we discuss the current dependence of the data at $T = 79.3$ K. Data were taken at $I = 20$, 50, 75, 100, 125, 150 and 200 mA. Figure 4 shows data for ρ_T, ρ_{ps} and ρ_{ff} as functions of field. ρ_{ff} is the difference between the value of voltages obtained at $\theta = 180°$ and 270°, while ρ_{ps} is the value at $\theta = 180°$. ρ_T is equal to the sum of ρ_{ps} and ρ_{ff}. The data shown here are for $I = 200$ mA at 79.3 K. The expressed used to fit ρ_{ff} is the modified flux flow expression, i.e. equation (1).

Since the equation requires the value of H_{c2}, this was obtained from the magnetization curves taken at different temperatures. The reversible magnetization was obtained from the hysteresis loops using the standard prescription [28], after incorporating the superconducting fraction $\eta = 0.22$. The intermediate field equation [29]

$$M_{rev} = \gamma \log \frac{H_{c2}}{H} \qquad (4)$$

was used to fit the data. A value $H_{c2} = 95 \times 10^3$ Oe was obtained for 79.3 K, while lower values were obtained for the higher temperatures. The values for H_{c2} and normal-state resistivity ρ_n were used to determine n from the fit of ρ_{ff} to (1). Interestingly we find for n a value close to 0.9 for 20 mA, which consistently decreased as the current was increased. The variation of n with the current can be seen in figure 5. For the larger currents used, 200 mA, n has decreased to 0.4. Thus it is clear that the exponent n can be made to cover the entire range $0.4 < n < 0.9$, i.e. the range of values quoted for BSCCO and YBCO samples, by varying the current. As discussed earlier in this text, we believe that the decrease of n reflects the increased lack

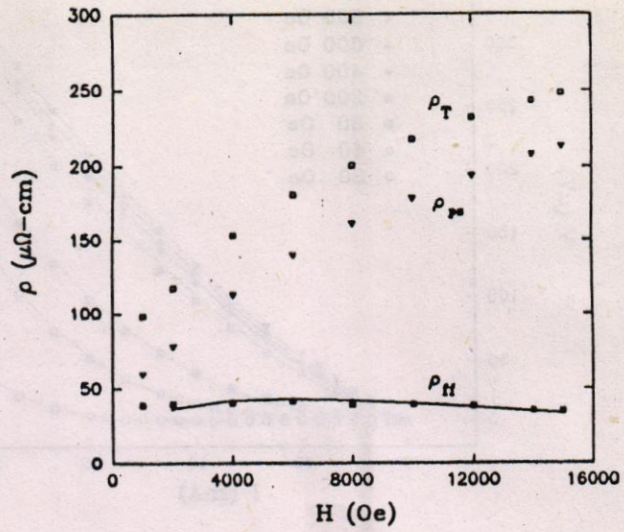

Figure 4. Total (ρ_T), phase slip (ρ_{ps}) and flux flow (ρ_f) resistivities as functions of applied field at 79.3 K and $I = 200$ mA. The solid line is a fit of ρ_f to (1) with $n = 0.46 \pm 0.01$.

of coherence of the vortex segments. The other noticeable feature in these data which is again very similar to that reported by Blackstead's group for the case of BSCCO, is the gradual development of a maximum in ρ_{ff} as a function of field with increasing currents. There is no maximum up to $I = 75$ mA, ($n = 0.63$), while a maximum develops around 10 kOe for the 100 mA data ($n = 0.5$). This peak becomes more pronounced with increasing currents, as can be seen in figure 4. For these data the peak occurs at $H = 4500$ Oe and this is followed by a clear decrease. Thus it is evident that our data for increasing current densities ($I > 100$ mA) begin to look identical to those reported by Blackstead and coworkers for BSCCO. On the other hand, at low current densities ($I = 20$ mA) our data are very close to theirs for YBCO, both in terms of the value of n and the absence of a maximum in ρ_{ff}.

A similar trend is noticeable when the data for ρ_{ff} are compared at different temperatures. The data at 79.3, 80.7 and 86 K were taken at currents $I = 20$ mA. The data for ρ_{ff} are fit to equation (2) and the values of H_{c2} for each temperature are those obtained from the reversible magnetization data. The fit of the data to (1) is indicated in figure 6 for $T = 86$ K. Again we find that the exponent n decreases from 0.87 at 79.3 K, to 0.56 at 86 K. While there is no maximum in ρ_{ff} at $T = 79.3$ K, we do observe a very clear development of a maximum in ρ_{ff} at 86 K at $H = 6$ kOe. With increasing temperatures in this range, the ratio ρ_{ff}/ρ_{ps}, a rough estimate of the relative significance of the two parts of the dissipation, decreases, e.g. $\rho_{ff}/\rho_{ps} = 0.44$ at $T = 79.3$ K. while it is 0.18 at $T = 86$ K, at the same field $H = 84$ kOe (figure 7). Qualitatively, a similar trend has also been observed for this ratio with increasing currents. Thus these data clearly indicate that both with increasing temperature and current, the exponent n decreases from the value of one. Furthermore a maximum in the flux flow resistivity ρ_{ff} as

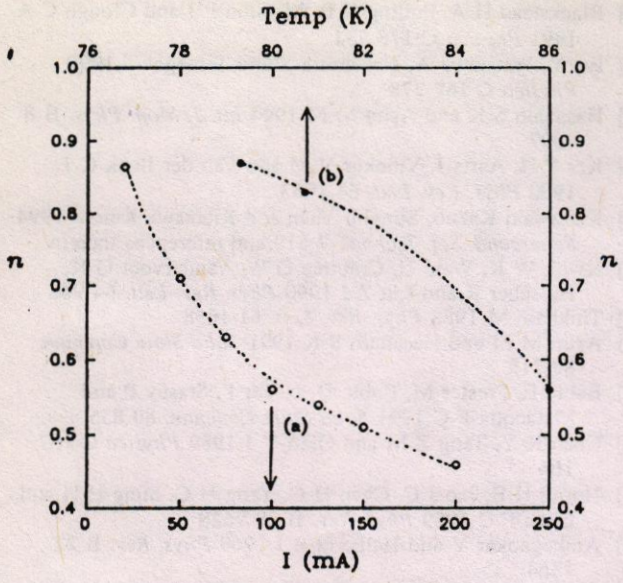

Figure 5. The variation of the n obtained from $\rho_f(H)$ behaviours. (*a*) For different values of transport current at $T = 77$ K. Note that n decreases from almost unity at low currents to almost 0.45 at high currents. (*b*) For increasing temperatures at a fixed current, $I = 20$ mA. The decrease in n with increasing temperatures and currents is apparent. Arrows indicate the relevant axes for each case. Dashed lines are guides to the eye.

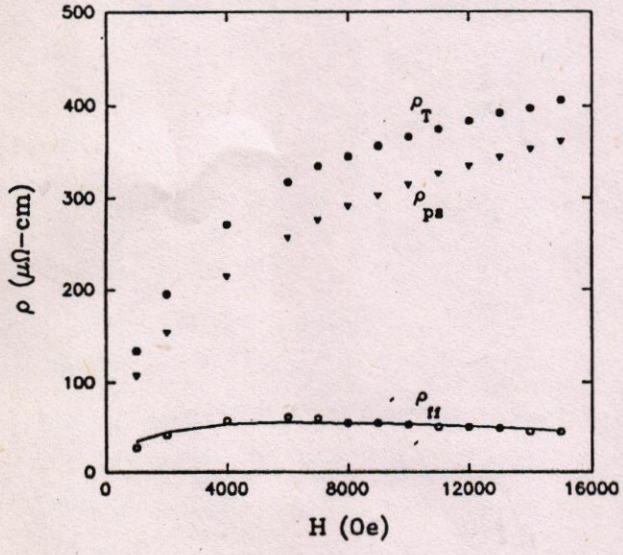

Figure 6. Total (ρ_T), phase slip (ρ_{ps}) and flux flow (ρ_f) resistivities as functions of applied field at 86 K and $I = 20$ mA. The solid line is a fit of ρ_f to (1) with $n = 0.56 \pm 0.02$.

a function of field is observed, indicating that for higher fields flux-flow-type dissipation is suppressed in favour of the angle-independent phase-slip-type dissipation ρ_{ps}.

The decrease of n with increasing current and temperature is understood by us as being reflective of a decrease in the coherence of the vortices or their division into smaller, decoupled segments. The increased degree of disorder, created by the thermal fluctuations or by the

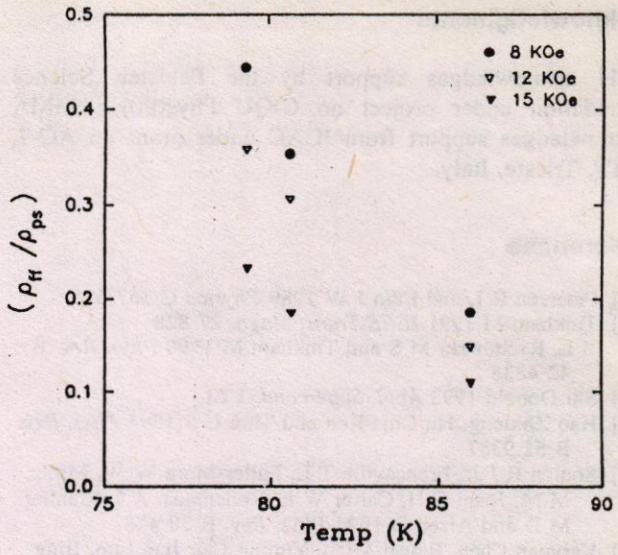

Figure 7. The variation of ρ_f/ρ_{ps} ratio as a function of temperature at different fields and $I = 20$ mA. At higher temperatures the relative significance of the ρ_f component decreases. (Qualitatively, a similar trend is observed with increasing currents.)

larger values of current which has to follow a meandering path in the granular material, is expected to lead to a lack of coherence of vortices along their length. Thus while at 77 K and at low currents $n = 1$, it tends to 0.5 at higher currents or temperatures, similarly to the case of the BSCCO sample. There, this observation was attributed to the two-dimensional pancake-type vortices in the plane. We suggest that the similarity between the results for BSCCO and YBCO at higher currents and temperatures is consistent with the increased disorder driving the YBCO towards increased decoupling of the vortex segments. While no formal justification for the $H^{1/2}$ dependence of ρ_{ff} is known to us, we note that the intervortex separation is expected to vary roughly as $B^{-1/2}$. Thus the $H^{1/2}$ dependence data may be reflective of the increasing density of vortices.

4. Conclusion

Our angle-dependent resistivity measurements on granular YBCO samples yield results which strongly support the model of a modified flux flow, incorporating both the dominant phase slip and a smaller flux flow ($\sin^2\theta$) part. The low-angle anomaly in $V(\theta)$ is also seen to be reflective of the Lorentz force in the sense that for higher currents and fields, the angular extent of the anomaly is reduced. The variation of the flux flow exponent n with currents and temperatures indicates that with increasing disorder of the vortices, the behaviour of the YBCO becomes very similar to that reported for BSCCO. This clearly demonstrates the crucial role of degree of vortex coherence in determining the form of the dissipation. However, a clear reason for the value $n = 0.5$ with increasing disorder in the modified flux flow is not understood.

Acknowledgments

SKH acknowledges support by the Pakistan Science Foundation under project no C-QU Phys(90). MMA acknowledges support from ICAC under grant no AC-7, ICTP, Trieste, Italy.

References

[1] Peterson R L and Ekin J W 1989 *Physica* C **157** 325
[2] Tinkham M 1991 *IEEE Trans. Magn.* **27** 828
Ji L, Rzchowski M S and Tinkham M 1990 *Phys. Rev.* B **42** 4838
[3] Shi Donglu 1993 *Appl. Supercond.* **1** 61
[4] Hao Zhidong, Hu Chia-Ren and Ting C S 1995 *Phys. Rev.* B **51** 9387
[5] Soulen R J Jr, Francavilla T L, Fuller-Mora W W, Miller M M, Joshi C H, Carter W L, Rodenbush A J, Manlief M D and Aized D. 1994 *Phys. Rev.* B **50** 478
[6] Kaiyuan Chen, Baicai Miao, Yiming Cai, Jian Luo, Bing Zhou and Yongjia Qian 1988 *Solid State Commun.* **66** 613
[7] Kim D H, Gray K E, Kampwirth R T and McKay D M 1990 *Phys. Rev.* B **42** 6249
[8] Kim D H, Goldman A M, Kang J H, Gray K E and Kampwirth R T 1989 *Phys. Rev.* B **40** 8834
[9] Kim Y B, Hempstead C F and Strnad A R 1964 *Phys. Rev. Lett.* **12** 145
[10] Blackstead H A, Pulling D B, Keiffer D G, Sanakararaman M and Sato H 1992 *Phys. Lett.* **170A** 130
[11] Blackstead H A, Pulling D B, McGinn P J and Liu J Z 1991 *Physica* C **174** 394
[12] Blackstead H A, Pulling D B, McGinn P J and Clough C A 1991 *Physica* C **175** 534
[13] Iye Y, Watanabe A, Nakamura S and Tamegai T 1990 *Physica* C **167** 278
[14] Hasanain S K and Asim M M 1994 *Int. J. Mod. Phys.* B **8** 4007
[15] Kes P H, Aarts J, Vinokur V M and Van der Beek C J 1990 *Phys. Rev. Lett.* **64** 1063
[16] Kadowaki Kazuo, Songliu Yuan and Kitazawa Koichi 1994 *Supercond. Sci. Technol.* **7** 519 and references therein
[17] Kwok W K, Welp U, Crabtree G W, Vandervoot G K, Hulscher R and Liu Z J 1990 *Phys. Rev. Lett.* **64** 966
[18] Tinkham M 1988 *Phys. Rev. Lett.* **61** 1658
[19] Asim M M and Hasanain S K 1991 *Solid State Commun.* **80** 719
[20] Babic E, Prester M, Babic D, Nozar P, Stasny P and Matacotta F C 1991 *Solid State Commun.* **80** 855
[21] Chen K Y, Tang Z M and Qian Y J 1989 *Physica* C **157** 164
[22] Horng H E, Jao J C, Chen H C, Yang H C, Sung H H and Chen F C 1989 *Phys. Rev.* B **39** 9628
[23] Ambegaokar V and Halperin B I 1969 *Phys. Rev.* B **22** 1364
[24] Wright A C, Zhang K and Erbil A 1991 *Phys. Rev.* B **44** 863
[25] Gaffney C, Petersen H and Bednar R 1993 *Phys. Rev.* B **48** 3388
[26] Hasanain S K and Shahzada S 1995 *Physica* C submitted
[27] Taylor K N R, Wang J and Russel G J 1993 *Mod. Phys. Lett.* B **7** 83
[28] Stancil D D, Schlesinger T E, Stamper A K and Wong D 1988 *J. Appl. Phys.* **64** 5899
[29] See e.g. Tinkham M 1975 *Introduction to Superconductivity* (Tokyo: McGraw-Hill Kogakusha) p 154

ELSEVIER

Physica C 269 (1996) 149–156

PHYSICA C

AC susceptibility hysteresis in granular superconductors

S.K. Hasanain [a,*], Shaista Shahzada [a], A. Mumtaz [a], G.S. Bhatti [b]

[a] *Department of Physics, Quaid-i-Azam University, Islamabad 45320, Pakistan*
[b] *Department of Electronics, Quaid-i-Azam University, Islamabad 45320, Pakistan*

Received 11 April 1996; revised manuscript received 24 June 1996

Abstract

We have investigated the hysteresis in the AC susceptibility of granular YBCO superconductors when the DC field is cycled. A crossover point is observed where the susceptibility χ' in decreasing fields becomes more diamagnetic than for increasing fields, and this is investigated as a function of temperature, AC field amplitude and frequency. The behavior is consistent with the variation of the AC penetration depth with these variables and with a reduced flux density of the intergrain regions on field reversal. The zero field cooled behavior of the second harmonic χ_2 as well as the behavior of χ' in field cooled conditions, are also reported. The DC field dependence of χ' is analyzed using the low amplitude, linear response region approximations.

1. Introduction

The use of a low amplitude AC field (superposed on a large DC field) to investigate the flux penetration in the mixed state of superconductors, is a well established technique [1,2]. In high-T_c materials this technique has also been applied with success in a variety of experiments. Some efforts have also been directed towards investigating the hysteresis of the AC response when the DC field is cycled [3]. Li et al. [4] used the onset of irreversibility of the $\chi'(H_{dc})$ as indicative of the lower critical field of the grains H_{clg}. Taylor et al. [5] explained the qualitative nature of the hysteresis at low fields in granular YBCO sample, as arising from the flux density changes in the intergrain region. This latter explanation was motivated by the observation that on decreasing the field the AC response was more diamagnetic than in increasing fields. They argued that while in the increasing field branch the DC flux is concentrated in the intergrain region, in the decreasing field branch the excess trapped flux within the grains has to close and does so by passing through the intergrain region. This reduces the effective flux density in the intergrain region and a higher AC response is observed.

The above pattern of the hysteresis viz. larger χ' in decreasing fields is therefore expected to be dominant in materials where the granularity is large and the choice of operating variables is such that the AC flux penetration into the grains themselves is very small, i.e. the AC response is dominated by the intergrain behavior. As the AC penetration depth λ increases (e.g. due to decrease of frequency or increase of temperature as in the Campbell (linear) regime [1,6,7]), the AC response will begin to be reflective of the DC flux penetration into the grains

* Corresponding author. Fax: +92 51 21 0256.

PII S0921-4534(96)00444-3

themselves. Thus by varying the parameters which control the penetration depth the AC response, in particular its hysteresis, can be made to be reflective of the inter or intragrain critical state properties.

This is the focus of the present work. We shall show that the AC susceptibility hysteresis in moderate DC fields ($H_{dc} \leq 1$ kOe) reflects both the intragrain pinning and penetration as well as the lower field intergrain hysteresis discussed by Taylor et al. [5]. We observe a definite crossover point in the hysteresis of $\chi'(H_{dc})$ which defines the dominance of inter or intragrain effects. By varying the frequency or amplitude of the AC field or the sample temperature, we are able to observe this crossover effect shift to lower DC field values as the intragrain penetration increases and persists down to lower field values.

We have also investigated the harmonics χ_n of the AC response in superposed DC fields, and their hysteresis. The DC field dependence of χ' in the intragrain region ($H > 250$ Oe) has been analyzed and compared to the behavior expected in the linear response regime. The effects of field cooling on the AC hysteresis and the cross over point have also been studied.

Finally, the hysteresis behavior in the YBCO granular and melt textured samples is compared amongst themselves and also with a weaker pinning BSCCO sample to observe the effects of varying extent of pinning.

2. Experiment

Most of the experimental work has been performed on two granular YBCO samples, labelled YCRA, and YCRE. These were prepared by standard solid state reaction technique and details have been reported previously [8]. The superconducting fraction identified by DC magnetization was approximately 22% for both of them. The YCRA and YCRE samples had dimensions of ($8 \times 2.4 \times 1.5$ mm^3) and ($12 \times 2.3 \times 1.4$ mm^3) respectively. The resistive $T_c(R = 0)$ was at $T = 89$ K while the $\chi'(T)$ and $\chi''(T)$ gave onset point of transition at 91 K.

A typical DC magnetization loop of the sample YCRA indicates significant flux pinning. The width of the $M(H)$ loop, which is understood to be proportional to J_c was found to obey an Anderson–Kim form [8] $\Delta m = [\alpha/(B + B_0)]$ for $H > 250$ Oe. This is to be contrasted to the case of the Bi sample used. The composition for the BSCCO sample used was $Bi_{1.6}Pb_{0.4}Sr_2Ca_2Cu_3O_{9+\delta}$ and it was prepared by standard solid reaction technique. Thereafter it was annealed for over 100 h at a temperature of 865 K. The resistive T_c was 110 K. For this sample the hysteresis loops are fully reversible above $\simeq 1.5$ KOe and the $M(H)$ curve almost passes through zero, when the field is decreased to zero. Thus the BSCCO sample exhibits weaker pinning behavior characteristic of these materials. The difference of pinning will be seen to be reflective in the hysteresis response, both at low and high fields. The $M(H)$ loop for the melt texture grown MT sample has a much larger hysteresis and reflects the stronger pinning. (Details of the sample growth and its characteristics are given else where [9].) Electron microscopy on the melt textured and granular YBCO samples gave average grain sizes of 150 and 5 μm respectively. The presence of voids was also much less for the melt grown samples as compared to the granular samples.

The measurements at 77 K were made in a glass cryostat while for the higher temperature measurements we used an Oxford Instruments, DN-1710 cryostat. The AC susceptibility χ' was measured using a standard balanced coil and self made AC bridge whose output was fed to a lockin amplifier. The harmonics of χ' were studied using a commercial signal analyzer (Advantest model TR 9402). The AC field could be applied in the range 1–20 Oe while the DC field from the solenoidal electromagnet used was in the range $0 \leq H \leq 1100$ Oe.

2.1. Hysteresis in χ'_{ac} with DC field

Firstly, we measured the variation of χ' for increasing AC fields, at some fixed DC field. This was done to ascertain whether the sample is in the linear regime for the combination of T, H, h_{ac} used. At $T = 77$ K, $f = 135$ Hz and $H_{dc} = 500$ Oe the AC magnetization was seen to be linear upto $h_{ac} = 10$ Oe. For a lowered DC field $H_{dc} = 200$ Oe, the response was seen to be linear upto higher AC fields viz. $h_{ac} = 18$ Oe. At elevated temperatures the response begins to get nonlinear even at lower AC

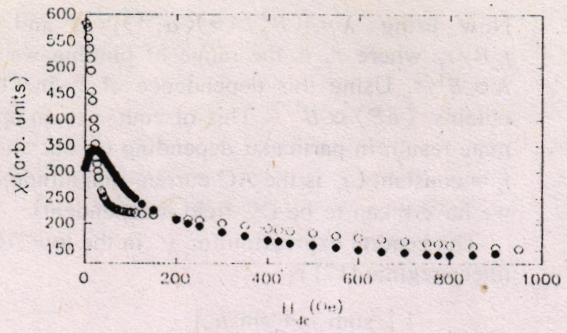

Fig. 1. Variation of the in phase part of AC susceptibility χ' with DC field for sample YCRA at $h_{ac} = 4.5$ Oe, $f = 510$ Hz and $T = 77$ K in ZFC condition. ○ and ● represent the increasing and decreasing field data, respectively.

fields. This is consistent with the weakening of pinning and increased vortex oscillation amplitude δ with increasing temperatures, as discussed by Van der Beek et al. [7] for the low AC amplitude, linear response region. The temperature dependence will be discussed in more detail later. The high value of the DC field ($H_{dc} = 500$ Oe) ensured that the linear response originated from the grains themselves. (Note that the lower critical field of the grains is $H_{clg} \simeq 125$ Oe.) As later data will show the nonlinear response from the *intergrain* region is strongly suppressed at these high fields, but is significant in the region $H < 100$ Oe.

Thus the AC field used in the hysteresis tests were always fixed at values below the nonlinearity onset field to ensure that the intragrain response was linear. In these experiments the DC field is swept, at a fixed f and h_{ac} from 0 to 1100 Oe and back, and hysteresis in χ_{ac} is studied. In Fig. 1 we show the $\chi'(H_{dc})$ data for YCRA, for $h_{ac} = 4.5$ Oe, $f = 510$ Hz and $T = 77$ K. In Fig. 1 the hysteresis of χ' is noticeable. Before discussing this we note that if the field is reversed before $H \simeq 120$ Oe there is no hysteresis in χ'. Since $H_{clg} \simeq 125$ Oe this clearly indicates that as long as the flux is confined to the intergrain region there is no hysteresis in χ'. This is similar to the observation of Lee et al. [4]. We also notice the rapid initial decrease of χ' as H_{dc} is increased. This is understood to be due to flux penetration into the intergrain regions and breakdown of macroscopic shielding currents. This rapid initial variation changes into a slow change beyond approximately 150 Oe i.e., close to H_{c1}. The fie dependence of χ' in this region will be discusse later.

We observe (Fig. 1) that on reversing the field th values of χ' are initially less diamagnetic than fo the field increasing branch. However as the field i reduced below about 200 Oe, the value of χ' i observed to become more diamagnetic than in th increasing field branch. This is the trend observed b Lee et al. [4] and Taylor et al. [5] and has bee explained by the latter as being due to the cancella tion of part of the intergrain fields by the reverse fields due to the closure loops of the trapped intra grain flux. It is apparent that when the field i reversed at e.g., 1 kOe, the response is initiall dominated by the large quantity of flux trapped i the grains, leading to a higher flux density B, an consequently to a lower value of χ' on the descend ing field branch. This trend changes at $H \sim 200$ Oe (the crossover point) where the net response may be said to change from being dominated by the intra-grain to the intergrain. This is understandable because the reduced flux density in the grains implies a small AC penetration depth $\lambda = [(B^2/4\pi)\langle \alpha_L^{-1} \rangle]^{1/2}$ [7] where α_L is the Labusch constant [10]. Thus at low flux densities B, AC response is dominated by the intergrain region.

2.1.1. *Effect of AC amplitude*

We next studied the effect of variation of h_{ac} on the crossover point. All the data was taken on one of the polycrystalline samples YCRA. At fixed frequency $f = 135$ Hz and temperature $T = 77$ K there is a clear shift in the crossover point with varying AC field values e.g., at $h_{ac} = 1.84$ Oe the crossover occurs at $H_{dc} = 300$ Oe, whereas at $h_{ac} = 3.75$ Oe, 7.44 Oe, and 9.92 Oe the crossover occurred at $H_{dc} = 175$ Oe, 110 Oe and 100 Oe respectively, while there is no crossover for $h_{ac} = 15$ Oe (i.e., χ' is always less diamagnetic on the way back). In general we found that increasing h_{ac} pushed the crossover point to lower DC field values. We explain this behavior by noting that the pinning of flux in the intergrain region is itself a function of h_{ac}. For large AC amplitudes the intergrain pinning is negligible and the hysteresis is dominated by the higher flux density of grains on field decrease.

2.1.2. Effects of temperature

We further studied the trend by varying the temperature of the sample. Since increasing the temperature will act to increase the penetration depth in the grains we would expect the crossover point to shift to lower DC fields. At a temperature of 83 K, and $h_{ac} = 7.44$ Oe, the crossover had shifted to 74 Oe (from 110 Oe at 77 K). On further increasing the temperature no crossover could be seen. At this point we reduced the AC amplitude to 3.75 Oe, and again obtained a crossover at 70 Oe. (Note that at 77 K, the crossover for $h_{ac} = 3.75$ Oe occurs at 175 Oe.) Thus it is evident that the crossover shifts to lower AC and DC fields as the temperature is increased, consistent with larger penetration depth.

2.1.3. Effects of frequency

We further sought to confirm the trend of penetration into the grains using frequency as a variable. In the linear regime, $\lambda_{ac} \propto \omega^{-1/2}$ [7] for frequencies where viscous damping effects are nonnegligible i.e., with increasing frequency the higher velocities and increased viscous forces $F \sim -\eta v$ [11] damp out the AC field closer to the surface of the grains. Thus with increasing frequencies we expect the flux penetration into the grains themselves to become negligible at relatively higher DC fields, as λ_{ac} becomes progressively smaller. This implies that the crossover field (which essentially indicates the field below which the intergrain hysteresis dominates) should shift to higher values with increasing frequency. This is the actual trend we observe. Data were taken at 77 K in the region $93 < f < 1060$ Hz, with $h_{ac} = 4$ Oe. The crossover field increased (linearly) over this range of frequency from $H_{dc} = 85$ to 225 Oe, consistent with the expectations.

2.2. DC field dependence of χ'_{ac}

We further analyzed the field dependence of χ' in the light of linear response model. We recall that in this region the AC flux penetration is given by [7] $\delta B = h_{ac} e^{-x/\lambda}$. Averaging over x and using the approximation $D \gg x$, (where D is half the sample thickness), we obtain

$$\langle \delta B \rangle \cong h_{ac} \lambda / D. \tag{1}$$

Now using $\lambda = [(B^2/4\pi)\langle \alpha_L^{-1} \rangle]^{1/2}$, and $\alpha_L = j_c B / r_f$ where r_f is the range of pinning we obtain $\lambda \propto B^{1/2}$. Using this dependence of λ in (1), one obtains, $\langle \delta B \rangle \propto B^{1/2}$. This of course is an approximate result, in particular depending on our choice of j_c = constant (j_c is the AC current magnitude, which we have taken to be DC field independent).

The general expression for χ' in the low AC field linear regime [12] is

$$4\pi\chi' = \frac{1}{u}\left[\frac{\sinh u + \sin u}{\cosh u + \cos u}\right] - 1, \tag{2}$$

where

$$u = \frac{d}{\lambda} = \left[\frac{\omega}{\rho}\frac{2\pi d^2}{c^2}\right]^{1/2}, \tag{3}$$

d is the sample size and ρ the resistivity.

Simplification of Eq. (1) for the case $u = d/\lambda \gg 1$ yields

$$4\pi\chi' \simeq \frac{1}{u} - 1. \tag{4}$$

If the resistivity ρ follows a power law, e.g., if $\rho = KB^n$ (K is a constant factor), then substituting ρ in Eq. (3) and the so obtained $u(B)$ in Eq. (4) yields

$$\chi' = \chi_0\left[1 - \frac{B^{n/2}}{a}\right], \quad (\chi_0 = -1/4\pi). \tag{5}$$

Here a is a frequency dependent constant. For example in the thermally activated flux flow (TAFF) regime [13] where $\rho \propto B$,

$$\chi' = \chi_0\left[1 - \frac{B^{1/2}}{a}\right]. \tag{6}$$

Thus we have fit the data $\chi'(H_{dc})$ for both field increasing and decreasing branches to the expression $\chi' = \chi_0[1 - H^n/a]$. We leave n and a as fit parameters to be obtained from the fit.

In Fig. 2 we show the results for both increasing and decreasing field branches. Here $h_{ac} = 4$ Oe and $f = 510$ Hz. The data is fit above 200 Oe to exclude the contribution from the intergrain part. We obtain $n = 0.36$, $a = 20.2$ for the field decreasing branch, while $n = 0.32$, $a = 20.25$ for the field increasing

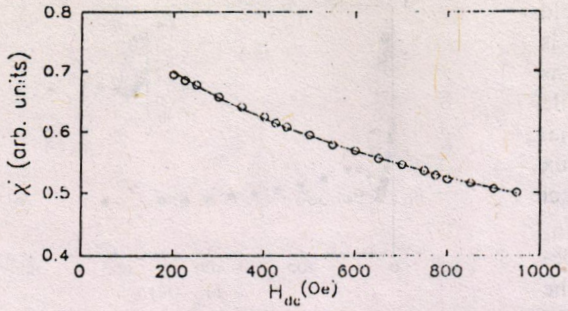

Fig. 2. Expanded part of Fig. 1 for the case of increasing DC field. Solid line is the fit to Eq. (6) (see text).

branch. There is an implicit simplification when Eq. (5) is applied to the granular samples, i.e., while the actual flux penetration take place in both the inter and intragrain regions, Eq. (5) assumes a uniform flux penetration. Thus our application of Eq. (5) to the data implicitly uses a response averaged over the two regions.

The value of $n = 0.36$ obtained from our fit can be compared to the $n = 0.5$ predicted on the basis of $\rho \propto B$, in Eq. (5) and the discrepancy most probably is due to the effect of granularity discussed above.

2.3. *Effect of field cooling on* $\chi'_{ac}(dc)$

It is well known [14,15,16] that field cooling of a granular superconducting sample produces new rearrangement and distribution of flux density compared to the zero field cooling situation. Therefore we may expect field cooling to influence the AC susceptibility and its hysteresis.

The field cooling tests were performed on the piece of granular YBCO sample labelled as YCRE. For zero field cooling condition, and $h_{ac} = 5.5$ Oe, the $\chi'(H)$ curve displayed the crossover effect at 60 Oe. All field cooled data were also taken at $h_{ac} = 5.5$ Oe. The cooling fields used were 40, 80, 120 Oe respectively. After cooling the sample to 77 K in the required field (e.g. 40 Oe) and allowing to stabilize, the field was raised to the maximum value. For the 40 Oe data the maximum field applied was 300 Oe, while for 80 and 120 Oe, the maximum field applied was 400 Oe. The data for $H_{FC} = 40$ Oe is shown in Fig. 3.

Three features distinguished this data from zero field cooled ZFC data. Firstly the value of diamagnetic signal increased significantly compa to the ZFC data at the same AC and DC fields e. the value obtained at 40 Oe after field cooling 12% higher than that for ZFC case. Similarly af 80 Oe field cooling the value is 7% higher, while 120 Oe there is again an almost 12% increase. Th in contrast to the DC magnetization data whi always shows *less* diamagnetism in the field cool condition, the χ'_{ac} data indicates lesser flux penet tion or higher diamagnetism.

Secondly we note that in the field cooled case t crossover effect moves to slightly higher DC fie values e.g., at $H_{FC} = 40$ Oe the crossover occurs $H \sim 70$ Oe while for $H_{FC} = 80$ and 120 Oe it o curred at 90 and 120, respectively. Thirdly we no that after field cooling there is a field region whe χ' actually increases slightly as H_{dc} is increase This trend is most evident in the $H_{FC} = 120$ Oe da where χ' increases with H_{dc} between 120 and 20 Oe. For lower cooling fields the effect though pr sent is small.

The first effect of field cooling, viz. higher χ', i explained by us on the basis that the flux trappe during cooling is primarily within the grains (due t their stronger pinning) while the *intergrain* flu density is actually *lower* than for the ZFC case Thus the low amplitude AC fields, (particularly a low DC fields), being confined to the intergrai region, "see" a lower DC flux density and penetrat

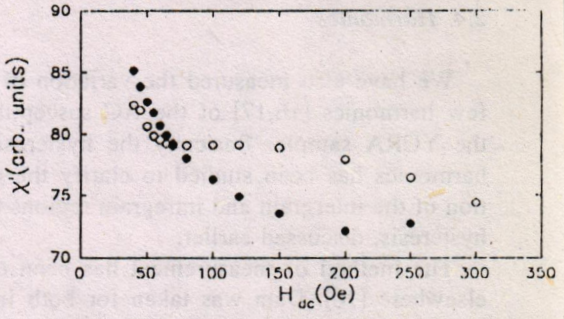

Fig. 3. Variation of χ' with DC field sweep for the YCRE sampl cooled in a DC field of 40 Oe, $h_{ac} = 5.5$ Oe and $f = 135$ Hz ○ and ● represent the increasing and decreasing field data respectively.

lesser ($\lambda \propto B$). Secondly, we note that the field cooled flux density within the grains themselves is expected to be lower near the surface region as compared to the bulk. Thus the flux density profile of the F.C. grains should be quite different from that of the ZFC case in increasing fields, where the flux is more concentrated at the surface. This latter effect is borne out by the observation that even for $H > H_{clg}$ (e.g. at 300 Oe), there is significant difference between ZFC and FC χ' data. The χ' value for the F.C. case is higher, i.e. more diamagnetic, for the FC case than for the ZFC case. The lowered DC flux density close to the grain surface results in a smaller penetration depth λ_{ac} and hence a more diamagnetic AC response, for the FC case.

The second point viz. the shift of crossover effect to higher fields on field cooling is consistent with the above discussion. Lower DC flux density in the surface region of the grains, enables the contribution of the intergrain region to χ' to remain significant up to even higher DC fields. Finally, the observation of a region of increasing χ' with increasing H_{dc} is also consistent with the above discussion. Once the applied field becomes higher than H_{clg}, there is apparently a tendency [8] to move the flux from inter to intragrain regions (because of lower flux density in the surface region of the grains). This initially results in a reduced flux density in the intergrain region, which decreases λ and δB and increases χ'. As the field is further increased this effect is over come by the net increase in δB and χ' begins to decrease. (e.g. at ~225 Oe in the 120 Oe field cooled data).

2.4. Harmonics

We have also measured the variation of the first few harmonics [16,17] of the AC susceptibility for the YCRA sample. Basically the hysteresis in the harmonics has been studied to clarify the contribution of the intergrain and intragrain regions to the χ' hysteresis, discussed earlier.

The method of measurement has been described elsewhere [16]. Data was taken for both increasing and decreasing fields in the ZFC condition.

Typical data for the second harmonic χ_2, with $f = 135$ Hz, $h_{ac} = 3.2$ Oe is shown in Fig. 4. Inset shows the low field hysteresis. We observe that χ_2

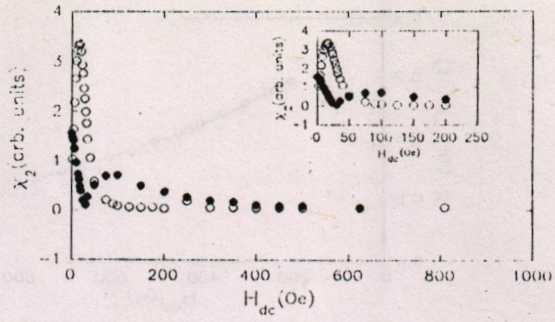

Fig. 4. Variation of the 2nd harmonic with DC field sweep, $h_{ac} = 3.2$ Oe, and $f = 135$ Hz. Inset shows expanded portion at low fields. ○ and ● represent the increasing and decreasing field data, respectively.

initially increases rapidly and then decreases continuously with increasing field and is almost negligible after ~100 Oe. In the decreasing field branch the signal becomes non zero at H ~ 350 Oe and is consistently *higher* than the increasing field values down to $H \sim 60$ Oe. We explain these features in the following terms. The initial increase of χ_2 and its subsequent decrease after the maximum are well established [16,17]. (The decline after the maximum is understood to be due to the decrease of J_c with field.)

The almost negligible values of χ_2 at higher DC fields, where the intragrain flux penetration is dominant, clearly shows that the intragrain response is linear.

The hysteresis in χ_2 is also fully consistent with the previous discussion. Note that the values of χ_2 in decreasing branch are higher than for the increasing field branch i.e., the effective or local field in the intergrain region are *lower* in *decreasing fields*. This follows from the fact that the second harmonic amplitude decreases with increasing DC flux density in this field region, $H > H^*$, where H^* denote the field for which χ_2 becomes maximum. Thus the *higher* values of χ_2 on decreasing field branch are indicative of *lower* effective fields. Note that if this contribution to the harmonics had been from the intragrain part, we would have obtained a lower value of χ_2 consistent with the higher flux density of grains due to the trapped flux in decreasing fields.

The third and fourth harmonics were also studied and led to the same conclusion viz. lower intergrain flux density on field decrease.

2.5. Hysteresis effects in textured (123) and bismuth samples

Finally we mention in comparison the hysteresis behavior in melt textured YBCO labelled as MT and the granular BSCCO samples. As discussed earlier the melt textured sample has larger grain sizes, higher density (less porosity) and larger flux pinning than the polycrystalline YCRA sample. The field dependence of χ' for this sample was much less than for the YCRA sample e.g., between 0 and 1 kOe there was barely a $\sim 4.6\%$ decrease of χ' as compared to 75% for the YCRA. Secondly, there is no rapid penetration of AC field at very low fields which is the characteristic of the intergrain region. Finally for most of the field range there is no hysteresis. On decreasing fields down to below 600 Oe from 1100 Oe there is a very small amount of hysteresis indicating slightly lower χ' (higher DC flux density) in decreasing fields. At most there is 1% hysteresis ($\Delta\chi'/\chi_0'$), where χ_0' is the value of χ' at $H = 0$ Oe. There is obviously no crossover effect in χ'.

The absence of the crossover effect and absence of hysteresis are explainable on the basis of low granularity and low intragrain penetration depth respectively. The absence of an extended intergrain region implies that the χ' response is essentially due to grains. The larger pinning forces in the case of the melt textured sample imply a smaller intragrain penetration depth. This can be seen from the expression $\lambda_c \sim [(B^2/4\pi)\langle \alpha_L^{-1}\rangle]^{1/2}$, i.e., λ_c decreases as the pinning force parameter α_L increases. Hence the AC field is more completely confined to the surface regions, where the magnetization is dominated by the equilibrium behavior. Hence the reversibility in the case of melt textured sample. We also conducted $\chi'(H_{dc})$ hysteresis test on the BSCCO sample with similar average grain sizes as in the case of YCRA. The $M(H)$ loop of the sample is fully reversible for the fields greater than 1 kOe. The noticeable point is the weak pinning of this sample as well as its granularity. The behavior of the χ' hysteresis in this sample is very similar to the strong pinning melt textured sample i.e., no hysteresis at high fields, and finally some small hysteresis below 175 Oe (Fig. 5). The sense of the hysteresis is also similar to that of the melt textured sample i.e., the value of χ' in the decreasing branch is less.

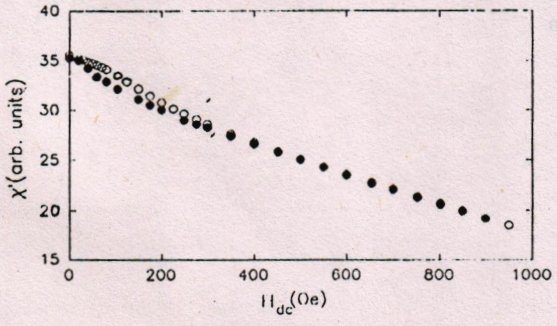

Fig. 5. $\chi'(H)$ for Bi sample, with $h_{ac} = 6$ Oe, $f = 135$ Hz. ○ and ● represent the increasing and decreasing field data, respectively.

The absence of hysteresis or any crossover effects in this sample are understandable in terms of very weak pinning and hysteresis of both inter- and intragranular flux. The very small quantity of inter- and intragrain pinned flux ensured negligible hysteresis.

Thus we conclude from the data on MT and BSCCO samples that at low AC fields hysteresis effects are negligible both in the relatively stronger pinning melt textured samples where λ_c is very small and only reversible surface flux is measured, and for the very weak pinning bismuth samples. The absence of flux density hysteresis even in the bulk of the bismuth sample, ensures a more or less hysteresis free AC response. It is in the moderate pinning and granular YBCO that one sees both the hysteresis and the crossover from intra- to intergrain dominated response.

3. Conclusion

We have seen that the AC susceptibility hysteresis in granular (ceramic and melt textured) samples varies in accordance with the role of both inter- and intragrain regions. At low amplitude AC fields the penetration depth λ_{ac} is the main physical quantity which determines the response. λ_{ac} in turn is understood to depend on the flux density, temperature and frequency. Hence the net response, i.e., the sum of the inter- and intragrain responses exhibits a field dependence and hysteresis which reflects the effect of the above variables on λ. We obtain a $\chi' \propto [1 - B^n]$ ($n \simeq 0.34 \pm 0.05$) dependence which appears ex-

plainable on the lines of a power law behavior of the resistivity $\rho \propto B^{2n}$. The variation of the crossover point with temperature, h_{ac} and f, are also consistent with the low amplitude (linear response) theory indicating that as the intragrain penetration increases, the crossover point shifts to lower DC fields. The crossover point thus serves as a rough guide of the DC fields above which the intragrain flux density variation dominates the net response. The harmonic response also confirms the explanations outlined above viz. lowered flux density of the intergrain region in the field decreasing branch of the $\chi'(H)$ data.

Differences between FC and ZFC data, show that while DC magnetization indicates a higher flux density, the AC response is consistent with a lowered flux density, because the AC response is sensitive to the surface or intergrain region where the FC samples apparently have lowered flux density values.

We observe that the complex pattern of hysteresis is observable in materials which have significant degree of intragrain penetration as well as some degree of intergrain pinning. The melt textured and BSCCO samples do not show any such complex behavior for different reasons as explained in the text.

Finally we note that this work has been confined to the low amplitude linear response regime. We intend to extend the studies to observe how the hysteresis behavior changes as the field begins to excite the non linear regime.

Acknowledgement

A. Mumtaz is supported by a grant from Pakistan Science Foundation PSF-C:QU-Phys-90; S. Shahzada is supported by a grant from Mrs. Mumtaz Riazuddin Pre-doctoral Fellowship.

References

[1] A.M. Campbell, J. Phys. C 2 (1969) 1492.
[2] R.W. Rollins, H. Kupfer and W. Gey, J. Appl. Phys. 45 (1974) 5392.
[3] K.H. Muller, Physica C 159 (1989) 717.
[4] C.Y. Lee, L.W. Song and Y.H. Kao, Physica C 101 (1992) 429.
[5] K.N.R. Taylor, J. Wang and G.J. Russell, Mod. Phys. Lett. B 7 (1993) 83.
[6] A.M. Campbell and J.E. Evetts, Adv. Phys. 21 (1972) 199.
[7] C.J. Van Der Beek, V.V. Geshkenbein and V.M. Vinokur, Phys. Rev. B 48 (1993) 3393.
[8] S.K. Hasanain and M. Asim, Int. J. Mod. Phys. B 8 (1994) 4007.
[9] G.H. Khosa, S.K. Hasanain and A.N. Kayani, Supercond. Sci. Technol. 8 (1995) 534.
[10] R. Labusch, Crystal Lattice Defects 1 (1969) 1.
[11] J. Bardeen and M.J. Stephen, Phys. Rev. 140 (1965) 1197A.
[12] G. Blatter, M.V. Feigel'man, V.V. Geshkenbein, A.I. Larkin and V.M. Vinokur, Rev. Mod. Phys. 166 (1994) 1125.
[13] P.H. Kes, J. Arts, J. Van der Berg, C.J. Van der Beek and J.A. Mydosh, Supercond. Sci. Technol. 1 (1989) 242.
[14] D. Lopez and F. de la Cruz, Phys. Rev. B 43 (1991) 11478.
[15] L. Ji, M.S. Rzchowski, N. Anand and M. Tinkham, Phys. Rev. B 47 (1993) 470;
L. Ji, M.S. Rzchowski and M. Tinkham, Phys. Rev. B 42 (1990) 4838.
[16] S. Manzoor, S.K. Hasanain and M.A. Noman, Int. J. Mod. Phys. 9 (1995) 177.
[17] C. Jeffries, Q.H. Lam, Y. Kim, L.C. Bourne and A. Zettl, Phys. Rev. B 37 (1988) 9840;
K.H. Muller, J.C. Macfarlane and R. Driver, Physica C 158 (1989) 69;
S.F. Wahid and N.K. Jaggi, Physica C 194 (1992) 211.

ELSEVIER

Physica C 272 (1996) 43–50

PHYSICA C

Peak shifts in magnetization rotation effects of anisotropy and pinning

S.K. Hasanain *, Sadia Manzoor, M. Aftab

Department of Physics, Quaid-i-Azam University, Islamabad 45320, Pakistan

Received 29 July 1996; revised manuscript received 1 October 1996

Abstract

Magnetization rotation experiments have been performed on a melt-textured $YBa_2Cu_3O_{7-x}$ sample in the field cooled and zero field cooled conditions. The data show significant shifts of the maxima and minima from their expected positions in $M(\theta)$, both in increasing angles as well as on the reversal of the sense of rotation. Our results have been explained using the concepts of the anisotropy of the flux line energy and the intrinsic torque within the framework of the generalized critical state model, which invokes the idea of a flux orientation gradient in addition to a gradient of flux density.

1. Introduction

Magnetization rotation measurements are among a wide variety of experiments performed on high T_c superconductors to explore their magnetic anisotropy [1–4]. In these experiments a sample with bulk anisotropy is rotated with respect to a fixed field direction and the magnetization component along the field direction is measured for different angles θ between the field and the reference c-axis. By varying the experimental parameters, e.g. field cooling, zero field cooling, temperature etc., one can obtain information both on the anisotropy of magnetization and pinning. Theoretical and experimental studies of pinning free samples have yielded additional information on the intrinsic torque in the HTSC [5–7]. Related to this are the ideas of the anisotropy of self energy and line tension. The first of these viz. the self energy E of a vortex is understood to be minimum for H lying in the ab-plane and maximum for $H \parallel c$-axis. The line tension $(\partial^2 E/\partial\theta^2)$ (which is essentially a measure of the ease of rotation of the line at a given orientation), is however a maximum for $H \parallel ab$-plane and minimum for $H \parallel c$. In other words, moving a line away from the ab-plane is energetically more difficult than moving it away from the c-direction.

It will be shown that our results for magnetization rotation in YBCO samples are explainable in terms of the anisotropy of these physical quantities. We shall show that the angular dependence of magnetization, in particular the position of maxima and minima are shifted systematically from their expected positions in a manner consistent with the anisotropy of the line energy and line tension. While our samples are not pinning free, it will be seen that as long as the sense of rotation (clockwise or anticlockwise) is not changed, the peak position for the applied field $H_{app} \perp c$ are shifted towards lower angles while the peak at $\theta = \pi$ or $H_{app} \parallel c$ is almost unaffected. The field dependence of these shifts and their analysis form a major part of this study. A

* Corresponding author.

PII S0921-4534(96)00557-6

second part of this study focuses on the hysteresis in $M(\theta)$ on reversal of the sense of rotation and its temperature and field dependence. This latter aspect is explained in terms of a generalized critical state involving the gradients both of the flux density and the flux orientation. We show that the reversal of sense of rotation has a pronounced effect on the $M(\theta)$ behavior thereafter. This effect of reversal is seen to be confined to a limited angular range, whereafter the peak positions occur *at the same intervals*, though not at the same positions as on the way up.

At this point we shall elaborate the generalized critical state model referred to above. This model was developed originally by Boyer et al. [9,10], and has been widely used in both experimental and theoretical investigations [11–14]. In this picture when a hysterectic type-2 material is rotated with respect to a magnetic field, the penetration of flux within the superconductors occurs in the following way. The flux closest to the surface remains aligned along the field direction, while deeper within it is tilted away from the field and towards the original orientation of the sample. Thus with respect to orientation, the flux is divided into two regions, (a) a core region which lies deeper within the sample and where the flux rotates rigidly with the sample, and (b) a shoulder region where the flux orientation varies form being along the field at the surface to being parallel to the core direction at its extremity. Thus in the shoulder region there exists a *gradient of the flux orientation* $\partial\psi(x)/\partial x$ where ψ is the orientation of flux with respect to the field at a distance x inside the sample.

As rotation progresses, the shoulder region extends inwards until either:

(a) the flux density $B(x)$ in the shoulder becomes zero at some $|x| < D/2$, where D is the sample dimension across which flux is penetrating, while the mid-plane of the sample is straddled by the core, or

(b) the expanding shoulders meet at the mid-plane of the sample.

(a) occurs if the applied field $H_{app} < H^*$, the penetration field of the sample, while for (b) to happen $H_{app} \geq H^*$. Once either of these states is reached, the sample is said to be in a quasi-steady state defined by a critical angle of rotation θ_c. Further rotation of the sample does not bring about any change in $\partial\psi(x)/\partial x$.

It follows from the above that for *isotropic materials* and $H_{app} \geq H^*$, rotation beyond θ_c would be manifested by a constant value of M. For an anisotropic material however the region above θ_c would also show variation in M as different orientations of the sample with respect to H produce different magnetizations. On the other hand for $H < H^*$, where a core of pinned flux persists even above θ_c, we would observe an in addition a superposed cos θ type contribution from the rigidly rotating core region on a vibrating sample type magnetometer.

In our context where we have a melt textured YBCO sample with bulk pinning and anisotropy, the above ideas of the generalized critical state imply that on rotation of the sample the flux could not in general be aligned along the applied field direction, e.g. if the orientation of the sample is at $H \perp c$ (after rotation through 90°), then the flux lines within it would be tilted away from this $H \perp c$ orientation as we go in deeper. Since the generalized critical state model takes into account flux density as well as flux orientation gradients,

$$J = J_{\parallel} e_{\parallel} + J_{\perp} e_{\perp},$$

where $e_{\parallel}$ and $e_{\perp}$ are unit vectors parallel and perpendicular to the applied field respectively. The parallel and perpendicular components of the current density are defined as follows [12]:

$$J = (B/\mu_0)\partial\psi(x)/\partial x,$$

$$J_{\perp} = (-1/\mu_0)\partial B(x)/\partial x.$$

Both $J_{\parallel}$ and $J_{\perp}$ are limited by a critical value J_c: for $J_{\perp} > J_{c\perp}$ flux flow will ensue, and $J_{\parallel} > J_{c\parallel}$ leads to the onset of flux cutting.

When the sense of rotation is reversed, hysteresis will be developed. This has been demonstrated by Cave et al. [11]. Essentially the idea is that on reversal of the sense of rotation, the original shoulder region gets divided into two parts (see Fig. 1). In the part close to the surface $x < x_0$, flux has a angular gradient in one sense while for $x > x_0$, where the changes have not yet propagated, the gradient retains the original sense. As the reversal is continued the new shoulder extends deeper and eventually extends over the entire sample. Thus it is obvious that $M(\theta)$ behavior would exhibit hysteresis immediately following reversal of sense of rotation.

2. Experimental procedure

The measurements have been carried out on a $Y_1Ba_2Cu_3O_{7-x}$ sample grown by the standard melt texture procedure. Details of preparation are given in Ref. [4]. The dimensions of the sample used were $a = 3$ mm, $b = 3$ mm and $c = 1.8$ mm where a, b, c refer to the crystalline a, b, c axes respectively.

The magnetization measurements reported were carried out on a vibrating sample magnetometer (VSM) which enabled the rotation of he sample relative to the applied field. The sample was mostly rotated in 5° or 10° steps from its initial state and corresponding M values were obtained. The accuracy of θ measurement is 1°. We obtained the data on the rotation of the sample under the zero field cooled (ZFC) condition and field cooled (FC) condition. The experimental procedures of these conditions are described in Ref. [4].

3. Results

3.1. Field cooling

We first describe the data obtained after field cooling the sample. The data is shown in Fig. 2 for applied fields H_{app} equal to 23 Oe, 100 Oe and 200

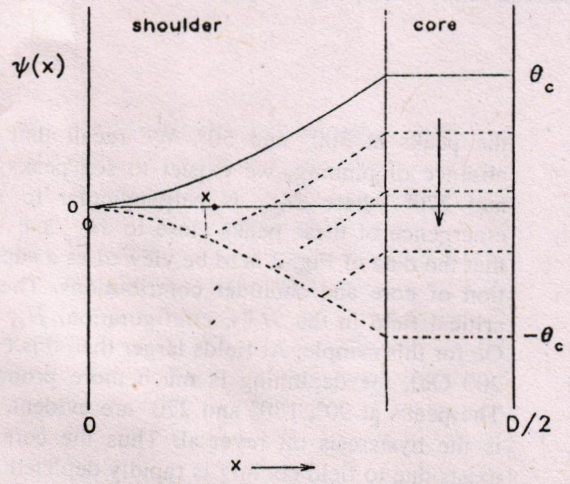

Fig. 1. Flux orientation profiles $\psi(x)$ in the generalized critical state model for increasing angles (—), and upon reversal of rotation (- - - - -).

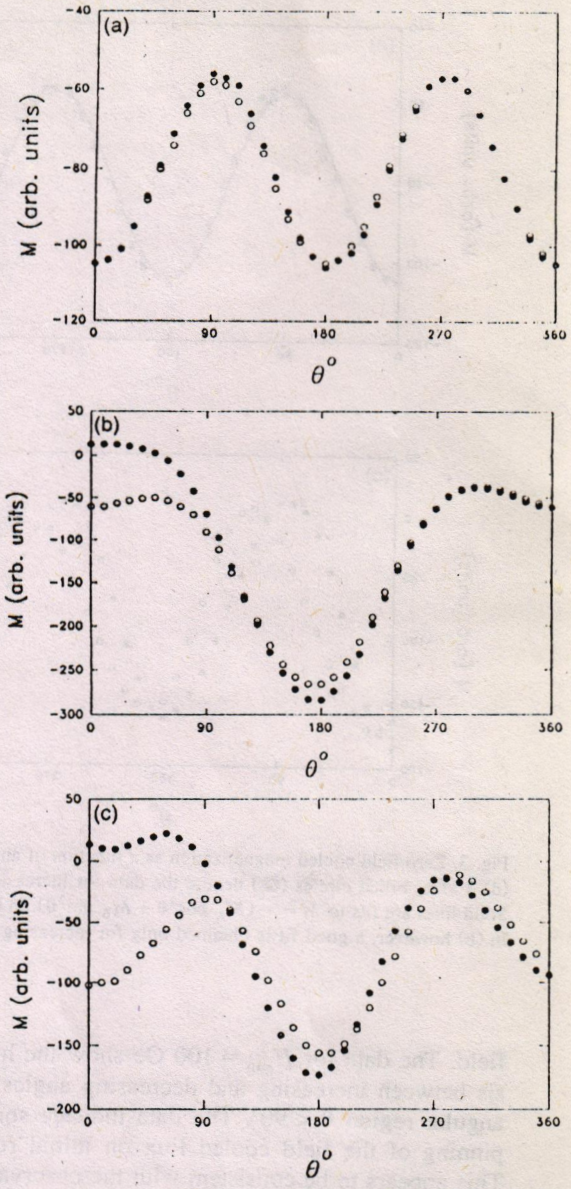

Fig. 2. Variation of the field cooled magnetization M with angle for applied field parallel to the c-axis H_{app} = (a) 23 Oe, (b) 100 Oe (c) 200 Oe. Data is shown for increasing angles (●) and upon reversal of rotation (○).

Oe ($H_{app} \parallel c$-axis). For the lowest field $M(\theta)$ varies as a cosine function indicating rigidly pinned flux as one would expect from the core region. Note that there is no indication of a shoulder region at this

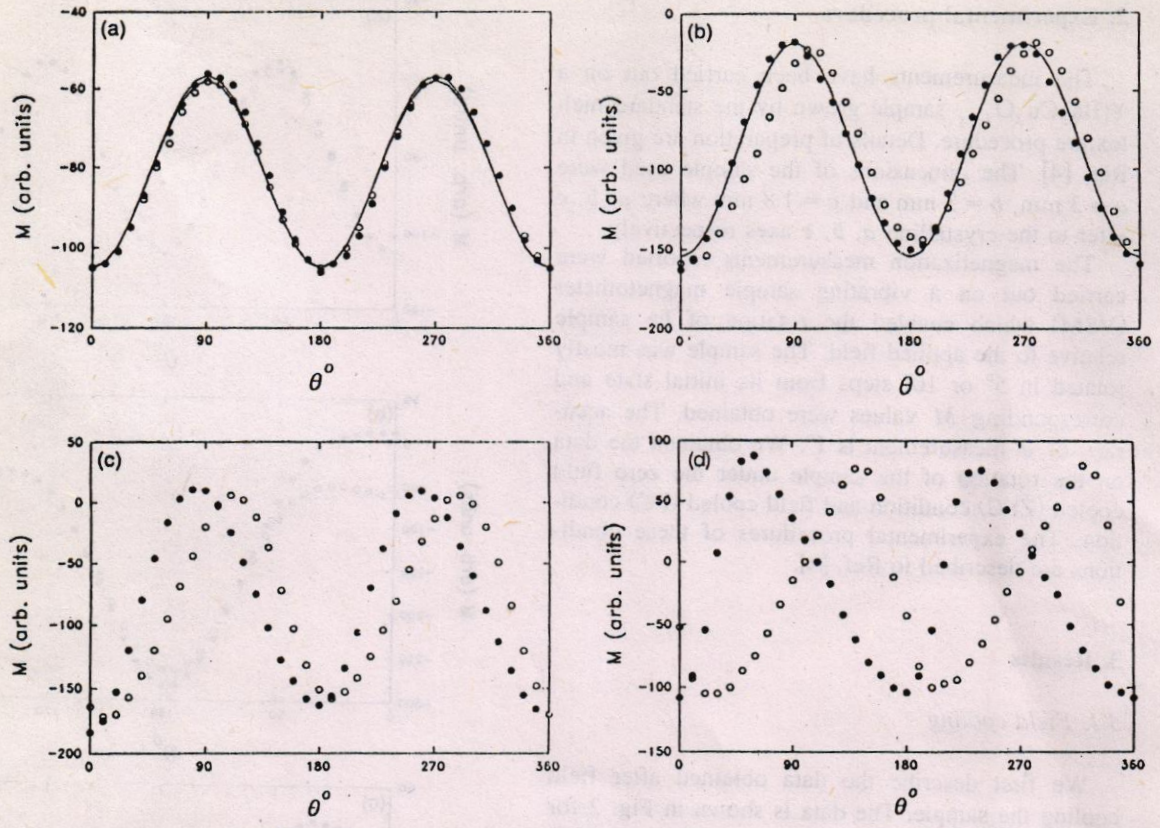

Fig. 3. Zero field cooled magnetization as a function of angle for H_{app} parallel to the c-axis equal to (a) 23 Oe, (b) 300 Oe, (c) 500 Oe, and (d) 3 kOe. Filled circles (●) denote the data for increasing angles, and hollow circles (○) are for the data taken on reversal of rotation. Solid lines are fits to $M = -(M_A \cos^2\theta + M_B \sin^2\theta)$. In (a) the data could be fit to this equation for both increasing and decreasing angles. In (b) however, a good fit is obtained only for increasing angles.

field. The data for $H_{app} = 100$ Oe show the hysteresis between increasing and decreasing angles in the angular region $\theta < 90°$. The data indicate some depinning of the field cooled flux on initial rotation. This appears to be consistent with the observation of an initial "transient regime" as discussed in Ref. [15], where apparently the magnitudes of the flux in the shoulder and core regions undergo changes before reaching their steady state values. The core and shoulder regions can be identified with the "rotational" and "frictional" components of the flux, B_R and B_F of Ref. [15]. This comparison will be discussed in greater detail later.

The evidence of the development of a shoulder region can be seen in this data from the presence of the peaks at 300° and 50°. We recall that in the absence of pinning, we expect to see peaks at 90° and 270° where H_{app} is perpendicular to c. The emergence of these peaks close to $H_{app} \perp c$ implies that the data of Fig. 2 is to be viewed as a superposition of core and shoulder contributions. The lower critical field in the $H \| c$ configuration, H_{c1} is 110 Oe for this sample. At fields larger than this ($H_{app} =$ 200 Oe), the depinning is much more pronounced. The peaks at 90°, 180° and 270° are evident, and so is the hysteresis on reversal. Thus the core which exists due to field cooling is rapidly depleted and the variation of $M(\theta)$ due to the equilibrium magnetization becomes dominant. Data taken upto much higher cooling fields basically reinforce these conclusions.

3.2. Zero field cooling

The ZFC data on the other hand shows a qualitatively different behavior (see Fig. 3). In contrast to the field cooled data, there is no evidence of depinning in the low angle regime $\theta < 90°$. The absence of depinning is not surprising considering the comparatively elevated temperatures of our study. As shown in Ref. [15] the rigidly rotating component of the flux decreases strongly with increasing temperatures, so that at the relatively high ambient temperature of 77 K, it can be considered to be negligible. We note that there may exist a "transient regime" at $\theta < 90°$ associated with the development of the orientational gradient of flux in the shoulder region (as has been discussed in the introduction).

For $H_{app} \leq 100$ Oe, there is almost no hysteresis between up and down going data and the peak positions are at 90°, 180°, 270° and 360°. However for $H_{app} > H_{c1}$, it begins to be apparent that there is pronounced hysteresis between up and down going data. This aspect will be discussed later. We note that for $H_{app} < 500$ Oe, the peaks on the way up occur at regular 90° intervals i.e., at $\theta = 90°$, 180° and 270°. Also that the oscillations are perfectly even and harmonic, and can be fit to

$$M \propto -(\sin^2\theta + \cos^2\theta).$$

At a field of 500 Oe, the peak position for $\theta = 90°$, 270° (i.e. in the $H_{app} \perp c$ orientation) no longer occur at these angles. Both the peaks are shifted downwards by 10°. The peak for $H_{app} \parallel c$ ($\theta = 180°$) still continues to occur at 180°. Thus the angular span in going from nominally $H_{app} \parallel c$ orientation to $H_{app} \perp c$ is reduced to 80°, while the angular span in going from $H_{app} \perp c$ orientation to $H_{app} \parallel c$ increases to 100°. This trend continues systematically with increasing field. The peak of the $H_{app} \perp c$ orientation is shifted downward by a maximum of 30° by the time H_{app} is equal to 1200 Oe, while the $H_{app} \parallel c$ peak still occurs at $\theta = 180°$. Increasing the field further upto 3 kOe had no effect on the peak position.

As a check to verify that the shift of the peak position, as elaborated above, was not dependent on the initial state of the sample, we initiated the experiment with $\theta = 90°$ (instead of the usual case of $\theta = 0°$). We again observed that the shifts in th peaks were maximum for the $H_{app} \parallel ab$-planes, an minimum for the $H_{app} \parallel c$ orientations, as in th previous case. The field dependence of the phas shifts and the effects of reversal of rotation wer very similar to those observed when rotation wa initiated at $\theta = 0°$.

It is immediately obvious from these data that th net orientation of the flux becomes parallel to th ab-planes well before the field has aligned itself ir that direction. This tilting of the flux away from th field direction becomes as large as 30°. However nc such effect occurs when the sample approaches the $H_{app} \parallel c$ orientation. We explain this behavior in the following way. When the sample is rotated towards the *ab*-planes, the mean flux orientation would ideally follow the field. Thus if $\theta < 90°$, the response M would correspond to this angle. However due to the anisotropy of the line energy, there is an additional effect. Since the lines will reduce their self energy by aligning themselves along the *ab*-planes, they tend to do so, and become parallel to the *ab*-plane earlier than the sample as a whole. This results in the observed peak occurring at $\theta < 90°$ or 270°. We note that this is not a torque due to the field, because there is no change in the phase shift as the field is increased from 1200 Oe to a maximum field of 3 kOe. We also observe that it is not a torque related to the pinning. Such an effect would be manifested in the flux tending to align closer to the *c*-axis along which the pinning is higher. The above arguments also explain the larger angular range in going from $H_{app} \parallel ab$-planes to $H_{app} \parallel c$ orientations, and the constancy of the peak at $\theta = 180°$. As the sample is rotated towards the *c*-axis, the flux has to be rotated away from *ab*-planes. Due to larger values of line tension in *ab*-planes, this requires higher energy and consequently a larger rotation. There will now be no tendency for the flux to align itself parallel to *c*-axis because of the larger self energy in this direction.

We observe that despite the fact that the sample has very pronounced hysteresis in the $M(H)$ loops indicating the presence of flux pinning, the $M(\theta)$ behavior exhibits a high degree of orientational freedom of the flux lines. (Note for example the equality of the peaks heights and the line shapes at $\theta = 90°$ and 270° or between $\theta = 180°$ and 360°). This could

occur in two ways: (a) complete absence of pinning, or (b) the presence of pinning leading to a shoulder in the sense described in the introduction. The flux lines in the shoulder are free to adjust themselves with respect to the field direction consistent with the angular gradient.

The possibility (a) above, viz. no pinning is ruled out not only because of the $M(H)$ loops characteristics mentioned but also because of the hysteresis on reversal of sense of rotation. Both these effects testify to the existence of flux pinning in our sample. Thus our operating picture is one where the pinning determines the angular gradient and the anisotropy determines the magnitude of the magnetization for various orientations. The flux lines in the shoulder rotate frictionally with respect to the sample, in the terminology of Refs. [15,16], where they are identified as B_F, the "frictional component" of the flux.

We have also investigated the angular dependence of the deviation of M(θ) from the low field behavior where there is no phase shift. The procedure we adopted is as follows. The low field data at H_{app} = 300 Oe was fit to the equation:

$$M(\theta) = -\left[M_A \cos^2\theta + M_B \sin^2\theta\right], \qquad (1)$$

Here M_A and M_B are the values of M for $H_{app} \| c$ and $H_{app} \| ab$-planes respectively. A very good fit to Eq. (1) was obtained indicating the functional form of $M(\theta)$ for ZFC case where there is no phase shift. We next used the obtained $M(\theta)$ at H_{app} = 1000 Oe, where there is a pronounced phase shift, and obtained from it the values of M_A and M_B as the values at $\theta = 180°$ and $\theta = 270° - \delta$ (where δ is the shift in the peak). Using these M_A and M_B values, magnetization $M(\theta)$ values were generated according to Eq. (1). This would be the form of $M(\theta)$ if there had been no phase shift at this field. We call these values M_{calc}. We next took the difference between the measured magnetization $M(\theta)$ and M_{calc},

$$\Delta M(\theta) = M(\theta) - M_{calc}(\theta).$$

This deviation $\Delta M(\theta)$ is plotted in Fig. 4 for the region $\theta = 180°$ to 270° and for $\theta = 270°$ to 360°. It is clear that the deviations have a maximum around 230°, i.e. around 40° away from the direction of *ab*-planes. This variation interestingly enough looks

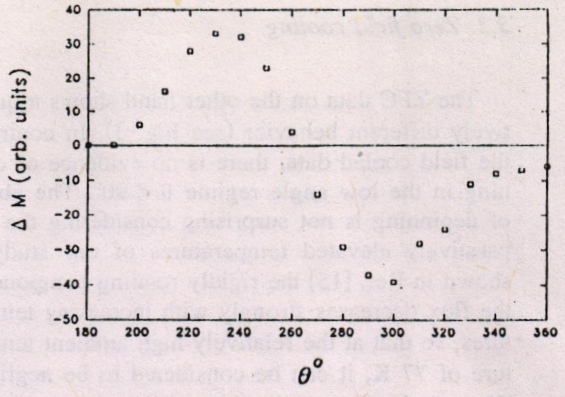

Fig. 4. ΔM versus θ for H_{ZFC} = 1 kOe, for the angular regime $180° \leq \theta \leq 360°$.

qualitatively similar to the behavior of intrinsic torque as a function of angle as described in Ref. [5] peaking around 30°–40° from the *ab*-planes. As pointed out by Farrell et al. [17], the detailed behavior of this intrinsic torque with angle depends on the degree of anisotropy, with the maximum shifting towards 45° with decreasing anisotropy.

For the angular region $270° \leq \theta \leq 360°$, the peak in ΔM occurred at 300°, and the values of ΔM are negative in this range. This is in contrast to the values of ΔM in the range 180°–270°, where $\Delta M = M(\theta) - M_{calc} > 0$. This indicates that $|M(\theta)| < |M_{calc}|$, or that the quantity of flux within the sample is higher at a given angle than the calculated value. This latter trend is also reasonable, because the region $180° \leq \theta \leq 270°$ is where the sample is being moved towards the orientation $H_{app} \| ab$-planes. As discussed earlier, flux entry becomes easier in this case, and the tilted flux orients itself readily along the ab-planes. In comparison the $\Delta M < 0$ behavior for $270° \leq \theta \leq 360°$ (i.e. during rotation away from the *ab*-planes) indicates that there is less flux inside the sample than the calculated values.

3.3. Reversal of rotation

The differences in the peak positions on the reversal of the sense of rotation are understood to be due to the anisotropy of pinning. We show that the effect of reversing the sense of rotation (at e.g. $\theta = 360°$) is

to create an additional phase shift in the peak positions. This effect is completed at most on rotating by 90°. This is the hysteresis associated with the change in the orientation of the flux in the shoulder region, as has been discussed in the introduction. It will be shown that rotations beyond this angle ($\approx 90°$) reproduce the effects on the way up in the sense of the angular span between successive peaks, and the changes in the same with applied field.

As mentioned earlier, the irreversibility in $M(\theta)$ on reversal is observed to occur for $H_{app} > H_{c1}$. The peak for the $H_{app} \parallel ab$-plane orientation becomes shifted. This can be seen for example in Fig. 2 ($H_{app} = 200$ Oe), where the peak in the upgoing path is at $\theta = 270°$. The peak in decreasing angles is now at 280°, i.e. it occurs 10° earlier than the actual orientation of the ab-planes along the field direction. On subsequent rotation, however, there are no further shifts. The peak positions at $\theta = 180°$ and $\theta = 90°$ also occur shifted by 10° in the same sense. With increasing field the shift on reversal is increased, e.g. at $H_{app} = 500$ Oe, the peak occurs at 290° (i.e. after a 70° rotation from 360°). Since the peak on the way up was at 260°, (i.e. already shifted by 10°), the net difference in the peak positions is of 30°. We find that the angular span in going from $H_{app} \parallel ab$ to $H_{app} \parallel c$ (100°), or vice versa (80°) is preserved on the reversal, once the initial changes (in the region $\theta = 360° \rightarrow 270°$) have been completed. This pattern is consistently followed at higher fields. At a field of 2 kOe, the first peak after reversal occurs after a rotation of only 40°. Since the peak on the way up was at 240°, this amounts to a net shift of 80° (for $H_{app} \parallel ab$). The angular span in going from the $H_{app} \parallel ab$ to $H_{app} \parallel c$ orientation is 120° both on the way up and down, and is equal to 60° for the angular path $H_{app} \parallel c$ to $H_{app} \parallel ab$.

Thus the pattern to emerge is that the reversal of the sense of rotation alters the response in the region $360° \rightarrow 270°$. Thereafter the effects, at least in the sense of the angular span between consecutive peaks, are identical to those on the way up. This means that the shifts produced by the reversal and the anisotropy related effects can be viewed separately. The shift in the peaks produced by reversing the sense of rotation adds to the shifts produced by the anisotropy of the line tension.

4. Conclusions

We have shown that the magnetization changes on rotation, specifically their deviations from perfect harmonicity and reversibility can be divided into two parts. The first part originates from the tendency of the flux lines to be aligned parallel to the ab-planes, and pushes the flux lines to be oriented thus before the actual 90° rotation from the c-axis has been completed. These deviations have been shown to reach a maximum at about 30° from the ab-planes and are zero for $H_{app} \parallel c$ orientation. There exists a strong similarity to the behavior of the intrinsic torque, suggesting that the peak shifts originate in the aforementioned tendency of the flux lines to lie parallel to the ab-planes. The second part of the behavior relates to the irreversibilities in the $M(\theta)$ curves on reversal of the sense of rotation. We have shown that this essentially originates in a region of about 90° angular span, where the moments in the shoulder region gradually reverse their orientation gradient. Once this region is traversed, the subsequent maxima and minima occur at the same intervals as in increasing angles. The increase and ultimate saturation of the phase shifts with field, and the fact that these are large for $H_{app} \perp c$ (and vice versa) indicate that these shifts are not essentially defined by the pinning.

Our current analysis is in many ways complimentary, and extends the existing picture of $M(\theta)$ behavior in high T_c materials. Detailed $M(\theta)$ studies [16] have indicated that the magnetization can be divided into two parts viz. a frictional part B_F, and a rotational part B_R. When the sample is rotated, B_F rotates with the field, while B_R is rigidly fixed and rotates with the sample. In zero field cooled samples B_R is negligible, while in field cooled samples both components are present. It was also concluded in Ref. [16] that B_F represents the rotational steady state, and is located in regions adjacent to the surfaces of the sample. It is obvious that our division of the flux into a "shoulder" and 'core' region coincides exactly with the description in terms of B_F and B_R respectively. This coincidence extends to the field and history dependence of the two components. Our picture however enables one to start from a more fundamental point, viz. the equations of th

generalized critical state, and gives a logical explanation of the existence of these two components. We also note that the model we have used is built on the existence of a flux line orientation gradient, an important aspect which has not been stressed in the context of high T_c materials. This model can be used to analyze the angular gradients of the magnetization, and to determine such useful quantities as the longitudinal critical current density $J_{c\parallel}$, and its relation to the transverse critical current density $J_{c\perp}$. Some of these aspects will be addressed by us in future work.

Acknowledgments

S.K. Hasanain acknowledges support from Pakistan Science Foundation grant no. PSF-C-QU-Phys-90. S. Manzoor is grateful for support from the Akhter Ali Memorial Fellowship Fund.

References

[1] U. Yaron, I. Felner and Y. Yeshurun, Phys. Rev. B 44 (1991) 12531.
[2] I. Felner, U. Yaron, Y. Yeshurun, G.V. Chandrashekar and F. Holtzberg, Phys. Rev. B 40 (1989) 5239.
[3] S.K. Hasanain, G.H. Khosa, M.Z. Iqbal and N.A. Khan, Supercond. Sci. Technol. 6 (1993) 691.
[4] G.H. Khosa, S.K. Hasanain and A.N. Kayani, Supercond. Sci. Technol. 8 (1995) 534.
[5] M.M. Doria and I.G. de Oliveira, Phys. Rev. B 49 (1994) 6205.
[6] V.G. Kogan, Phys. Rev. B 38 (1988) 7049.
[7] L.N. Bulaevskii, Phys. Rev. B 44 (1991) 910.
[8] A. Sudbø and E.H. Brandt, Phys. Rev. Lett. 67 (1991) 3176.
[9] R. Boyer and M.A.R. LeBlanc, Solid State Commun. 24 (1977) 261.
[10] R. Boyer, G. Fillion and M.A.R. LeBlanc, J. Appl. Phys. 51 (1980) 1692.
[11] J.R. Cave and M.A.R. LeBlanc, J. Appl. Phys. 53 (1982) 1631.
[12] J.R. Clem, Phys. Rev. B 26 (1982) 2463.
[13] J.R. Clem and A. Perez-Gonzalez, Phys. Rev. B 33 (1986) 1601.
[14] A. Perez-Gonzalez and J.R. Clem, Phys. Rev. B 42 (1990) 4100.
[15] M.K. Hasan and J.S. Kouvel, Physica C 254 (1995) 323.
[16] H.P. Goeckner and J.S. Kouvel, Phys. Rev. B 50 (1994) 3435.
[17] D.E. Farrell, C.M. Williams, S.A. Wolf, N.P. Bansal and V.G. Kogan, Phys. Rev. Lett. 61 (1988) 2805.